Publ. Astron. Soc. Japan (2014) 66 (5), 90 (1–71)
doi: 10.1093/pasj/psu072

Survey of period variations of superhumps in SU UMa-type dwarf novae. VI. The sixth year (2013–2014)

Taichi Kato,[1,*] Pavol A. Dubovsky,[2] Igor Kudzej,[2] Franz-Josef Hambsch,[3,4,5] Ian Miller,[6] Tomohito Ohshima,[1] Chikako Nakata,[1] Miho Kawabata,[7] Hirochika Nishino,[7] Kazunari Masumoto,[7] Sahori Mizoguchi,[7,8] Masayuki Yamanaka,[7,9,10] Katsura Matsumoto,[7] Daisuke Sakai,[7] Daiki Fukushima,[7] Minami Matsuura,[7] Genki Bouno,[7] Megumi Takenaka,[7] Shinichi Nakagawa,[7] Ryo Noguchi,[7] Eriko Iino,[7] Roger D. Pickard,[11,12] Yutaka Maeda,[13] Arne Henden,[14] Kiyoshi Kasai,[15] Seiichiro Kiyota,[16] Hidehiko Akazawa,[17] Kazuyoshi Imamura,[17] Enrique de Miguel,[18,19] Hiroyuki Maehara,[20] Berto Monard,[21,22] Elena P. Pavlenko,[23,1] Kirill Antonyuk,[23] Nikolaj Pit,[23] Oksana I. Antonyuk,[23] Aleksei V. Baklanov,[23] Javier Ruiz,[24,25,26] Michael Richmond,[27] Arto Oksanen,[28] Caisey Harlingten,[29] Sergey Yu. Shugarov,[30,31] Drahomir Chochol,[31] Gianluca Masi,[32] Francesca Nocentini,[32] Patrick Schmeer,[33] Greg Bolt,[34] Peter Nelson,[35] Joseph Ulowetz,[36] Richard Sabo,[37] William N. Goff,[38] William Stein,[39] Raúl Michel,[40] Shawn Dvorak,[41] Irina B. Voloshina,[30] Vladimir Metlov,[30] Natalia Katysheva,[30] Vitaly V. Neustroev,[42] George Sjoberg,[14,43] Colin Littlefield,[44] Bartłomiej Dębski,[45] Paulina Sowicka,[45] Marcin Klimaszewski,[45] Małgorzata Curyło,[45] Etienne Morelle,[46] Ivan A. Curtis,[47] Hidetoshi Iwamatsu,[1,48] Neil D. Butterworth,[49] Maksim V. Andreev,[50,51] Nikolai Parakhin,[50] Aleksandr Sklyanov,[52] Kazuhiko Shiokawa,[53] Rudolf Novák,[54] Tat'yana R. Irsmambetova,[30] Hiroshi Itoh,[55] Yoshiharu Ito,[56] Kenji Hirosawa,[57] Denis Denisenko,[58] Christopher S. Kochanek,[59] Benjamin Shappee,[59] Krzysztof Z. Stanek,[59] José L. Prieto,[60,61] Koh-ichi Itagaki,[62] Rod Stubbings,[63] Jose Ripero,[64] Eddy Muyllaert,[65] and Gary Poyner[66]

[1]Department of Astronomy, Kyoto University, Kitashiakawa-Oiwake-cho, Sakyo-ku, Kyoto, Kyoto 606-8502, Japan
[2]Vihorlat Observatory, Mierova 4, Humenne, Slovakia
[3]Groupe Européen d'Observations Stellaires (GEOS), 23 Parc de Levesville, 28300 Bailleau l'Evêque, France
[4]Bundesdeutsche Arbeitsgemeinschaft für Veränderliche Sterne (BAV), Munsterdamm 90, 12169 Berlin, Germany
[5]Vereniging Voor Sterrenkunde (VVS), Oude Bleken 12, 2400 Mol, Belgium
[6]Furzehill House, Ilston, Swansea, SA2 7LE, UK
[7]Osaka Kyoiku University, 4-698-1 Asahigaoka, Kashiwara, Osaka 582-8582, Japan
[8]Sendai Astronomical Observatory, Nishikigaoka, Aoba-ku, Sendai, Miyagi 989-3123, Japan

[9]Department of Physics, Faculty of Science and Engineering, Konan University, Okamoto, Higashinada-ku, Kobe, Hyogo 658-8501, Japan
[10]Kwasan and Hida Observatories, Kyoto University, Kitakazan-Ohmine-cho, Yamashina-ku, Kyoto, Kyoto 607-8471, Japan
[11]The British Astronomical Association, Variable Star Section (BAA VSS), Burlington House, Piccadilly, London, W1J 0DU, UK
[12]3 The Birches, Shobdon, Leominster, Herefordshire, HR6 9NG, UK
[13]12-14 Kaminishiyama-machi, Nagasaki, Nagasaki 850-0006, Japan
[14]American Association of Variable Star Observers, 49 Bay State Rd., Cambridge, MA 02138, USA
[15]Baselstrasse 133D, CH-4132 Muttenz, Switzerland
[16]Variable Star Observers League in Japan (VSOLJ), 7-1 Kitahatsutomi, Kamagaya, Chiba 273-0126, Japan
[17]Department of Biosphere-Geosphere System Science, Faculty of Informatics, Okayama University of Science, 1-1 Ridai-cho, Okayama, Okayama 700-0005, Japan
[18]Departamento de Física Aplicada, Facultad de Ciencias Experimentales, Universidad de Huelva, 21071 Huelva, Spain
[19]Center for Backyard Astrophysics, Observatorio del CIECEM, Parque Dunar, Matalascañas, 21760 Almonte, Huelva, Spain
[20]Kiso Observatory, Institute of Astronomy, School of Science, The University of Tokyo, 10762-30 Mitake, Kiso-machi, Kiso-gun, Nagano 397-0101, Japan
[21]Bronberg Observatory, Center for Backyard Astronomy Pretoria, PO Box 11426, Tiegerpoort 0056, South Africa
[22]Kleinkaroo Observatory, Center for Backyard Astronomy Kleinkaroo, Sint Helena 1B, PO Box 281, Calitzdorp 6660, South Africa
[23]Crimean Astrophysical Observatory, 98409, Nauchny, Crimea, Ukraine
[24]Observatorio de Cantabria, Ctra. de Rocamundo s/n, Valderredible, Cantabria, Spain
[25]Instituto de Física de Cantabria (CSIC-UC), Avenida Los Castros s/n, E-39005 Santander, Cantabria, Spain
[26]Agrupación Astronómica Cántabra, Apartado 573, 39080, Santander, Spain
[27]Physics Department, Rochester Institute of Technology, 85 Lomb Memorial Drive, Rochester, NY 14623, USA
[28]Nyrola Observatory, Jyvaskylan Sirius ry, Vertaalantie 419, FI-40270 Palokka, Finland
[29]Searchlight Observatory Network, The Grange, Erpingham, Norfolk, NR11 7QX, UK
[30]Sternberg Astronomical Institute, Lomonosov Moscow University, Universitetsky avenyu, 13, Moscow 119992, Russia
[31]Astronomical Institute of the Slovak Academy of Sciences, 05960, Tatranska Lomnica, the Slovak Republic
[32]The Virtual Telescope Project, Via Madonna del Loco 47, 03023 Ceccano (FR), Italy
[33]Bischmisheim, Am Probstbaum 10, 66132 Saarbrücken, Germany
[34]Camberwarra Drive, Craigie, Western Australia 6025, Australia
[35]1105 Hazeldean Rd, Ellinbank 3820, Australia
[36]Center for Backyard Astrophysics Illinois, Northbrook Meadow Observatory, 855 Fair Ln, Northbrook, IL 60062, USA
[37]2336 Trailcrest Dr., Bozeman, MT 59718, USA
[38]13508 Monitor Ln., Sutter Creek, CA 95685, USA
[39]6025 Calle Paraiso, Las Cruces, NM 88012, USA
[40]Instituto de Astronomía UNAM, Apartado Postal 877, 22800 Ensenada B.C., México
[41]Rolling Hills Observatory, 1643 Nightfall Drive, Clermont, FL 34711, USA
[42]Astronomy Division, Department of Physics, PO Box 3000, FIN-90014 University of Oulu, Finland
[43]The George-Elma Observatory, 9 Contentment Crest, #182, Mayhill, NM 88339, USA
[44]Department of Physics, University of Notre Dame, Notre Dame, IN 46556, USA
[45]Astronomical Observatory, Jagiellonian University, ul. Orla 171 30-244 Kraków, Poland
[46]9 rue Vasco de GAMA, 59553 Lauwin Planque, France

[47]2 Yandra Street, Vale Park, Adelaide, South Australia 5081, Australia
[48]St. Dominic Junior and Senior High School, 2-2-14 Tsunogorou, Aoba-ku, Sendai, Miyagi 980-0874, Japan
[49]24 Payne Street, Mount Louisa, Queensland 4814, Australia
[50]Institute of Astronomy, Russian Academy of Sciences, 361605 Peak Terskol, Kabardino-Balkaria, Russia
[51]International Center for Astronomical, Medical and Ecological Research of NASU, 27 Akademika Zabolotnoho str., 03680 Kiev, Ukraine
[52]Kazan Federal University, Kremlevskaya str., 18, Kazan, 420008, Russia
[53]810 Moriyama, Komoro, Nagano 384-0085, Japan
[54]Research Centre for Toxic Compounds in the Environment, Faculty of Science, Masaryk University, Kamenice 3, 625 00 Brno, Czech Republic
[55]VSOLJ, 1001-105 Nishiterakata-cho, Hachioji, Tokyo 192-0153, Japan
[56]VSOLJ, 6-2-69 Kamisugi, Aoba-ku, Sendai, Miyagi 980-0011, Japan
[57]216-4 Maeda, Inazawa-cho, Inazawa, Aichi 492-8217, Japan
[58]Space Research Institute (IKI), Russian Academy of Sciences, Moscow, Russia
[59]Department of Astronomy, the Ohio State University, Columbia, OH 43210, USA
[60]Núcleo de Astronomía de la Facultad de Ingeniería, Universidad Diego Portales, Av. Ejército 441, Santiago, Chile
[61]Department of Astrophysical Sciences, Princeton University, NJ 08544, USA
[62]Itagaki Astronomical Observatory, Teppo-cho, Yamagata, Yamagata 990-2492, Japan
[63]Tetoora Observatory, Tetoora Road, Victoria, Australia
[64]President of CAA (Centro Astronómico de Avila) and Variable and SNe Group M1, Buenavista 7, Ciudad Sto. Domingo, 28110 Algete/Madrid, Spain
[65]Vereniging Voor Sterrenkunde (VVS), Moffelstraat 13 3370 Boutersem, Belgium
[66]BAA Variable Star Section, 67 Ellerton Road, Kingstanding, Birmingham B44 0QE, UK

*E-mail: tkato@kusastro.kyoto-u.ac.jp

Received 2014 March 9; Accepted 2014 June 24

Abstract

Continuing the project undertaken by Kato et al. (2009), we collected times of superhump maxima for 56 SU UMa-type dwarf novae mainly observed during the 2013–2014 season and characterized these objects. We detected negative superhumps in VW Hyi and indicated that the low number of normal outbursts in some supercycles can be interpreted as a result of disk tilt. This finding, combined with the Kepler observation of V1504 Cyg and V344 Lyr, suggests that disk tilt is responsible for modulating the outburst pattern in SU UMa-type dwarf novae. We also studied the deeply eclipsing WZ Sge-type dwarf nova MASTER OT J005740.99+443101.5 and found evidence of a sharp eclipse during the phase of early superhumps. The profile can be reproduced by a combination of the eclipse of the axisymmetric disk and the uneclipsed light source of early superhumps. This finding shows the lack of evidence for a greatly enhanced hot spot during the early stage of WZ Sge-type outburst. We detected growing (stage A) superhumps in MN Dra and give a suggestion that some of SU UMa-type dwarf novae situated near the critical condition of tidal instability may show long-lasting stage A superhumps. The large negative period derivatives reported in such systems can be understood as a result of the combination of stage A and B superhumps. Two WZ Sge-type dwarf novae, AL Com and ASASSN-13ck, showed a long-lasting (plateau-type) rebrightening. In the early phase of their rebrightenings, both objects showed a precursor-like outburst, suggesting that the long-lasting rebrightening is triggered by a precursor outburst.

Key words: accretion, accretion disks — novae, cataclysmic variables — stars: dwarf novae

1 Introduction

Cataclysmic variables (CVs) are close binary systems transferring matter from a low-mass dwarf secondary to a white dwarf. The transferred matter forms an accretion disk. In dwarf novae (DNe), a class of CVs, thermal-viscous instability in the accretion disk causes outbursts. SU UMa-type dwarf novae, a subclass of DNe, show long outbursts (superoutburst) in addition to ordinary short outbursts, and semiperiodic modulations called superhumps are detected during the superoutbursts. The superhumps have periods a few percent longer than the orbital period. It is now widely believed that the 3:1 resonance in the accretion disk brings about the eccentric deformation of the disk, resulting in superhumps (tidal instability: Whitehurst 1988; Hirose & Osaki 1990; Lubow 1991). The superoutburst can be understood as a result of the increased tidal dissipation and the removal of the angular momentum when the tidal instability works [thermal tidal instability (TTI) model: Osaki 1989, 1996]. This process produces a relaxation oscillation in the total angular momentum of the disk, and superoutbursts recur. The interval between the successive superoutbursts is called a supercycle. For general information on CVs, DNe, SU UMa-type dwarf novae, and superhumps, see, e.g., Warner (1995).

In a series of papers, Kato et al. (2009, 2010, 2012b, 2013b, 2014a), we systematically surveyed SU UMa-type dwarf novae particularly on variations in the superhump period. The change in the superhump period reflects the precession angular velocity of the eccentric (or flexing) disk, and is expected to be an excellent probe for studying the structure of the accretion disk during dwarf nova outbursts. In a recent series of papers, we dealt with various topics related to SU UMa-type dwarf novae and superhumps; in Kato et al. (2012b), we also studied Kepler data and made a pilot study on variations in the superhump amplitude motivated by Smak (2010). In Kato et al. (2013b), we systematically studied ER UMa-type dwarf novae (a class of SU UMa-type dwarf novae with a very short supercycle, see, e.g., Kato & Kunjaya 1995; Robertson et al. 1995; Kato et al. 1999) and helium dwarf novae (AM CVn-type objects). In Kato et al. (2014a), we made a pilot study on the decline rate of the superoutburst motivated by Cannizzo et al. (2010) and studied negative superhumps (having periods shorter than the orbital period and being considered as a manifestation of a tilted disk, see, e.g., Harvey et al. 1995; Patterson et al. 1997; Wood & Burke 2007) particularly in BK Lyn, which displays two states: a nova-like variable (a thermally stable CV) and an ER UMa-type dwarf nova.

We continue this extended, comprehensive research of SU UMa-type dwarf novae and superhumps in general in this paper. Since most of the objects treated in this paper have been little documented in the past, and since a compilation from historical descriptions of dwarf novae has not been issued for a long time since Glasby (1970), we intend this series of papers to also be a compiled source of information as to individual dwarf novae.

The present advances in understanding superhump periods and their variations started with a new interpretation of the Kepler observation (Osaki & Kato 2013a), who used the negative superhump as a probe for the variation in the disk radius over a supercycle period, and confirmed the radius variation predicted by the TTI model. Combined with Osaki and Kato (2013b, 2014), the TTI model is currently the only viable model of the SU UMa-type phenomenon.

In Kato et al. (2009), we demonstrated that most of the $O-C$ diagrams of superhumps in SU UMa-type dwarf novae can be expressed by three distinct stages: an initial growing stage (stage A) with a long period, a fully developed stage (stage B) with a systematically varying period, and a later stage (stage C) with a shorter, almost constant period (see Kato et al. 2009 for the notation of stages A–B–C of superhumps). The origin of these three stages of superhumps was a mystery when it was documented in Kato et al. (2009). Through analysis of the Kepler data, Osaki and Kato (2013b) proposed that the appearance of the pressure effect is responsible for the transition from stage A to stage B. From this interpretation, stage A reflects the state of the 3:1 resonance that is confined to the resonance region. This interpretation allowed a new method for determining the mass ratio ($q = M_2/M_1$) only from superhump observations and the orbital period (Kato & Osaki 2013b). This method is particularly suitable for measuring mass ratios in WZ Sge-type dwarf novae (SU UMa-type dwarf novae with a very long supercycle, considered to be the terminal stage of the CV evolution) and for distinguishing hitherto very poorly known period bouncers (CVs which have passed the minimum orbital period in evolution) from ordinary CVs (Kato et al. 2013a; Nakata et al. 2013b). Superhumps are now not only a powerful tool for diagnosing the accretion disk, but also an important one for illuminating CV evolution.

Materials and methods of analyses are given in section 2; observations and analyses of individual objects, including short discussions on individual objects, are given in section 3; general discussion is described in section 4 and the summary in section 5.

2 Observation and analysis

The data were obtained in the campaign led by the VSNET Collaboration (Kato et al. 2004b). For some objects,

Table 1. List of superoutbursts.

Subsection	Object	Year	Observers or references*	ID†
3.1	FO And	2013	Aka	
3.2	DH Aql	2000	Oud, Btw	
3.3	BB Ari	2013	GFB, OkC, HaC, Mhh	
3.4	UZ Boo	2013	KU, GFB, DPV, RIT, Rui, Mhh, AAVSO, RPc, Kai, CRI, IMi, Mdy, Iak, Ioh	
3.5	V342 Cam	2013	DPV	
3.6	V452 Cas	2013	IMi, RPc, DPV	
3.7	V359 Cen	2014	HaC	
3.9	YZ Cnc	2014	Aka, Mdy, HaC	
3.10	GZ Cnc	2014	Kis, Mdy, IMi, Kai, Aka	
3.11	AL Com	2013	OKU, NKa, KU, Irs, CRI, DKS, Kis, IMi, AAVSO	
3.12	V503 Cyg	2013	RPc	
3.13	IX Dra	2012	MEV, AAVSO, UJH	
3.14	MN Dra	2012	Ast, CRI	
		2013	CRI, Kai, Ter, KU	
3.15	CP Eri	2013	OkC, SWI	
3.16	V1239 Her	2013	RPc, IMi	
3.17	CT Hya	2014	Mdy	
3.18	VW Hyi	2012	HaC, CTA, Han	
3.19	WX Hyi	1977	Bailey (1979a)	
		2014	HaC	
3.20	AY Lyr	2013	Aka	
3.21	AO Oct	2013	HaC	
3.22	DT Oct	2014	OkC	
3.23	V521 Peg	2013	KU, Mdy, Aka, DPV, RPc, IMi, Hsk, Mhh	
3.24	TY Psc	2013	Aka	
3.25	V893 Sco	2007	MLF, OKU	
		2008	GBo	
		2010	GBo, OKU	
		2013	HaC, MLF	
3.26	RZ Sge	2013	AAVSO, IMi, Rui	
3.27	AW Sge	2013	Vol, SRI	
3.28	V1265 Tau	2013	GFB, HaC, KU	
3.29	SU UMa	2013	OKU, DPV, Kis, Iha	
3.30	SS UMi	2013	DPV, Kai, Krw	
3.31	CU Vel	2013	HaC, Nel	
3.32	1RXS J231935	2013	DPV	1RXS J231935.0+364705
3.33	ASAS J224349	2013	Krw, HaC, Mdy, DPV, Shu, IMi, Rui, Mhh	ASAS J224349+0809.5
3.34	ASASSN-13cf	2013	LCO, IMi, RPc	

we used the public data from the AAVSO International Database.[1]

The majority of the data were acquired by time-resolved CCD photometry by using telescopes in the 30 cm class located world-wide, and their observational details will be presented in future papers with analysis and discussion on individual objects of interest. The list of outbursts and observers is summarized in table 1. The data analysis was performed in the same way as described in Kato et al. (2009, 2014a), and we mainly used R software[2] for data analysis. In de-trending the data, we used both lower (first- to fifth-order) polynomial fitting and locally weighted polynomial regression (LOWESS: Cleveland 1979). The times of superhump maxima were determined by such a template fitting method as is described in Kato et al. (2009). The times of all observations are expressed in Barycentric Julian Date (BJD).

The abbreviations used in this paper are the same as in Kato et al. (2014a); $P_{\rm orb}$ means the orbital

[1] ⟨http://www.aavso.org/data-download⟩.

[2] The R Foundation for Statistical Computing: ⟨http://cran.r-project.org/⟩.

Table 1. (Continued)

Subsection	Object	Year	Observers or references*	ID†
3.35	ASASSN-13cg	2013	LCO, CRI	
3.36	ASASSN-13ck	2013	deM, OkC, HaC, Mas, Han, DPV, UJH, IMi, RPc, AAVSO, Nel, Mdy, Mic, RIT	
3.37	ASASSN-13cv	2013	Kai	
3.38	ASASSN-13cz	2013	IMi	
3.39	ASASSN-13da	2013	HaC	
3.40	ASASSN-14ac	2014	OKU, Kis, Mdy, DPV, RPc, KU, RIT, Mic	
3.41	CSS J024354	2013	MLF	CSS131026:024354−160314
3.42	DDE 31	2014	Mdy	
3.43	MASTER J004527	2013	OKU, UJH, deM, AAVSO, IMi, Kai, SRI, RPc, DKS, DPV, Neu, RIT	MASTER OT J004527.52+503213.8
3.44	MASTER J005740	2013	deM, NKa, Shu, Mas, SWI, UJH, AAVSO, KU, SRI, OKU, DPV, RPc	MASTER OT J005740.99+443101.5
3.45	MASTER J024847	2013	IMi	MASTER OT J024847.86+501239.7
3.46	MASTER J061335	2013	OKU, Ter, DPV, KU, Mas, Nov	MASTER OT J061335.30+395714.7
3.47	MASTER J073208	2013	Shu	MASTER OT J073208.11+064149.5
3.48	MASTER J095018	2013	HaC, OKU	MASTER OT J095018.04−063921.9
3.49	MASTER J141143	2014	DPV	MASTER OT J141143.46+262051.5
3.50	MASTER J162323	2013	Shu, IMi, Neu, Rui, DPV	MASTER OT J162323.48+782603.3
3.51	MASTER J234843	2013	OKU, Mas, DPV	MASTER OT J234843.23+250250.4
3.52	OT J013741	2014	deM, Kai	CSS140104:013741+220312
3.53	OT J210016	2013	MLF, deM, OKU, DKS	CSS130905:210016−024258
3.54	PNV J191501	2013	KU, deM, AAVSO, GBo, Vol, OkC, SWI, OKU, Mic, HaC, DPV, SRI, Mdy, MEV, RIT, Aka, Siz, GFB, RPc, Kis, IMi, Mhh, Nel, Ioh	PNV J19150199+0719471
3.55	SSS J094327	2013	Kis	SSS J094327.3−272038
		2014	GBo, Kis, HaC	
3.56	TCP J233822	2013	MLF, HaC, Nel	TCP J23382254−2049518

*Key to observers: Aka (H. Akazawa, OUS), Ast (Astrotel telescope, by A. Sklyanov), Btw (N. Butterworth), CRI (Crimean Astrophys. Obs.), CTA (I. Curtis), deM (E. de Miguel), DKS‡(S. Dvorak), DPV (P. Dubovsky), GBo (G. Bolt), GFB‡(W. Goff), HaC (F.-J. Hambsch, remote obs. in Chile), Han (Hankasalmi Obs., by A. Oksanen), Hsk (K. Hirosawa), IaK (K. Imamura), Iha (Y. Ito), IMi‡(I. Miller), Ioh (H. Itoh), Irs (T. Irsmambetova), Kai (K. Kasai), Kis (S. Kiyota), Krw (Krakow team), KU (Kyoto Univ., campus obs.), LCO (C. Littlefield), Mas (G. Masi team), Mdy (Y. Maeda), MEV‡(E. Morelle), Mhh (H. Maehara), Mic (R. Michel-Murillo team), MLF (B. Monard), Nel‡(P. Nelson), Neu (V. Neustroev), NKa (N. Katysheva), Nov (R. Novák), OkC‡(A. Oksanen, remote obs. in Chile), OKU (Osaka Kyoiku Univ.), Oud (Ouda station, Kyoto Univ.), RIT (M. Richmond), RPc‡(R. Pickard), Rui (J. Ruiz), Shu (S. Shugarov), Siz (K. Shiokawa), SRI‡(R. Sabo), SWI‡(W. Stein), Ter (Terskol Obs.), UJH‡(J. Ulowetz), Vol (I. Voloshina), and AAVSO (AAVSO database).

†Original identifications, discoverers, or data source.

‡Inclusive of observations from the AAVSO database.

period and $\varepsilon \equiv P_{\rm SH}/P_{\rm orb} - 1$ is the fractional superhump excess. Since Osaki and Kato (2013a), the alternative fractional superhump excess in the frequency unit, $\varepsilon^* \equiv 1 - P_{\rm orb}/P_{\rm SH} = \varepsilon/(1+\varepsilon)$, has been introduced because this fractional superhump excess can be directly compared to the precession rate. We therefore used ε^* for referring to the precession rate.

We used phase dispersion minimization (PDM: Stellingwerf 1978) for period analysis, and $1\,\sigma$ errors for the PDM analysis were evaluated from the methods of Fernie (1989) and Kato et al. (2010). We also used the least absolute shrinkage and selection operator (Lasso) method (Tibshirani 1996; Kato & Uemura 2012), which has proved to be effective in yielding very sharp signals. In this paper, we used the two-dimensional Lasso power spectra, introduced in some analyses of the Kepler data such as Kato and Maehara (2013), Osaki and Kato (2013b), and Kato and Osaki (2013a). These two-dimensional Lasso power spectra have proved to be helpful in detecting negative superhumps (cf. Osaki & Kato 2013b) as well as positive superhumps with varying frequencies (cf. Kato & Maehara 2013). Although the application of two-dimensional Lasso power spectra to the Kepler data is limited to almost uniformly sampled data, we have demonstrated in Kato et al. (2014a) and Ohshima et al. (2014) that two-dimensional Lasso power spectra are also effective in detecting multiple signals and their variations in non-uniformly sampled ground-based data.

The resultant $P_{\rm SH}$, $P_{\rm dot}$, and other parameters are listed in table 2 in the same format as in Kato et al. (2009).

Table 2. Superhump periods and period derivatives.

Object	Year	P_1*(d)	Error*	E_1*		P_{dot}†	Error†	P_2*(d)	Error*	E_2*		P_{orb} (d)‡	Q§
FO And	2013	0.074412	0.000070	1	70	—	—	—	—	—	—	0.07161	CGM
DH Aql	2000	0.080005	0.000067	0	39	—	—	—	—	—	—	—	C
BB Ari	2013	0.072544	0.000097	0	42	—	—	0.072135	0.000046	40	111	—	B
UZ Boo	2013	0.062066	0.000029	15	85	5.1	5.1	—	—	—	—	—	B
V342 Cam	2013	—	—	—	—	—	—	0.078067	0.000080	0	65	0.07531	C
V452 Cas	2013	0.088596	0.000068	0	92	−14.9	2.9	—	—	—	—	—	CG
V359 Cen	2014	0.081064	0.000026	0	49	−6.3	4.2	0.080744	0.000052	60	86	—	B
FZ Cet	2014	0.058547	0.000062	0	43	—	—	—	—	—	—	—	C
YZ Cnc	2014	0.090422	0.000069	0	41	−3.9	11.2	—	—	—	—	0.0868	CG
GZ Cnc	2014	0.092699	0.000056	12	92	−2.5	4.8	—	—	—	—	0.08825	C
AL Com	2013	0.057323	0.000022	87	210	4.9	1.9	—	—	—	—	0.056669	B
IX Dra	2012	0.066955	0.000021	0	146	0.4	1.5	—	—	—	—	—	B
MN Dra	2012	0.105299	0.000061	47	115	—	—	—	—	—	—	0.0998	C
MN Dra	2013	0.105040	0.000066	26	66	−14.8	9.5	—	—	—	—	0.0998	C
CP Eri	2013	0.019897	0.000003	0	111	3.1	0.9	—	—	—	—	0.019692	B
CT Hya	2014	—	—	—	—	—	—	0.066178	0.000064	0	46	—	C
VW Hyi	2012	0.076916	0.000014	11	90	2.9	1.3	0.076579	0.000019	87	159	0.074271	A
WX Hyi	1977	0.077612	0.000113	0	14	—	—	0.077106	0.000091	26	40	0.074813	C
WX Hyi	2014	0.077616	0.000037	0	52	—	—	0.077367	0.000072	52	103	0.074813	C
AO Oct	2013	0.067326	0.000046	0	59	19.6	6.4	0.066776	0.000064	59	91	0.06535	B
DT Oct	2014	—	—	—	—	—	—	0.074022	0.000113	54	81	—	C
V521 Peg	2013	0.061503	0.000032	0	67	13.8	5.8	0.061006	0.000029	67	199	0.0599	B
TY Psc	2013	—	—	—	—	—	—	0.070381	0.000030	27	57	0.068348	C
V893 Sco	2013	0.078675	0.000025	0	52	—	—	0.078288	0.000054	51	153	0.075961	B
RZ Sge	2013	0.070642	0.000026	0	58	11.5	4.2	—	—	—	—	0.06828	C
AW Sge	2013	—	—	—	—	—	—	0.074293	0.000025	62	90	—	C
V1265 Tau	2013	0.053428	0.000024	0	187	1.9	1.9	0.053086	0.000043	186	319	—	B
SU UMa	2013	—	—	—	—	—	—	0.078775	0.000131	0	51	0.07635	C
SS UMi	2013	—	—	—	—	—	—	0.069936	0.000095	0	59	0.06778	C
CU Vel	2013	—	—	—	—	—	—	0.080573	0.000043	0	63	0.078054	B
ASAS J224349	2013	0.069719	0.000048	0	55	25.2	7.5	0.069513	0.000015	87	149	—	B
ASASSN-13cf	2013	0.058407	0.000028	0	115	7.1	1.9	—	—	—	—	—	B
ASASSN-13cg	2013	0.060228	0.000037	0	63	24.4	6.9	—	—	—	—	—	C
ASASSN-13ck	2013	0.056186	0.000010	35	185	5.6	0.4	—	—	—	—	0.055348	AE
ASASSN-13cz	2013	0.079773	0.000058	0	13	—	—	—	—	—	—	—	C
ASASSN-13da	2013	0.071781	0.000037	56	140	6.5	4.1	0.071259	0.000309	154	182	—	C
ASASSN-14ac	2014	0.058550	0.000009	57	188	−1.7	1.2	—	—	—	—	—	B
CSS J024354	2013	0.062076	0.000042	0	129	—	—	—	—	—	—	—	CGM

The definitions for parameters P_1, P_2, E_1, E_2, and P_{dot} are the same as in Kato et al. (2009). We also presented comparisons of different superoutbursts in the $O-C$ diagram since this has been one of the motivations for these surveys (cf. Uemura et al. 2005) and it has been demonstrated that a combination of $O-C$ diagrams showing a comparison of different superoutbursts can better describe the overall pattern of the period variation (Kato et al. 2009). In drawing combined $O-C$ diagrams, we usually used $E=0$ for the start of a superoutburst, which is usually referred to the first positive detection of the outburst. This epoch usually has an accuracy of $\sim$1 d for a well-observed object, and if the outburst was not sufficiently observed, we mentioned how to define $E=0$ in such an outburst. We also present representative $O-C$ diagrams and light curves, especially for WZ Sge-type dwarf novae, which are not expected to undergo outbursts in the near future. In all figures, the binned magnitude and $O-C$ value are accompanied by 1σ error bars, which are omitted when the error is smaller than the plotted mark.

We used the same terminology of superhumps as we summarized in Kato et al. (2012b). We especially call reader's attention to the term "late superhumps." We only used "traditional" late superhumps when an $\sim$0.5 phase shift is confirmed (Vogt 1983; see also table 1 in Kato et al. 2012b for various types of superhumps), since we suspect that many of the past claims of detections of "late

Table 2. (Continued)

Object	Year	P_1*(d)	Error*	E_1*		P_{dot}†	Error†	P_2*(d)	Error*	E_2*		P_{orb} (d)‡	Q§
MASTER J004527	2013	0.080365	0.000020	12	50	−3.8	4.8	0.080004	0.000012	50	144	—	A
MASTER J005740	2013	0.057067	0.000011	14	144	4.0	1.0	—	—	—	—	0.056190	B
MASTER J024847	2013	0.0644	0.0003	0	2	—	—	—	—	—	—	—	C
MASTER J061335	2013	0.056091	0.000021	61	269	5.1	0.6	0.055950	0.000072	268	321	—	B
MASTER J073208	2013	0.058836	0.000081	0	38	—	—	—	—	—	—	—	C
MASTER J162323	2013	0.088661	0.000020	35	192	3.9	0.9	—	—	—	—	—	B
MASTER J234843	2013	0.032007	0.000005	0	255	1.3	0.5	0.031977	0.000010	249	438	—	C
OT J210016	2013	0.058502	0.000020	17	160	2.3	1.5	—	—	—	—	0.05787	CE
PNV J191501	2013	0.058382	0.000010	58	297	5.2	0.2	0.058176	0.000033	292	366	0.05706	AE
SSS J094327	2014	0.070500	0.000010	14	60	5.6	2.3	0.070241	0.000048	57	88	—	C
TCP J233822	2013	0.057868	0.000014	39	206	2.7	1.1	—	—	—	—	0.057255	AE

*P_1 (P_2): the superhump period during stage B (stage C); Error: the 1 σ error; E_1 (E_2): the interval used for calculating the period P_1 (period P_2), corresponding to E in the superhump maxima table of section 3).

†P_{dot}: the period derivative in units of 10^{-5}.

‡References: FO And (Thorstensen et al. 1996), V342 Cam (Shears et al. 2011b), YZ Cnc (Shafter & Hessman 1988), GZ Cnc (Tappert & Bianchini 2003), AL Com (this work), MN Dra (Pavlenko et al. 2010), CP Eri (Armstrong et al. 2012), VW Hyi (this work), WX Hyi (Schoembs & Vogt 1981), AO Oct (Woudt et al. 2004), V521 Peg (Rodríguez-Gil et al. 2005), TY Psc (Thorstensen et al. 1996), V893 Sco (this work), RZ Sge (Patterson et al. 2003), SU UMa (Thorstensen et al. 1986), SS UMi (Thorstensen et al. 1996), CU Vel (this work), and ASASSN-13ck–TCP J233822 (this work).

§Data quality and comments. A: excellent, B: partial coverage or slightly low quality, C: insufficient coverage or observations with large scatter, G: P_{dot} denotes global P_{dot}, M: observational gap in middle stage, 2: late-stage coverage, the listed period may refer to P_2, E: P_{orb} refers to the period of early superhumps, P: P_{orb} refers to a shorter stable periodicity recorded in outburst.

superhumps" were likely to be stage C superhumps—cf. Kato et al. (2009); note that the Kepler observation of V585 Lyr also demonstrated persistent stage C superhumps without a phase shift (Kato & Osaki 2013a).

Early superhumps are double-wave humps seen during the early stage of WZ Sge-type dwarf novae, and have a period close to the orbital period (Kato et al. 1996b; Kato 2002; Osaki & Meyer 2002). We used the period of early superhumps as the approximate orbital period. The validity of this assumption is also reviewed in this paper.

The same as in Kato et al. (2009), we used coordinate-based optical transient (OT) designations for some objects, such as Catalina Real-time Transient Survey (CRTS: Drake et al. 2009)[3] transients, and listed the original identifiers in table 1. When available, we have preferred using the International Astronomical Union (IAU)-format names provided by the CRTS team in the public data release.[4]

3 Individual objects

3.1 FO Andromedae

FO And was discovered to be a dwarf nova by Hoffmeister (1967). Meinunger (1984b) showed that its outbursts occur with intervals of 10–30 d, and there was probably already a superoutburst. Meinunger (1984a) reported on the detection of three superoutbursts and that the intervals between normal outbursts ranged from 15 to 23 d. This object has been monitored by amateur observers since 1982, and both AAVSO and VSOLJ observers detected superoutbursts. Bruch (1989) obtained a spectrum in quiescence and detected Balmer and He II emission lines. Szkody et al. (1989) reported on the time-resolved photometry in quiescence without detecting a significant period. According to Szkody et al. (1989), Grauer and Bond (1986) detected superhumps with a period of $\sim$105 min, but this result was not published.

The first periodically printed matter of the superhumps in this object was Kato (1995b), whose result was refined in Kato et al. (2009). Thorstensen et al. (1996) determined the orbital period through a radial velocity study. Kato et al. (2012b) reported on superhumps in the 2010 and 2011 superoutbursts.

The 2013 November–December superoutburst was detected on November 24 by J. Ripero (vsnet-alert 16647). A time-series of observations started two nights later, and a total of three-night observations was obtained (vsnet-alert 16696). The times of superhump maxima are listed in table 3. A comparison of the $O-C$ diagrams (figure 1) suggests that the obtained global period is a mixture of different stages.

3.2 DH Aquilae

DH Aql was discovered to be a Mira-type variable (=HV 3899) with a range of 12.5 to fainter than 16 in the photographic magnitude (Cannon 1925). This

[3] ⟨http://nesssi.cacr.caltech.edu/catalina/⟩. For information on the individual Catalina CVs, see ⟨http://nesssi.cacr.caltech.edu/catalina/AllCV.html⟩.

[4] ⟨http://nesssi.cacr.caltech.edu/DataRelease/⟩.

Table 3. Superhump maxima of FO And (2013).

E	Max*	Error	$O-C^{\dagger}$	$N^{\ddagger}$
0	56622.9587	0.0016	−0.0015	51
1	56623.0348	0.0006	0.0001	48
56	56627.1334	0.0019	0.0048	56
57	56627.2050	0.0018	0.0020	50
68	56628.0242	0.0030	0.0024	55
69	56628.0944	0.0017	−0.0018	56
70	56628.1647	0.0028	−0.0060	55

*BJD − 2400000.
†Against max = 2456622.9602 + 0.074435 E.
†Number of points used to determine the maximum.

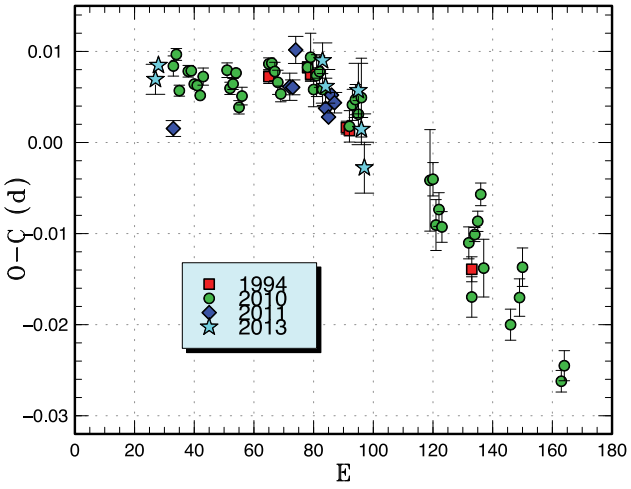

Fig. 1. Comparison of different superoutbursts of FO And in the $O-C$ diagram. A period of 0.07451 d was used to draw this figure. Approximate cycle counts (E) after the start of the superoutburst were used.

element was also used in Kholopov et al. (1985). Tsesevich (1969) recorded three outbursts and identified this object as a dwarf nova. The durations of outbursts were 3–4 d. Zhukov, Solov'ev, and Solovjev (1972) also reported another outburst and confirmed the periodicity suggested by Tsesevich (1969). This object has been regularly monitored since 1980 (e.g., Bateson 1982a, 1982b; also summarized in Mason & Howell 2003).

Nogami and Kato (1995) detected superhumps during the 1994 September outburst and established the SU UMa-type classification. Bateson (1998) reported on seven superoutbursts and supercycle lengths of 259–450 d (361 d on the average).

Kato et al. (2009) reported on the observations of superoutbursts in 2002, 2003, and 2008. We found the data of the unreported 2000 superoutburst (vsnet-alert 5163) and summarize the result here. The times of superhump maxima are listed in table 4. This superoutburst was observed in relatively early phase, and stages B and C can be recognized. The resultant $O-C$ diagram well agrees with the others (figure 2).

Table 4. Superhump maxima of DH Aql (2000).

E	Max*	Error	$O-C^{\dagger}$	$N^{\ddagger}$
0	51759.1254	0.0005	−0.0030	101
1	51759.2027	0.0005	−0.0055	161
11	51760.0042	0.0002	−0.0019	171
12	51760.0842	0.0002	−0.0016	172
13	51760.1645	0.0003	−0.0012	122
14	51760.2479	0.0009	0.0025	49
24	51761.0444	0.0008	0.0011	174
25	51761.1217	0.0003	−0.0013	173
26	51761.2045	0.0011	0.0017	150
36	51762.0026	0.0002	0.0019	138
37	51762.0812	0.0003	0.0007	170
38	51762.1621	0.0004	0.0019	171
39	51762.2527	0.0011	0.0127	44
85	51765.9083	0.0011	−0.0017	54
86	51765.9838	0.0011	−0.0061	66

*BJD − 2400000.
†Against max = 2451759.1285 + 0.079783 E.
‡Number of points used to determine the maximum.

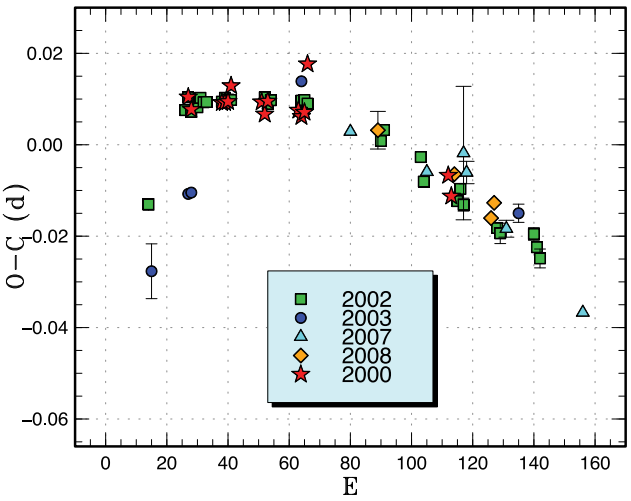

Fig. 2. Comparison of different superoutbursts of DH Aql in the $O-C$ diagram. A period of 0.08000 d was used to draw this figure. Approximate cycle counts (E) after the start of the outburst were used.

3.3 BB Arietis

This object (= NSV 907) was suspected as a dwarf nova because this suspected variable is located close to a ROSAT X-ray source (vsnet-chat 3317). In 2004, two outbursts were detected by P. Schmeer, confirming the dwarf-nova-type nature. Superhumps were detected during the second outburst (Kato et al. 2009).

On 2013 August 3, the ASAS-SN (Shappee et al. 2014a) team detected this object in outburst (vsnet-alert 16111). Although the object faded rapidly, it brightened five days later and showed superhumps, and the initial ASAS-SN detection turned out to be a precursor outburst (vsnet-alert 16169, 16170). The times of superhump maxima

Table 5. Superhump maxima of BB Ari (2013).

E	Max*	Error	$O-C^{\dagger}$	$N^{\ddagger}$
0	56514.8763	0.0030	−0.0029	17
1	56514.9473	0.0009	−0.0042	24
14	56515.8916	0.0011	−0.0001	44
26	56516.7491	0.0020	−0.0104	25
27	56516.8349	0.0004	0.0031	71
28	56516.9093	0.0004	0.0053	99
33	56517.2702	0.0007	0.0046	69
40	56517.7760	0.0045	0.0042	24
41	56517.8507	0.0007	0.0066	58
42	56517.9228	0.0004	0.0064	74
55	56518.8595	0.0003	0.0029	110
56	56518.9332	0.0005	0.0043	35
69	56519.8723	0.0006	0.0033	52
70	56519.9441	0.0008	0.0029	25
82	56520.7971	0.0068	−0.0119	37
83	56520.8779	0.0004	−0.0035	121
84	56520.9595	0.0009	0.0059	8
96	56521.8184	0.0013	−0.0031	23
97	56521.8884	0.0011	−0.0054	27
110	56522.8258	0.0012	−0.0080	24
111	56522.9022	0.0011	−0.0040	47
124	56523.8165	0.0020	−0.0297	25
137	56524.8159	0.0032	0.0296	56
138	56524.8508	0.0076	−0.0079	67
166	56526.8955	0.0029	0.0120	48

*BJD − 2400000.
†Against max = 2456514.8792 + 0.072315 E.
‡Number of points used to determine the maximum.

during the main superoutburst are listed in table 5. There was a stage B–C transition in the $O-C$ data. Although stage A superhumps were probably recorded between the precursor and the main superoutburst, we could not determine the period due to the insufficiency of observations. The present determination of superhump period confirmed the suggestion that we observed only stage C superhumps in 2004 (Kato et al. 2009)—figure 3.

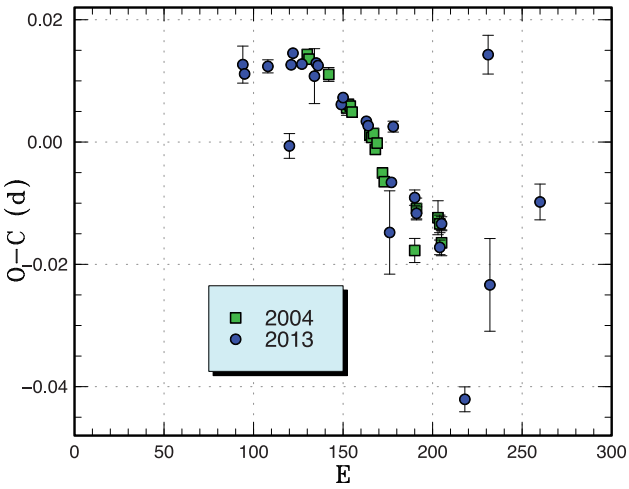

Fig. 3. Comparison of different superoutbursts of BB Ari in the $O-C$ diagram. A period of 0.07254 d was used to draw this figure. Approximate cycle counts (E) after the precursor outburst were used (2013). Since the start of the 2004 superoutburst was not well constrained, we shifted the $O-C$ diagram to best fit the 2013 one.

3.4 UZ Bootis

UZ Boo is renowned as an object of a small group of WZ Sge-type dwarf novae when this subclass was proposed (Bailey 1979b). Only a small number of outbursts were recorded: 1929 April, 1937 June, 1938 May, 1978 September (Richter 1986), 1994 August (Iida & York 1994), and 2003 December (Kato et al. 2009). Although superhumps were first recorded during the 1994 superoutburst, the period was only marginally estimated to be 0.0619 d (Kato et al. 2001a) under very unfavorable conditions. During the 2003 superoutburst, the superhump period was established as 0.06192(3) d (stage B, Kato et al. 2009) despite the unfavorable seasonal observing conditions. The presence of multiple post-superoutburst rebrightenings was suspected during the 1994 superoutburst (Kuulkers et al. 1996), although the detections of these rebrightenings were based on visual observations. It took us additional two years to establish the phenomenon of multiple post-superoutburst rebrightenings in dwarf novae (EG Cnc: cf. Osaki et al. 1997; Patterson et al. 1998; Kato et al. 2004a). During the 2003 superoutburst, UZ Boo showed four post-superoutburst rebrightenings (Kato et al. 2009) and its close resemblance to EG Cnc was highlighted.

The object was again detected in outburst on 2013 July 26 by C. Chiselbrook visually and confirmed by W. MacDonald II using a CCD. Since the object had not been detected by the same observer on July 25, the outburst appeared to be a young one. Although this outburst was supposed to provide an opportunity to detect early superhumps, no meaningful coherent period was detected (vsnet-alert 16064, 16065, 16075), partly due to the high air mass and the short visibility in the evening. Only three days after the outburst detection, likely growing ordinary superhumps were detected (vsnet-alert 16080, 16087). The duration in which early superhumps were present, if there were any, was very short when compared to other WZ Sge-type dwarf novae.

Since the comparison star was much redder than the variable and some observations were done at high air masses, we corrected observations by using the second-order atmospheric extinction whose coefficients were experimentally determined. The times of superhump maxima during the plateau phase are listed in table 6. The times of superhumps were not determined by the fitting method on 2013

Table 6. Superhump maxima of UZ Boo (2013).

E	Max*	Error	$O-C^{\dagger}$	$N^{\ddagger}$
0	56504.4170	0.0005	−0.0007	136
1	56504.4762	0.0006	−0.0034	110
5	56504.7297	0.0003	0.0020	90
15	56505.3481	0.0002	0.0004	106
16	56505.4120	0.0004	0.0024	52
21	56505.7209	0.0003	0.0013	91
26	56506.0283	0.0005	−0.0013	266
27	56506.0914	0.0009	−0.0002	171
30	56506.2797	0.0004	0.0022	127
31	56506.3391	0.0006	−0.0004	125
32	56506.4039	0.0004	0.0024	222
33	56506.4631	0.0008	−0.0004	52
37	56506.7129	0.0004	0.0014	106
38	56506.7725	0.0006	−0.0010	58
41	56506.9606	0.0039	0.0011	117
42	56507.0198	0.0002	−0.0017	424
43	56507.0811	0.0003	−0.0024	445
53	56507.7009	0.0005	−0.0026	91
54	56507.7644	0.0006	−0.0011	62
58	56508.0069	0.0024	−0.0065	93
64	56508.3879	0.0019	0.0025	25
69	56508.7038	0.0015	0.0084	84
70	56508.7620	0.0011	0.0046	88
80	56509.3604	0.0015	−0.0169	28
81	56509.4368	0.0008	−0.0025	129
83	56509.5668	0.0021	0.0035	63
84	56509.6294	0.0015	0.0041	76
85	56509.6910	0.0009	0.0038	69
86	56509.7519	0.0009	0.0026	89
95	56510.3080	0.0035	0.0007	64
96	56510.3681	0.0008	−0.0011	132
97	56510.4276	0.0013	−0.0037	61
101	56510.6821	0.0032	0.0029	55
102	56510.7407	0.0021	−0.0005	67

*BJD − 2400000.
†Against max = 2456504.4177 + 0.0619954 E.
‡Number of points used to determine the maximum.

July 29 (JD 2456503). Although the amplitudes of superhumps grew during the initial three nights and they were likely stage A superhumps, the stages were not distinct on the $O-C$ diagram. This was probably due to the shortness of stage A itself and the limited observation. We used $E \geq 15$ for determining the period in table 2 to avoid the inclusion of stage A superhumps. Using the data from BJD 2456503 to 2456506, we obtained a period of 0.06210(5) d by the PDM method. We regard it a likely period of stage A superhumps. The superhump period was almost constant during stage B and no clear transition to stage C was recorded.

After the rapid fading from the superoutburst, individual maximum times of superhumps could not be measured due to the faintness. We could, however, detect signals by the PDM method. During an observational interval between

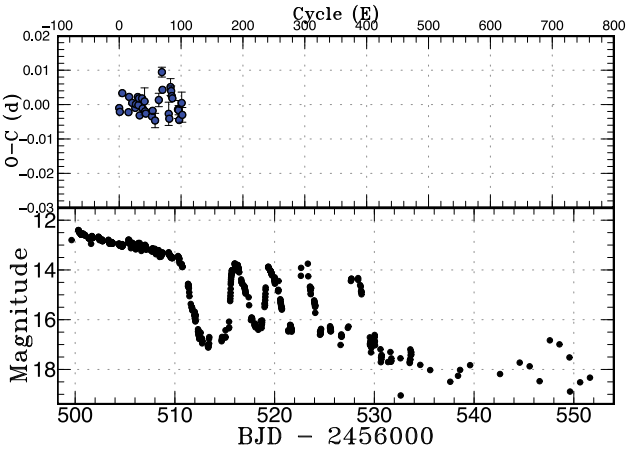

Fig. 4. $O-C$ diagram of superhumps in UZ Boo (2013). Upper: $O-C$ diagram. A period of 0.062032 d was used for drawing this figure. Lower: Light curve. The observations were binned to 0.012 d.

BJD 2456511–2456515 (the "dip" after the fading), we obtained a period of 0.0610(1) d. During the interval between BJD 2456515–2456522 (the first two rebrightenings), we detected a period of 0.06182(4) d. During the interval between BJD 2456522–2456532 (the last two rebrightenings), we detected a period of 0.06197(4) d. These periods suggest that superhumps persisted during the entire rebrightening phase.

The object underwent four post-superoutburst rebrightenings the same as in the 2003 superoutburst (figure 4). The object slightly brightened when superhumps appeared. This phenomenon is common to what was observed in objects with multiple rebrightenings—EG Cnc (Patterson et al. 1998), EZ Lyn (Kato et al. 2012b), MASTER OT J211258.65+242145.4 (Nakata et al. 2013b), and MASTER OT J203749.39+552210.3 (Nakata et al. 2013b); for a complete list, see Nakata et al. (2013b). It seems that this phenomenon is more apparent in systems with multiple rebrightenings.

The mean length of the supercycle has been updated; that is, 3170(110) d on the assumption that one superoutburst escaped detection around 1986.

3.5 V342 Camelopardalis

V342 Cam (= 1RXS J042332+745300 =HS 0417+7445) was selected as a CV from ROSAT X-ray sources (Wu et al. 2001) and from a spectroscopic survey (Aungwerojwit et al. 2006). Kato et al. (2009, 2010) reported observations of superhumps during the 2008 and 2010 superoutbursts, respectively. Shears et al. (2011b) also presented an analysis of the 2008 superoutburst and examined the outburst behavior during the period from 2005 to 2010. Shears et al. (2011b) photometrically obtained an orbital period of 0.07531(8) d.

Table 7. Superhump maxima of V342 Cam (2013).

E	Max*	Error	$O-C^{\dagger}$	$N^{\ddagger}$
0	56511.4451	0.0005	−0.0019	78
1	56511.5245	0.0005	−0.0006	72
12	56512.3914	0.0011	0.0076	70
13	56512.4645	0.0008	0.0025	78
14	56512.5410	0.0005	0.0010	70
25	56513.3975	0.0006	−0.0012	79
26	56513.4752	0.0006	−0.0016	73
27	56513.5465	0.0020	−0.0084	55
64	56516.4516	0.0022	0.0083	83
65	56516.5157	0.0016	−0.0057	83

*BJD − 2400000.
†Against max = 2456511.4471 + 0.078067 E.
‡Number of points used to determine the maximum.

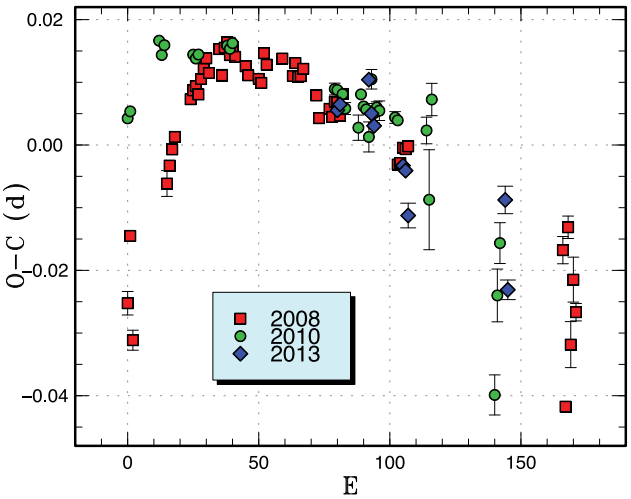

Fig. 5. Comparison of different superoutbursts of V342 Cam in the $O-C$ diagram. A period of 0.07845 d was used to draw this figure. Approximate cycle counts (E) after the start of the superoutburst were used. Since the start of the 2013 superoutburst was not well constrained, we shifted the $O-C$ diagram to best fit the others.

On 2013 August 1, ASAS-SN team detected an outburst (vsnet-alert 16096). The outburst was not young enough and only stage C superhumps were recorded (table 7). On the final night, the profile was double-humped. We show the maxima on the smooth extension of stage C superhumps in the table. A comparison of $O-C$ diagrams of different superoutbursts is shown in figure 5.

3.6 V452 Cassiopeiae

V452 Cas was discovered to be a dwarf nova (= S 10453) with a range of 14–17.5 (photographic magnitude) by Richter (1969). Bruch, Fischer, and Wilmsen (1987) also detected an outburst. Liu and Hu (2000) obtained a spectrum in quiescence and detected the Hα line in emission.

Table 8. Superhump maxima of V452 Cas (2013).

E	Max*	Error	$O-C^{\dagger}$	$N^{\ddagger}$
0	56616.2975	0.0004	−0.0086	117
23	56618.3469	0.0007	0.0031	92
24	56618.4347	0.0005	0.0023	131
25	56618.5273	0.0010	0.0063	69
91	56624.3651	0.0042	−0.0033	41
92	56624.4570	0.0029	0.0001	38

*BJD − 2400000.
†Against max = 2456616.3061 + 0.088596 E.
‡Number of points used to determine the maximum.

Although the object has been monitored visually by amateur observers since 1992, no secure outburst was detected until 1999 October 8, when P. Schmeer detected an outburst of 16.2 mag (unfiltered CCD; vsnet-alert 3561). P. Schmeer suspected that past possible visual detections were probably the close companion star rather than true outbursts. The object further brightened and attained to 15.52 mag on the next night. On 1999 November 9, P. Schmeer reported (private communication) a bright ($\sim$15.0 mag) outburst and suspected that it is a superoutburst. This bright outburst was also confirmed visually at a magnitude of 14.7–14.9 (vsnet-alert 3684). P. Schmeer suspected that this object is an SU UMa-type dwarf nova with (rather) frequent small-amplitude outbursts (vsnet-alert 3687). P. Vanmunster detected superhumps with a period of 0.0891 d (vsnet-alert 3698, 3707). Superhumps were also detected during the 2000 September outburst (vsnet-alert 5276).

Shears et al. (2009) systematically studied this object during the period from 2005 to 2008, and obtained a supercycle length of 146 ± 16 d. Shears et al. (2009) also reported superhumps during the 2007 September superoutburst. The long-period superhumps detected in the early stage were likely stage A superhumps. An analysis of the 1999 and 2008 superoutbursts was reported in Kato et al. (2009).

I. Miller detected a superoutburst on 2013 November 19 and detected a superhump (vsnet-alert 16632). The times of superhump maxima are listed in table 8. On BJD 2456624, secondary maxima of superhumps became strong. In the table, we list the maxima which are on a smooth extension of earlier times of maxima. A comparison of $O-C$ diagrams (figure 6) indicates that the evolution of superhumps during this superoutburst followed the trend previously recorded. The initial epoch probably indicated the time near the stage A–B transition. In table 2, a global $P_{\rm dot}$ in all stages is given.

Preceding superoutbursts occurred in 2013 January and June (BJD 2456305 and 2456445). Supercycles in a series of these three superoutbursts were 140 and 171 d, suggesting that the supercycle significantly varies.

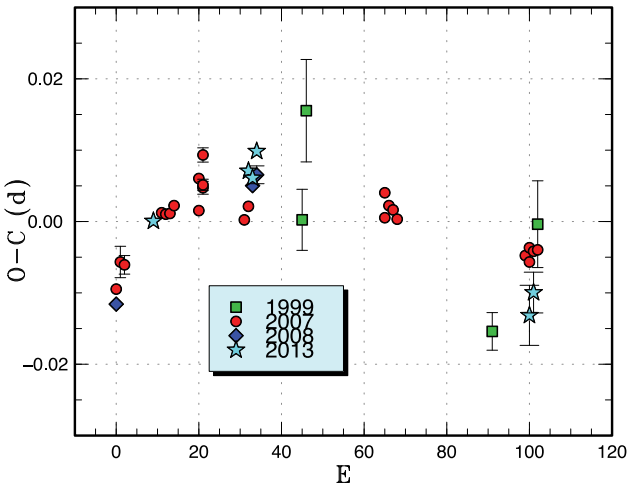

Fig. 6. Comparison of different superoutbursts of V452 Cas in the $O-C$ diagram. A period of 0.08880 d was used to draw this figure. Approximate cycle counts (E) after the start of the superoutburst were used.

3.7 V359 Centauri

V359 Cen was originally discovered to be a possible nova by A. Opolski (originally in Lwów Contr. 4; Prager & Shapley 1941). The object was visible from 1930 April 20 to 1930 April 27, and its brightness declined from 13.8 to 15.0 mag. On the assumption of a typical absolute maximum for a nova, a large distance of 160 kpc was inferred (McLaughlin 1945). McLaughlin (1945) already discussed the possibility of a dwarf nova. Duerbeck (1987) proposed a 21.0 mag quiescent counterpart. Munari and Zwitter (1998) tried to find the proposed quiescent counterpart spectroscopically, but their attempt failed due to its faintness. Gill and O'Brien (1998) could not find a nova shell in a deep image.

The second historical outburst was recorded by R. Stubbings on 1999 July 13. Woudt and Warner (2001) obtained time-resolved CCD photometry following the 1999 July outburst and detected a period of 0.0779 d. The object underwent more outbursts in 2000 May, 2001 April, and 2002 June, and the object was recognized as an SU UMa-type dwarf nova. The detection of superhumps during the 1999 and 2002 superoutbursts was reported in Kato et al. (2002d).

The 2014 superoutburst was detected by R. Stubbings (see vsnet-alert 16941). Subsequent observations detected superhumps (vsnet-alert 16946, 16948, 16952). The times of superhump maxima are listed in table 9. The observation recorded the middle and latter parts of the superoutburst. The epochs for $E \geq 97$ correspond to the rapidly fading part of the superoutburst. The times of maxima and the identification of superhumps was not secure due to faintness of the object. The two $O-C$ diagrams of the 2002 and 2014 superoutbursts agree with each other (figure 7).

Table 9. Superhump maxima of V359 Cen (2014).

E	Max*	Error	$O-C^{\dagger}$	$N^{\ddagger}$
0	56712.8358	0.0005	−0.0034	17
11	56713.7308	0.0006	0.0009	19
12	56713.8097	0.0008	−0.0011	20
23	56714.7021	0.0006	0.0007	16
24	56714.7848	0.0007	0.0025	19
36	56715.7553	0.0009	0.0014	20
37	56715.8362	0.0008	0.0013	19
48	56716.7291	0.0006	0.0037	20
49	56716.8086	0.0005	0.0021	20
60	56717.6975	0.0006	0.0004	17
61	56717.7794	0.0008	0.0014	20
73	56718.7461	0.0006	−0.0034	20
74	56718.8274	0.0006	−0.0031	20
86	56719.7978	0.0011	−0.0042	20
97	56720.6940	0.0021	0.0013	19
98	56720.7719	0.0016	−0.0017	19
99	56720.8513	0.0014	−0.0033	19
110	56721.7465	0.0053	0.0013	20
111	56721.8175	0.0032	−0.0087	20
122	56722.7259	0.0079	0.0091	15
123	56722.8006	0.0054	0.0029	16

*BJD − 2400000.
†Against max = 2456712.8393 + 0.080963 E.
‡Number of points used to determine the maximum.

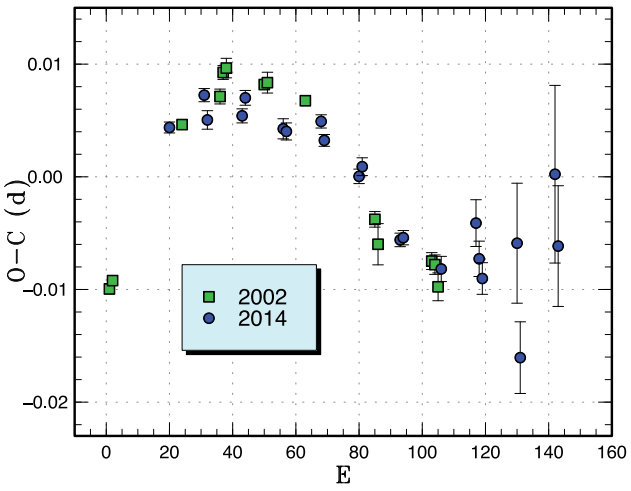

Fig. 7. Comparison of different superoutbursts of V359 Cen in the $O-C$ diagram. A period of 0.08110 d was used to draw this figure. Approximate cycle counts (E) after the start of the superoutburst were used. Since the start of the 2014 superoutburst was not well constrained, we shifted the $O-C$ diagram to best fit the 2002 one.

3.8 FZ Ceti

This object was discovered to be a variable star of unknown type (= BV 1187, NSV 601) with a range of 12.2 to fainter than 14.4 in the photographic magnitude (Avery & Sievers 1968). The object was also selected as a faint blue star

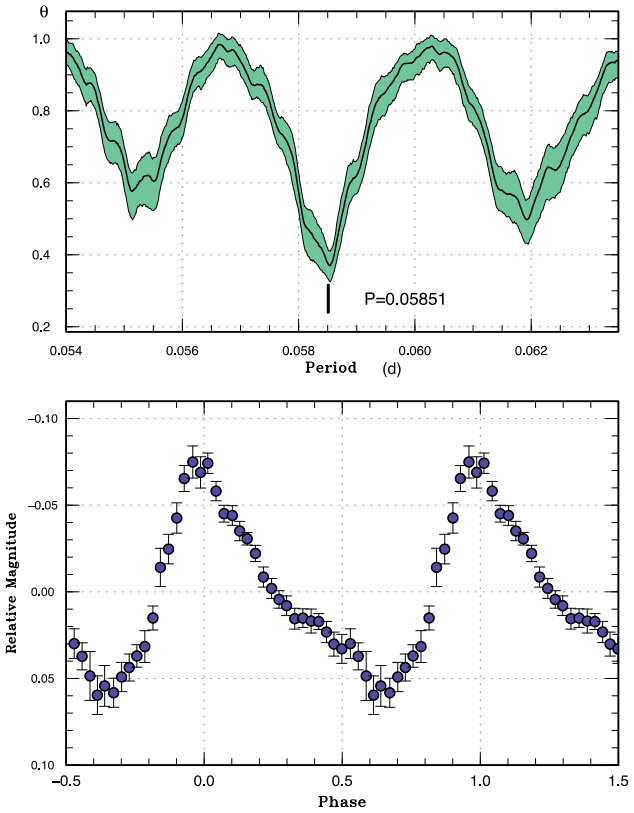

Fig. 8. Superhumps in FZ Cet (2014). Upper: PDM analysis. Lower: Phase-averaged profile.

(= PHL 3637)[5] with a photographic magnitude of 18.7 and a $(U-V)$ excess of −0.2. The identification in Demartino et al. (1996) was incorrect (Haro & Luyten 1962). S. Otero found in 2005 that this object is a dwarf nova based on ASAS-3 (Pojmański 2002) observations (vsnet-alert 8620). The ASAS-3 light curve immediately suggested that this object is an SU UMa-type dwarf nova showing superoutbursts (vsnet-alert 8621). The object was given the GCVS (General Catalogue of Variable Stars) name FZ Cet in Kazarovets et al. (2008). Despite its brightness in outburst, the two superoutbursts occurred in seasonally unfavorable conditions (2010 February and 2012 February) and their superhumps were not detected until 2014.

The 2014 outburst was detected by R. Stubbings on January 19 (vsnet-alert 16797). This outburst was in better seasonal conditions than the preceding two superoutbursts, and subsequent observations were useful for detecting superhumps (vsnet-alert 16803, 16808; figure 8). The times of superhump maxima are listed in table 10. The superoutburst lasted more than 11 d (vsnet-alert 16845).

[5] The name in the Downes CV catalog (Downes et al. 2001) is incorrect.

Table 10. Superhump maxima of FZ Cet (2014).

E	Max*	Error	$O-C$†	N‡
0	56678.0315	0.0002	0.0012	106
1	56678.0889	0.0003	0.0000	114
9	56678.5564	0.0006	−0.0008	17
17	56679.0233	0.0020	−0.0023	56
18	56679.0821	0.0003	−0.0020	107
19	56679.1463	0.0015	0.0036	33
43	56680.5482	0.0023	0.0004	12

*BJD − 2400000.
†Against max = 2456678.0303 + 0.058547 E.
‡Number of points used to determine the maximum.

Table 11. Superhump maxima of YZ Cnc (2014).

E	Max*	Error	$O-C$†	N‡
0	56678.6122	0.0016	−0.0023	23
1	56678.7048	0.0011	−0.0001	21
16	56680.0624	0.0006	0.0011	100
17	56680.1538	0.0007	0.0021	201
18	56680.2434	0.0005	0.0013	201
19	56680.3355	0.0013	0.0029	48
22	56680.6079	0.0032	0.0041	21
23	56680.6916	0.0040	−0.0026	20
27	56681.0546	0.0011	−0.0013	100
28	56681.1417	0.0011	−0.0046	101
29	56681.2380	0.0011	0.0013	99
30	56681.3224	0.0009	−0.0047	82
38	56682.0489	0.0017	−0.0016	55
39	56682.1466	0.0018	0.0056	48
41	56682.3205	0.0018	−0.0013	38

*BJD − 2400000.
†Against max = 2456678.6145 + 0.090422 E.
‡Number of points used to determine the maximum.

3.9 YZ Cancri

YZ Cnc is a well-known active SU UMa-type dwarf nova (e.g., Szkody & Mattei 1984). Although Patterson (1979) detected superhumps, the identification of the period was incorrect (Kato et al. 2009). The 2007 superoutburst was reported in Kato et al. (2009). The 2011 superoutburst was reported in Kato et al. (2014a). We reported on a superoutburst in 2014 January here. The times of superhump maxima during the main superoutburst are listed in table 11. Since we could not determine whether there was a jump in the phase (the same as in traditional late superhumps) after the fading in the main superoutburst, we listed the times of superhumps after the superoutburst separately (table 12). A comparison of the $O-C$ diagrams (figure 9) suggests that post-superoutburst superhumps in the 2014 superoutburst were indeed traditional late superhumps.

Table 12. Superhump maxima of YZ Cnc (2014) (post-superoutburst).

E	Max*	Error	$O-C^{\dagger}$	$N^{\ddagger}$
0	56684.9658	0.0015	−0.0020	68
1	56685.0488	0.0021	−0.0098	65
2	56685.1507	0.0024	0.0011	66
3	56685.2422	0.0016	0.0017	68
7	56685.6098	0.0021	0.0056	24
8	56685.6989	0.0011	0.0038	22
13	56686.1433	0.0015	−0.0064	68
14	56686.2429	0.0007	0.0023	68
18	56686.6070	0.0017	0.0027	19
19	56686.6994	0.0011	0.0042	22
45	56689.0553	0.0010	−0.0038	66
46	56689.1525	0.0015	0.0025	68
47	56689.2391	0.0012	−0.0019	67

*BJD − 2400000.
†Against max = 2456684.9678 + 0.090918 E.
‡Number of points used to determine the maximum.

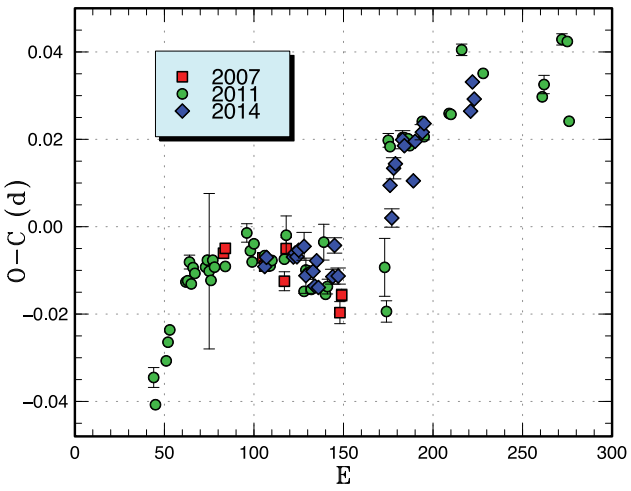

Fig. 9. Comparison of different superoutburstsof YZ Cnc in the $O-C$ diagram. A period of 0.09050 d was used to draw this figure. Approximate cycle counts (E) after the start of the superoutburst were used (in the case of YZ Cnc, this refers to the precursor outburst). Since the start of the 2014 superoutburst was not well constrained, we shifted the $O-C$ diagram to best fit the others.

3.10 GZ Cancri

GZ Cnc is a variable star (=TmzV34) discovered by K. Takamizawa. The object turned out to be an active dwarf nova (Kato et al. 2001c, 2002c). Tappert and Bianchini (2003) obtained an orbital period of 0.08825(28) d from radial velocity observations. This period indicates that GZ Cnc is located in the period gap, and it raised the interesting question whether GZ Cnc is an SU UMa-type dwarf nova. In 2010 March, a long outburst turned out to be a superoutburst (Kato et al. 2010). Another superoutburst was recorded in 2013 February (Kato et al. 2014a).

Table 13. Superhump maxima of GZ Cnc (2014).

E	Max*	Error	$O-C^{\dagger}$	$N^{\ddagger}$
0	56663.1487	0.0015	−0.0142	60
1	56663.2486	0.0003	−0.0073	181
2	56663.3478	0.0003	−0.0010	181
12	56664.2934	0.0005	0.0149	69
53	56668.1021	0.0004	0.0118	127
54	56668.1945	0.0004	0.0112	162
55	56668.2812	0.0018	0.0050	64
75	56670.1309	0.0008	−0.0048	160
79	56670.5059	0.0005	−0.0017	102
80	56670.5937	0.0008	−0.0068	76
90	56671.5261	0.0005	−0.0042	96
91	56671.6229	0.0006	−0.0002	91
92	56671.7136	0.0006	−0.0026	89

*BJD − 2400000.
†Against max = 2456663.1629 + 0.092970 E.
‡Number of points used to determine the maximum.

The 2014 January superoutburst was detected by R. Stubbings (vsnet-alert 16758). The bright magnitude immediately suggested a superoutburst. The initial observation recorded a long superhump period (vsnet-alert 16782). The times of superhump maxima are listed in table 13. The maxima $E \leq 2$ correspond to stage A superhumps (see also figures 10 and 11). A PDM analysis of this part of the data yielded a period of 0.0969(3) d (the period in vsnet-alert 16782 referred to $E \leq 12$). Due to the shortness of the run, the accuracy of this period of stage A superhumps is limited. This ε corresponds to $q = 0.30(2)$ (Kato & Osaki 2013b; see also subsection 4.2 of this paper). Although this estimate is based on a very limited observation, this observation seems to support that this object has a mass ratio near the borderline of the condition for the 3:1 resonance (q range of 0.25–0.33 depending on simulations). The object is indeed likely a "borderline" SU UMa-type dwarf nova.

3.11 AL Comae Berenices

AL Com has been one of the most renowned high-amplitude dwarf novae since its discovery in 1962 by L. Rosino (Bertola 1964). Szkody (1987) showed a large amplitude variation with a period of ∼40 min and suggested that AL Com may belong to either DQ Her-type magnetic systems or AM CVn-type double degenerate systems. Further spectroscopic observations by Mukai et al. (1990) precluded any possibility of the latter system. More extensive photometry by Abbott et al. (1992) showed two distinct periodicities of 41 min and 87–90 min; the latter was suggested to be the orbital period, and the former the rotation period of the white dwarf. From these periods, Abbott et al. (1992) concluded that AL Com bears the properties of

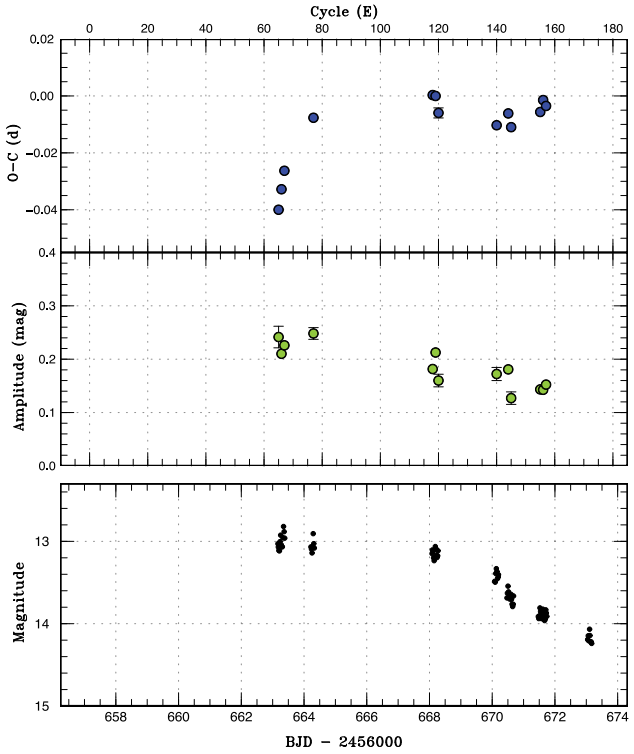

Fig. 10. $O-C$ diagram of superhumps in GZ Cnc (2014). Upper: $O-C$ diagram. A period of 0.09270 d was used for drawing this figure. Approximate cycle counts (E) after the start of the superoutburst were used. Middle: Amplitudes of the superhumps. Lower: Light curve. The observations were binned to 0.019 d.

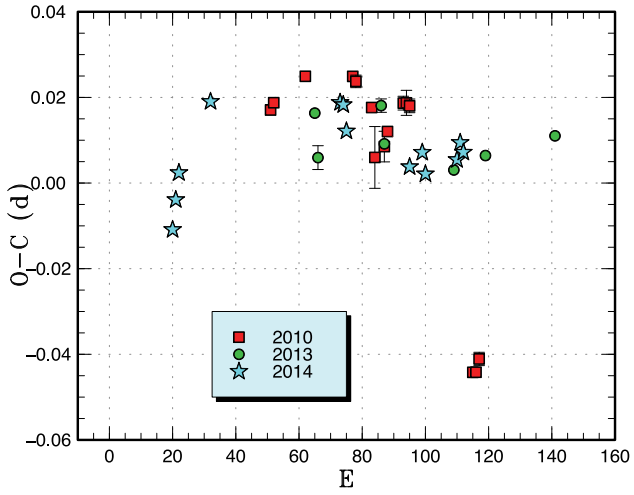

Fig. 11. Comparison of different superoutbursts of GZ Cnc in the $O-C$ diagram. A period of 0.09290 d was used to draw this figure. Approximate cycle counts (E) after the start of the superoutburst were used.

both an enigmatic dwarf nova WZ Sge and a unique intermediate polar EX Hya. The 1995 superoutburst clarified that this object is a WZ Sge-type dwarf nova, and it shows double-wave modulations (now called early superhumps) during the early stage of the superoutburst (Kato et al. 1996b). Based on the outburst light curve and the orbital

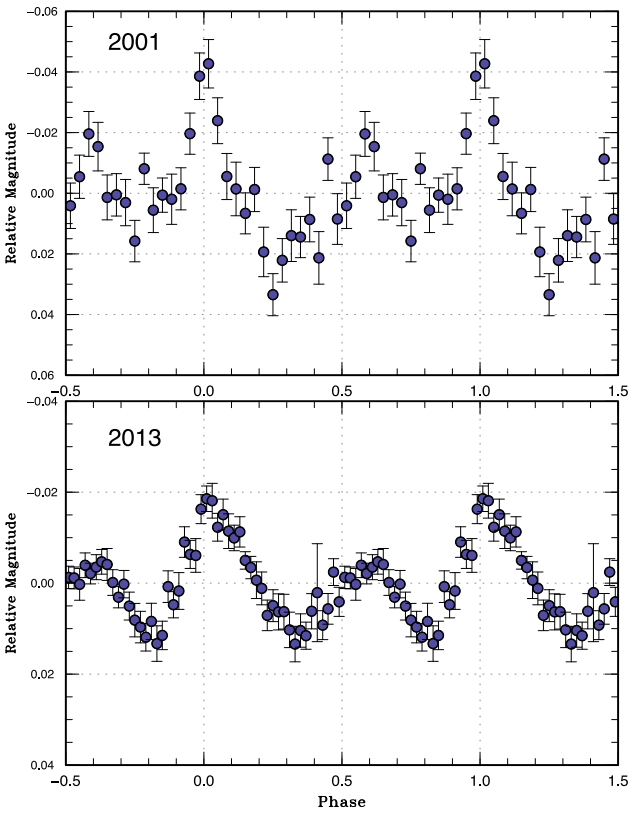

Fig. 12. Comparison in early superhumps of AL Com between 2001 and 2013.

parameters, AL Com was considered as a "twin" of WZ Sge. This superoutburst was particularly well documented (Patterson et al. 1996; Howell et al. 1996; Nogami et al. 1997).

Another superoutburst was recorded in 2001 (Ishioka et al. 2002). A less-observed superoutburst in 2007 indicated that the post-superoutburst rebrightenings are different between different superoutbursts (Uemura et al. 2008). There was an outburst in 2003 detected in SDSS, which was missed by visual observers.

The 2013 superoutburst was detected on December 6 by C. Gualdoni (cvnet-outburst 5738). Subsequent observations detected early superhumps (vsnet-alert 16695, 16712). The evolution of superhumps in the early stage was well observed (vsnet-alert 16718, 16724).

The period of early superhumps was found to be 0.056660(8) d by the PDM method from the observations before BJD 2456639.5. This value is in complete agreement with the 2001 measurement of early superhumps (figure 12; see subsection 4.4). The commonly accepted mechanism of early superhumps (cf. Osaki & Meyer 2002) suggests that the phases of early superhumps are constant in different superoutbursts (which is defined by the orientation of the observer against the binary's orbit). Assuming that the phases of early superhumps are the same during the

Table 14. Superhump maxima of AL Com (2013).

E	Max*	Error	$O-C^{\dagger}$	$N^{\ddagger}$
0	56639.5761	0.0015	−0.0141	92
1	56639.6341	0.0010	−0.0135	93
2	56639.6924	0.0006	−0.0126	95
12	56640.2813	0.0004	0.0018	70
13	56640.3382	0.0003	0.0013	50
17	56640.5715	0.0005	0.0049	73
18	56640.6271	0.0006	0.0030	89
19	56640.6910	0.0004	0.0094	80
87	56644.5997	0.0004	0.0122	28
88	56644.6527	0.0008	0.0077	19
104	56645.5709	0.0003	0.0068	24
105	56645.6283	0.0005	0.0069	26
106	56645.6877	0.0016	0.0088	12
116	56646.2574	0.0006	0.0041	50
158	56648.6687	0.0006	0.0028	72
159	56648.7228	0.0006	−0.0005	67
169	56649.2882	0.0010	−0.0095	90
170	56649.3523	0.0043	−0.0028	77
174	56649.5823	0.0005	−0.0026	29
175	56649.6354	0.0007	−0.0070	28
208	56651.5372	0.0033	−0.0007	26
209	56651.5924	0.0029	−0.0030	52
210	56651.6493	0.0012	−0.0035	73

*BJD − 2400000.
†Against max = 2456639.5902 + 0.057441 E.
‡Number of points used to determine the maximum.

Table 15. Superhump maxima of AL Com (2013) (post-superoutburst).

E	Max*	Error	$O-C^{\dagger}$	$N^{\ddagger}$
0	56655.3022	0.0011	0.0006	42
1	56655.3520	0.0021	−0.0070	39
40	56657.5992	0.0030	0.0023	65
41	56657.6493	0.0059	−0.0049	71
94	56660.6941	0.0083	−0.0014	28
104	56661.2776	0.0015	0.0083	59
138	56663.2230	0.0017	0.0028	16
155	56664.1963	0.0031	0.0007	55
156	56664.2582	0.0010	0.0051	60
157	56664.3123	0.0012	0.0018	60
158	56664.3666	0.0009	−0.0012	59
215	56667.6371	0.0023	−0.0014	58
244	56669.3019	0.0032	−0.0007	41
314	56673.3144	0.0044	−0.0048	30

*BJD − 2400000.
†Against max = 2456655.3017 + 0.057381 E.
‡Number of points used to determine the maximum.

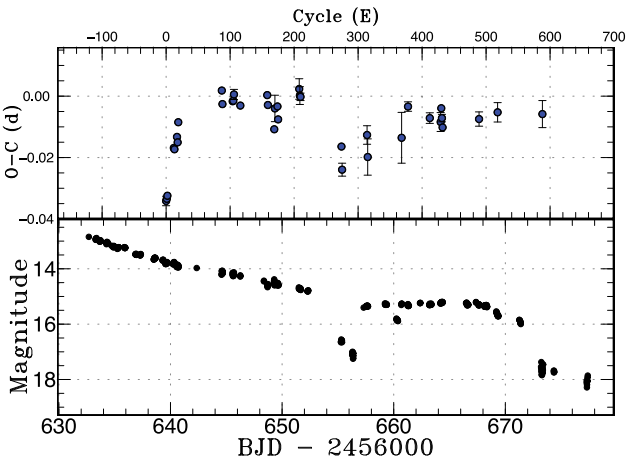

Fig. 13. $O-C$ diagram of superhumps in AL Com (2013). Upper: $O-C$ diagram. A period of 0.05733 d was used for drawing this figure. Lower: Light curve. The observations were binned to 0.011 d.

1995, 2001, and 2013 superoutbursts, we can determine the orbital period. A refined orbital period of 0.056668589(9) d are well fitted to all the observations. An alias by one cycle is 0.056667180(9) d and is not favored if we believe the identification of the period by Patterson et al. (1996).

The times of superhump maxima during the plateau phase of the superoutburst are listed in table 14. Stage A superhumps were better detected during the 2013 superoutburst than during the previous ones. The 2013 superoutburst showed a positive $P_{\rm dot}$ of $+4.9(19) \times 10^{-5}$. This value is larger than the 1995 and 2001 measurements. A comparison of $O-C$ diagrams of different superoutbursts is presented in figure 14.

The times of superhump maxima after the rapid fading are listed in table 15. A PDM analysis of the combined data in this interval yielded a period of 0.057393(10) d. Although the overall $O-C$ diagram (figure 13) suggests the presence of a phase jump around the dip, the later times of superhump maxima appear to be on a smooth extension line of stage B superhumps.

A comparison of light curves of different superoutbursts is shown in figure 15. All superoutbursts (except the poorly observed 2007 one) showed a dip and a plateau-type rebrightening. The second (rebrightening) plateau after the dip was almost flat in the 1995 superoutburst, and it was associated with an initial small dip in the 2013. The 2007 superoutburst was more structured, as reported in Uemura et al. (2008), but it is still unlike discrete rebrightenings such as EG Cnc showed (Patterson et al. 1998; Kato et al. 2004a). We consider that the 2007 superoutburst resembled the 2001 superoutburst of WZ Sge, though with small brightenings with amplitudes less than 1 mag. Although the duration of the rebrightening plateau in the 2001 superoutburst appears longer than those in other superoutbursts, this part of the observation was of low quality and it needs to be interpreted carefully. A variation in the rebrightening was also observed in EZ Lyn (Kato et al. 2012b) and suspected in WZ Sge (Patterson et al. 1981). Although there

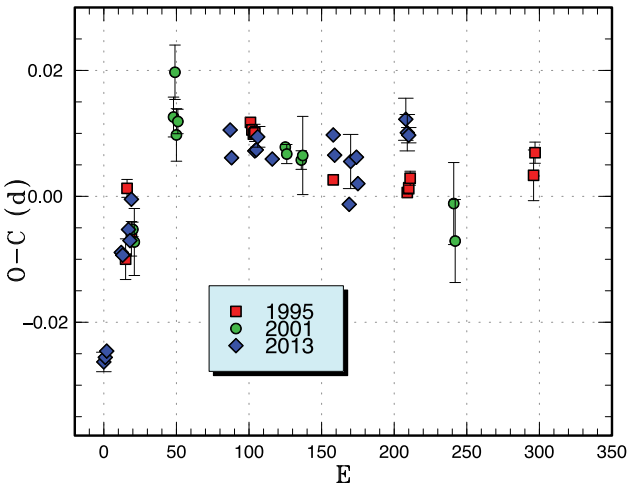

Fig. 14. Comparison of different superoutbursts of AL Com in the $O-C$ diagram. A period of 0.05732 d was used to draw this figure. Approximate cycle counts (E) after the emergence of the superhump were used. Assuming that the stage A in 2013 was best observed, the 1995 and 2001 $O-C$ diagrams were shifted within 20 cycles to best match the stage A–B transition in 2013.

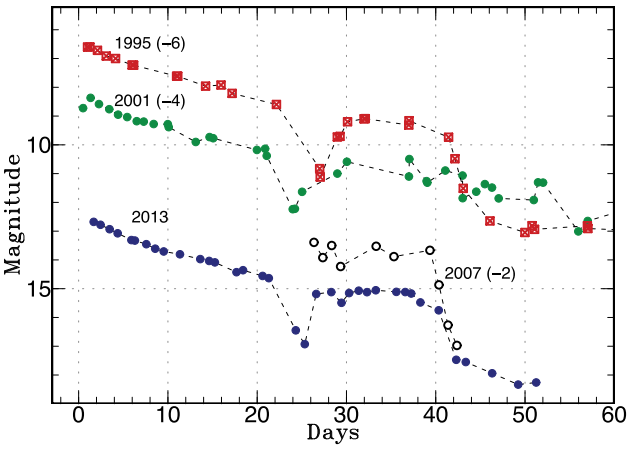

Fig. 15. Comparison of superoutbursts of AL Com. The data were binned to 1 d and shifted in magnitude. The dashed lines are added to make the variation easier to recognize. The data for the 2007 superoutburst were from Uemura et al. (2008).

is a subtle difference between patterns of rebrightening in the same object, the present comparison of the light curves in AL Com suggests that the pattern of rebrightening is generally reproducible.

The known outbursts of AL Com are listed in table 16. The supercycle appears to be 6–7 yr. Since the 2003 outburst escaped detection under visual observer's observations, the true frequency of normal outbursts may be higher than what this table suggests.

3.12 V503 Cygni

This SU UMa-type dwarf nova is notable for its unusually short (89 d) supercycle and the occasional presence of negative superhumps (Harvey et al. 1995). Kato, Ishioka, and Uemura (2002a) reported on a dramatic variation in the number of normal outbursts, and this finding led to the discovery of the state with negative superhumps suppressing the number of normal outbursts (Ohshima et al. 2012; Zemko et al. 2013; Osaki & Kato 2013a, 2013b).

The superoutburst in 2013 August was observed only for two nights during its final part. We obtained maxima of BJD 2456527.4717(11) ($N=88$), 2456527.5580(27) ($N=47$), 2456532.3896(20) ($N=67$), and 2456532.4696(13) ($N=63$). Since the phases of the last two maxima are different from the earlier ones by a phase of ~ 0.5, they may be traditional late superhumps.

3.13 IX Draconis

IX Dra was selected as an ultraviolet-excess object (= KUV 18126+6704) by Noguchi, Maehara, and Kondo (1980). Noguchi, Yutani, and Maehara (1982) detected its variability. Wegner and McMahan (1988) spectroscopically classified the object as a B subdwarf. Liu et al. (1999) classified the object as a dwarf nova by spectroscopy. Klose (1995) detected the variability of this object on photographic plates and obtained a period of ~ 45.7 d, although it was not strictly periodic. T. Vanmunster detected superhumps in 2000 (vsnet-alert 5368, 5369). Ishioka et al. (2001) studied this object and revealed that it is a new ER UMa-type dwarf nova with a supercycle of 53 d. Olech et al. (2004) studied the 2003 superoutburst and suggested a period of 0.06646(6) d, which they considered to be an orbital period. This period led to a very small fractional superhump excess, from which Olech et al. (2004) suggested that IX Dra is a period bouncer. Otulakowska-Hypka et al. (2013) further studied this object and found a longer supercycle. Otulakowska-Hypka et al. (2013) discussed the secular increase of supercycles in ER UMa-type dwarf novae. The identification of the orbital period, however, was less convincing the same as in Olech et al. (2004), and there is a possibility of another period which places IX Dra in a region of ordinary dwarf nova before the period minimum. Kato et al. (2013b) did not regard the orbital period by Otulakowska-Hypka et al. (2013) as a true orbital one based on a close similarity of IX Dra to ER UMa.

We analyzed the superoutburst in 2012 July–August. The times of superhump maxima are listed in table 17. The resultant $O-C$ data indicate that the superhumps can be expressed by a single period without a strong period variation. Such a phase reversal as can be seen in ER UMa (Kato et al. 1996a) was not apparent. Olech et al. (2004) also reported on only small period variations. Although Kato et al. (2009) recognized stages B and C in the data

Table 16. Outbursts of AL Com.

Date*	Maximum†	Type	References
1892 April 26	14.3p	—	Bertola (1964)
1941 June 25	13.8p	—	Lucchetti and Usher (1972)
1961 November 17–December 20	13.8p	super	Rosino (1961); Bertola (1964)
1965 March 26–27	13.4p	super	Zwicky (1965); Bertola (1965)
1974 April 19–20	14.1v	normal?	AAVSO
1975 March 16–June 29	12.8v	super (two outbursts?)	AAVSO
1995 April 5–May 19	12.4v	super	Patterson et al. (1996); Nogami et al. (1997)
2001 May 18–June 9?	12.6v	super	Ishioka et al. (2002)
2003 January 28	15.5g	normal	SDSS
2007 November 6–24‡	15.4v	super	Uemura et al. (2008)
2013 December 6–2014 January 15	12.7v	super	this work

*For modern data, the end date refers to the end of the (second) plateau phase.
†p: photographic, v: visual, g: green in the SDSS system.
‡Rebrightening part only.

Table 17. Superhump maxima of IX Dra (2012).

E	Max*	Error	$O-C$†	N‡
0	56130.7403	0.0003	−0.0017	58
1	56130.8082	0.0003	−0.0007	56
25	56132.4161	0.0003	0.0002	126
26	56132.4832	0.0003	0.0003	144
27	56132.5466	0.0003	−0.0032	144
28	56132.6215	0.0019	0.0047	45
40	56133.4199	0.0005	−0.0003	75
54	56134.3624	0.0109	0.0048	24
55	56134.4228	0.0006	−0.0018	70
56	56134.4939	0.0005	0.0024	75
57	56134.5590	0.0008	0.0005	75
58	56134.6268	0.0019	0.0013	58
59	56134.6898	0.0016	−0.0026	44
70	56135.4323	0.0019	0.0034	75
71	56135.4944	0.0006	−0.0015	66
105	56137.7717	0.0017	−0.0006	66
106	56137.8364	0.0011	−0.0029	68
107	56137.9039	0.0013	−0.0023	68
121	56138.8408	0.0011	−0.0028	88
130	56139.4364	0.0008	−0.0098	70
131	56139.5149	0.0024	0.0017	75
145	56140.4481	0.0012	−0.0025	61
146	56140.5307	0.0032	0.0132	59

*BJD − 2400000.
†Against max = 2456130.7420 + 0.066955 E.
‡Number of points used to determine the maximum.

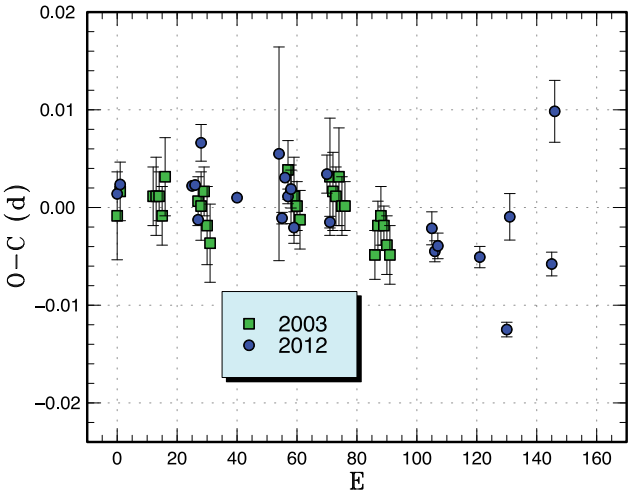

Fig. 16. Comparison of different superoutbursts of IX Dra in the $O-C$ diagram. A period of 0.06700 d was used to draw this figure. Approximate cycle counts (E) after the start of the observation were used. The starts of the superoutbursts were not well constrained.

of Olech et al. (2004), the present data did not show any strong sign of a stage transition (see also figure 16).

3.14 MN Draconis

This object is an SU UMa-type dwarf nova in the period gap (Antipin & Pavlenko 2002; Nogami et al. 2003). It is well-known that this object showed negative superhumps in quiescence (Pavlenko et al. 2010; Samsonov et al. 2010).

The 2012 July–August superoutburst was observed from the growing stage of superhumps. The times of superhump maxima are listed in table 18. Although the individual times of maxima were not well determined before $E = 10$, the $O-C$ diagram suggests that the interval $E \leq 39$ was stage A (figure 17). A PDM analysis of this segment yielded a period of 0.10993(9) d.

The 2013 November superoutburst (vsnet-alert 16611) was observed for eight nights. The times of superhump maxima are listed in table 19. A large variation of period was detected. Up to $E = 18$, the amplitudes of superhumps grew, and stage A superhumps were most likely recorded (figure 18). Although we identified the following phase as stage B, the identification for $E = 95$ is uncertain due to

Table 18. Superhump maxima of MN Dra (2012).

E	Max*	Error	$O-C^{\dagger}$	$N^{\ddagger}$
0	56130.3597	0.0048	−0.0239	42
1	56130.4483	0.0030	−0.0420	80
2	56130.5274	0.0017	−0.0696	56
10	56131.4246	0.0026	−0.0261	80
36	56134.2857	0.0011	0.0608	30
38	56134.4995	0.0006	0.0612	28
46	56135.3539	0.0015	0.0619	28
47	56135.4674	0.0012	0.0688	27
94	56140.4101	0.0017	−0.0035	27
95	56140.5155	0.0027	−0.0049	21
112	56142.3134	0.0042	−0.0209	32
113	56142.4136	0.0036	−0.0274	30
114	56142.5133	0.0045	−0.0344	28

*BJD − 2400000.

†Against max = 2456130.3836 + 0.106703 E.

‡Number of points used to determine the maximum.

Table 19. Superhump maxima of MN Dra (2013).

E	Max*	Error	$O-C^{\dagger}$	$N^{\ddagger}$
0	56602.2479	0.0011	−0.0287	114
1	56602.3594	0.0010	−0.0231	116
9	56603.2248	0.0004	−0.0042	198
10	56603.3341	0.0014	−0.0007	90
18	56604.1967	0.0019	0.0154	13
26	56605.0438	0.0088	0.0159	99
27	56605.1550	0.0034	0.0213	166
28	56605.2595	0.0015	0.0200	20
46	56607.1492	0.0011	0.0051	64
47	56607.2544	0.0006	0.0044	106
48	56607.3611	0.0007	0.0053	131
57	56608.3064	0.0037	−0.0018	59
66	56609.2469	0.0012	−0.0136	95
95	56612.3137	0.0043	−0.0153	37

*BJD − 2400000.

†Against max = 2456602.2767 + 0.105815 E.

‡Number of points used to determine the maximum.

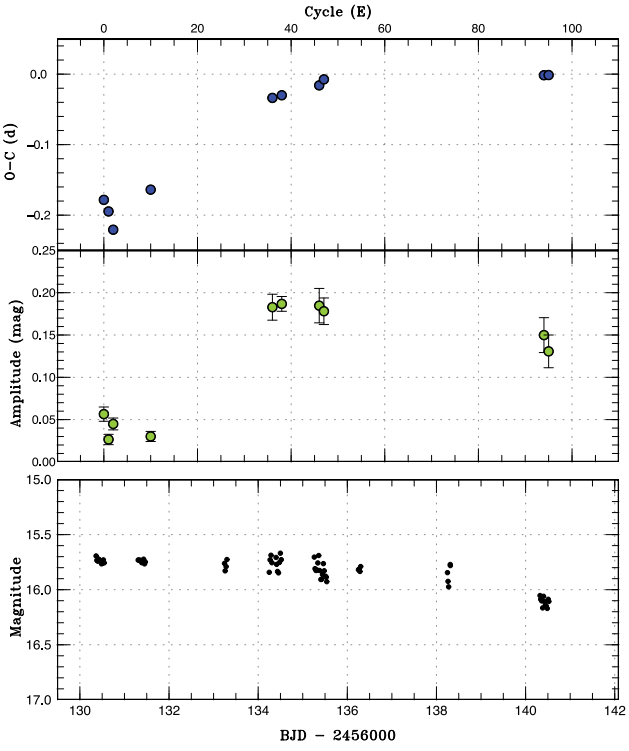

Fig. 17. $O-C$ diagram of superhumps in MN Dra (2012). Upper: $O-C$ diagram. A period of 0.10504 d was used for drawing this figure. Cycle counts (E) after the start of the observation were used. Middle: Amplitudes of the superhumps. Lower: Light curve. The observations were binned to 0.021 d.

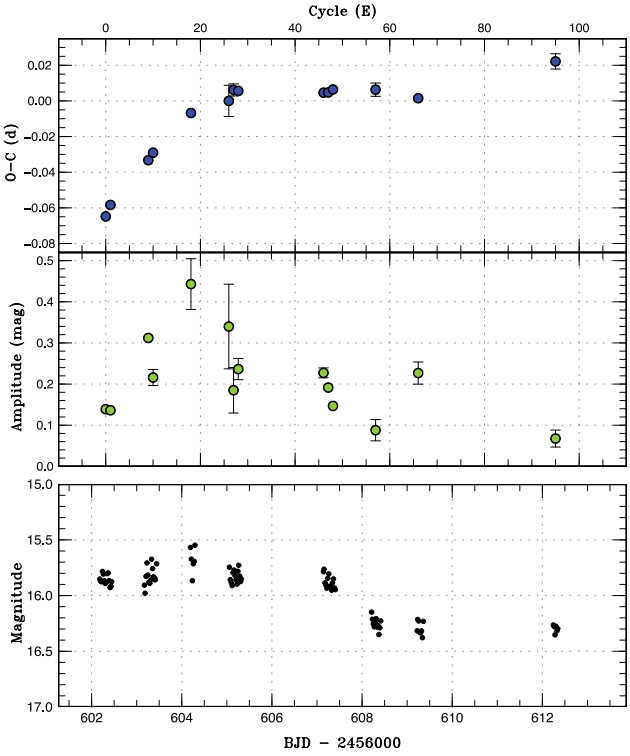

Fig. 18. $O-C$ diagram of superhumps in MN Dra (2013). Upper: $O-C$ diagram. A period of 0.10504 d was used for drawing this figure. Cycle counts (E) after the start of the observation were used. Middle: Amplitudes of the superhumps. Lower: Light curve. The observations were binned to 0.021 d.

the lower quality of the data. In table 2, we list the period derived from the data between $26 \leq E \leq 66$.

Assuming that the orbital period is 0.0998(2) d (Pavlenko et al. 2010), the values of ε^* for stage A superhumps are 0.092(1) for 2012 which corresponds to $q = 0.327(5)$ and 0.078(1) for 2013 to $q = 0.258(5)$. Since both observations were not ideal (due to lack of well-measured maxima for the 2012 observation and to lack of data for the early stage of the 2013), we simply take an average of these two values to obtain $q = 0.29(5)$. A comparison of $O-C$ diagrams of different superoutbursts (figure 19) suggests that the large negative $P_{\rm dot}$ in the 2002b

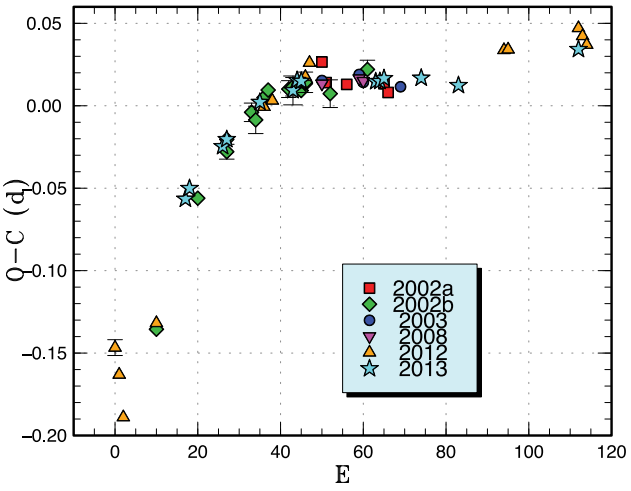

Fig. 19. Comparison of different superoutbursts of MN Dra in the $O-C$ diagram. A period of 0.1050 d was used to draw this figure. Approximate cycle counts (E) after the start of the outburst were used (2012). Since the start of the other superoutbursts was not well constrained, we shifted the $O-C$ diagrams to best fit the 2012 one.

superoutburst reported in Nogami et al. (2003) and Kato et al. (2009) reflected stage A–B transition.

3.15 CP Eridani

CP Eri was discovered to be a faint blue variable showing an outburst (Luyten & Haro 1959). Szkody et al. (1989) obtained a time-series of photometry in quiescence and detected sporadic variations of 0.2–0.4 mag without clear periodicity. Howell et al. (1991) observed this object again in quiescence and detected modulations with a period of 28.6–29.5 min. Due to its shortness, Howell et al. (1991) considered this period to be the spin period of the magnetic white dwarf. Abbott et al. (1992) obtained a time-series of higher quality photometry and identified a period of 1724(4) s (28.6 min). Furthermore, Abbott et al. (1992) obtained spectra in both high and low states, and revealed that this object lacks hydrogen lines. The helium lines were in emission in a low state and in absorption in a high state, and this behavior was very similar to that of CR Boo (Wood et al. 1987). Abbott et al. (1992) concluded that CP Eri is an interacting binary white dwarf (IBWD, or AM CVn-type star). Patterson et al. (1993), however, suggested that this photometric period is the superhump period since most AM CVn-type stars show superhumps. Zwitter and Munari (1995) obtained a spectrum with a featureless blue continuum.

Although this object was discovered to be an outbursting one, its outburst behavior was not clarified for a long time. Although J. Patterson (cba-info message on 1998 January 1) reported an outburst of 16.5 mag and its 0.2 mag superhumps, the result was published only in Armstrong, Patterson, and Kemp (2012). Since 2003, B. Monard regularly monitored this object and detected several outbursts between 16.0 and 17.5 mag. More recently, CRTS data suggested a cycle length of ~ 100 d (Kato et al. 2012b). Ramsay et al. (2012) presented the result of long-term monitoring of AM CVn-type stars and detected three outbursts in CP Eri. The duration of the outbursts was 15 d and the outburst duty cycle was 27%. Judging from the duration, these outbursts were likely superoutbursts.

Armstrong, Patterson, and Kemp (2012), following the interpretation in Patterson et al. (1993), identified the orbital and superhump periods from the 1998 data. According to this interpretation, the orbital modulation of 1701.4(2) s doubly humped.

On 2013 October 3, the ASAS-SN team detected an outburst of CP Eri (vsnet-alert 16501). Subsequent observations recorded its superhumps (vsnet-alert 16510, 16515). This outbursting state near the peak was observed for three nights (the outburst lasted at least 5 d including the ASAS-SN detection) and followed by a dip (vsnet-alert 16526). After the dip, the superhump signal at first became weaker, but then became detectable again (vsnet-alert 16530, 16537). The later part of the outburst consisted of oscillations as reported in Armstrong, Patterson, and Kemp (2012).

The times of superhump maxima during the initial peak are listed in table 20. A positive $P_{\rm dot}$ of $+3.1(9) \times 10^{-5}$ was for the first time recorded in CP Eri. Superhumps after the dip had a shorter period—0.019752(4) d by the PDM method. The times of maxima of these superhumps are listed in table 21. The interpretation of these superhumps (whether they are the same superhumps as in the initial peak or "traditional" late superhumps) is not clear. It was, however, likely that these superhumps were excited again after the dip phenomenon. The combined $O-C$ diagram (figure 20) may suggest that the phase of the superhumps was continuous if the superhump period continued to increase the same as in stage B of hydrogen-rich dwarf novae.

3.16 V1239 Herculis

This object (SDSS J170213.26+322954.1) is an eclipsing SU UMa-type dwarf nova in the period gap (Boyd et al. 2006; Littlefair et al. 2006). The 2005 and 2011 superoutbursts were reported in Boyd, Oksanen, and Henden (2006) and Kato et al. (2009) and in Kato et al. (2013b), respectively. On 2013 September 26, another outburst was reported (vsnet-alert 16462; also vsnet-alert 16464). Although this outburst was probably a superoutburst, only a single-night observation covering an eclipse was reported.

Table 20. Superhump maxima of CP Eri (2013).

E	Max*	Error	$O-C^{\dagger}$	$N^{\ddagger}$
0	56570.6649	0.0008	−0.0001	14
1	56570.6854	0.0003	0.0005	19
2	56570.7060	0.0002	0.0012	19
3	56570.7253	0.0003	0.0006	19
4	56570.7452	0.0003	0.0006	19
5	56570.7649	0.0003	0.0004	19
6	56570.7841	0.0003	−0.0003	15
7	56570.8050	0.0003	0.0007	38
8	56570.8250	0.0003	0.0008	40
9	56570.8439	0.0006	−0.0002	24
10	56570.8640	0.0005	−0.0000	21
11	56570.8836	0.0012	−0.0002	21
12	56570.9029	0.0005	−0.0009	21
13	56570.9217	0.0006	−0.0019	21
14	56570.9446	0.0006	0.0010	20
15	56570.9634	0.0004	−0.0001	21
56	56571.7790	0.0006	−0.0003	15
57	56571.7999	0.0005	0.0008	15
58	56571.8186	0.0010	−0.0005	14
59	56571.8378	0.0011	−0.0012	15
60	56571.8587	0.0005	−0.0001	19
61	56571.8780	0.0004	−0.0008	32
62	56571.8975	0.0005	−0.0011	19
63	56571.9172	0.0004	−0.0013	14
64	56571.9380	0.0006	−0.0004	14
65	56571.9584	0.0013	0.0001	14
66	56571.9779	0.0008	−0.0003	11
103	56572.7142	0.0004	−0.0002	19
104	56572.7344	0.0004	0.0001	20
105	56572.7540	0.0005	−0.0002	20
106	56572.7750	0.0004	0.0009	18
107	56572.7948	0.0004	0.0008	20
108	56572.8139	0.0004	0.0000	19
109	56572.8340	0.0003	0.0002	20
110	56572.8547	0.0003	0.0011	19
111	56572.8737	0.0008	0.0002	17

*BJD − 2400000.
†Against max = 2456570.6650 + 0.019897 E.
‡Number of points used to determine the maximum.

Table 21. Superhump maxima of CP Eri (2013) (after the dip).

E	Max*	Error	$O-C^{\dagger}$	$N^{\ddagger}$
0	56576.7433	0.0018	0.0013	19
1	56576.7615	0.0011	−0.0003	18
2	56576.7835	0.0030	0.0019	18
3	56576.7996	0.0006	−0.0017	20
4	56576.8203	0.0007	−0.0007	19
5	56576.8401	0.0006	−0.0007	19
6	56576.8609	0.0005	0.0003	20
7	56576.8804	0.0008	0.0001	19
51	56577.7487	0.0026	−0.0009	10
52	56577.7670	0.0010	−0.0024	16
53	56577.7869	0.0006	−0.0022	20
54	56577.8047	0.0011	−0.0042	20
102	56578.7619	0.0013	0.0047	17
103	56578.7822	0.0011	0.0052	19
104	56578.8009	0.0024	0.0042	19
203	56580.7519	0.0007	−0.0007	17
206	56580.8114	0.0009	−0.0006	19
207	56580.8308	0.0004	−0.0009	19
208	56580.8489	0.0007	−0.0025	19
209	56580.8715	0.0018	0.0003	19

*BJD − 2400000.
†Against max = 2456576.7420 + 0.019757 E.
‡Number of points used to determine the maximum.

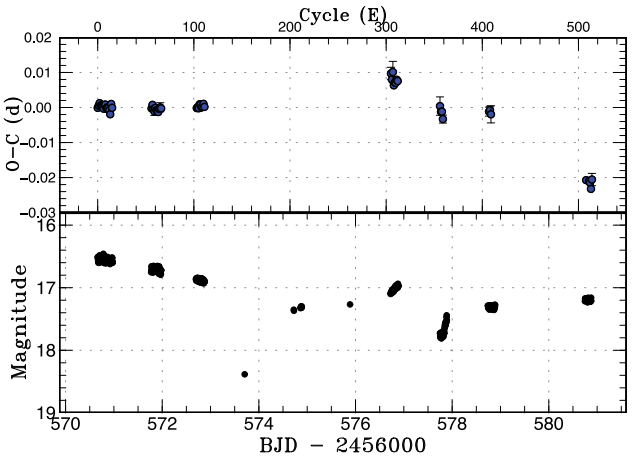

Fig. 20. $O-C$ diagram of superhumps in CP Eri (2013). Upper: $O-C$ diagram. A period of 0.019897 d was used for drawing this figure. Lower: Light curve. The observations were binned to 0.004 d.

By using these observations, we refined an ephemeris of

$$\mathrm{Min(BJD)} = 2453648.23651(1) + 0.1000822137(7)E \quad (1)$$

using the Markov-chain Monte Carlo (MCMC) modeling introduced in Kato et al. (2013b). This ephemeris supersedes the one reported in Kato et al. (2013b) which was determined by the traditional minimum finding method.

3.17 CT Hydrae

CT Hya was discovered to be a dwarf nova (= AN 114.1936) with a photographic range of 14.5 to fainter than 16.5 by Hoffmeister (1936). Hoffmeister (1936) recorded four outbursts during the period from 1929 to 1934. The finding chart was published in Hoffmeister (1957). Vogt and Bateson (1982) presented a photographic chart and identified the quiescent counterpart. The first secure outburst since the discovery was reported on 1995 February 22 from CCD observations by M. Iida (VSOLJ). Iida observed the object on the subsequent night and detected variations compatible with superhumps. The

Table 22. Superhump maxima of CT Hya (2014).

E	Max*	Error	$O-C^{\dagger}$	$N^{\ddagger}$
0	56708.1208	0.0004	0.0024	134
1	56708.1860	0.0004	0.0015	133
2	56708.2468	0.0012	−0.0039	123
45	56711.0947	0.0011	−0.0017	28
46	56711.1644	0.0007	0.0018	38

*BJD − 2400000.
†Against max = 2456708.1184 + 0.066178 E.
‡Number of points used to determine the maximum.

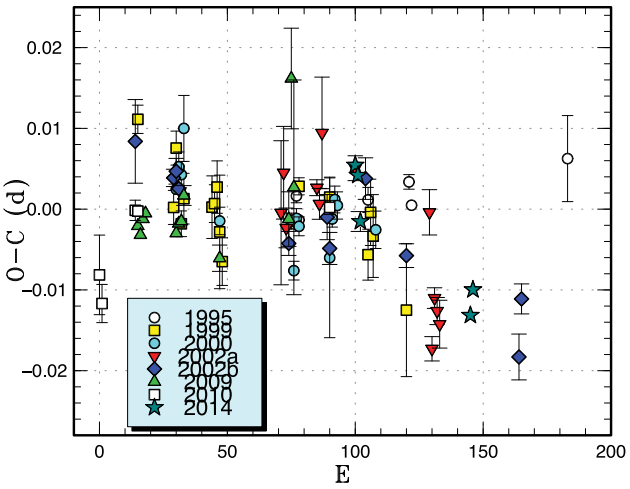

Fig. 21. Comparison of different superoutbursts of CT Hya in the $O-C$ diagram. A period of 0.06650 d was used to draw this figure. Approximate cycle counts (E) after the maximum of the superoutburst were used. This figure is updated from the corresponding one in Kato et al. (2010), and includes the 1995 and 2014 observations. Since the start of the 2014 superoutburst was not well constrained, we shifted the $O-C$ diagram to best fit the others. The shift value for the 2002a superoutburst was corrected.

same outburst was observed by Nogami, Kato, and Hirata (1996), who reported on the detection of superhumps. In Kato et al. (2009), superoutbursts in 1999, 2000, 2002 (two superoutbursts), and 2009 were reported. In Kato et al. (2010), another superoutburst in 2010 was reported.

The 2014 superoutburst was detected by CRTS (see vsnet-alert 16926) and observations on two nights were obtained. The times of superhump maxima are listed in table 22. The observation probably detected stage C superhumps (see figure 21).

3.18 VW Hydri

We observed the 2012 November–December superoutburst of this famous SU UMa-type dwarf nova. By using the 2011–2012 data, we have determined that the orbital period is 0.0742705(1) d and that the mean epoch of the maximum is BJD 2456116.7250(1). Combined these values

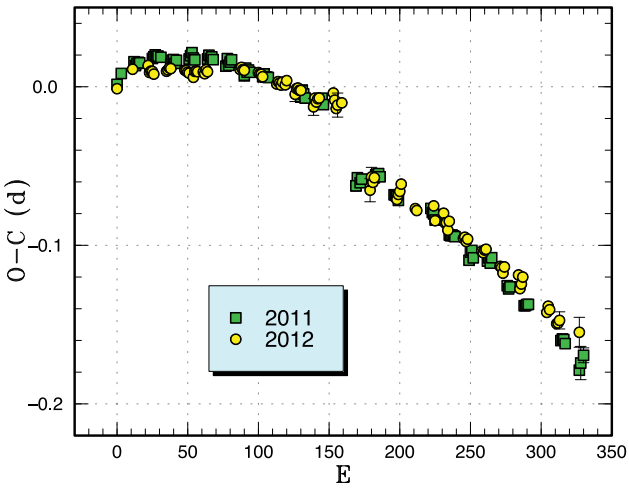

Fig. 22. Comparison of different superoutbursts of VW Hyi in the $O-C$ diagram. A period of 0.076914 d was used to draw this figure. Approximate cycle counts (E) after the maximum of the superoutburst were used.

with the ephemeris of Vogt (1974), we have obtained an updated ephemeris of

$$\mathrm{Max(BJD)} = 2456116.7250(1) + 0.074271061(4)E. \quad (2)$$

The times of superhump maxima during the superoutburst plateau are listed in table 23. Although the evolution of superhumps was similar to that in 2011 (Kato et al. 2013b), stage A superhumps were not well observed in the 2012 superoutburst. The precursor was not as apparent as that in the 2011 superoutburst. During the rapidly fading phase from the superoutburst, an ∼0.5 phase jump was observed the same as in 2011. These superhumps can be interpreted as "traditional" late superhumps. The times of these post-superoutburst superhumps were determined after the subtraction of the mean orbital profile (table 24).

A comparison between the 2011 (Kato et al. 2013b) and 2012 superoutbursts in the $O-C$ diagram shows a slight difference in the curvature of the $O-C$ diagram during the superoutburst plateau. Although the times of post-superoutburst superhumps in the 2012 superoutburst were given only before the next normal outburst, the signal remained detectable for ∼40 d after the termination of the superoutburst by the PDM method. The resultant periods in 5 d intervals are listed in table 25.

The detection of negative superhumps in this object is discussed in subsection 4.8.

3.19 WX Hydri

WX Hyi was originally discovered to be a variable star (= AN 9.1932) with a magnitude range of 10.7 to 14.2 (photographic scale at that time) by Luyten (1932).

Table 23. Superhump maxima of VW Hyi (2012).

E	Max*	Error	$O-C^{\dagger}$	$N^{\ddagger}$
0	56254.8352	0.0012	−0.0172	14
11	56255.6936	0.0022	−0.0034	21
22	56256.5420	0.0019	0.0005	22
23	56256.6145	0.0007	−0.0037	31
24	56256.6923	0.0004	−0.0028	29
25	56256.7690	0.0004	−0.0028	31
26	56256.8442	0.0017	−0.0044	11
35	56257.5382	0.0005	−0.0013	29
36	56257.6160	0.0005	−0.0003	31
37	56257.6942	0.0005	0.0011	28
38	56257.7707	0.0004	0.0008	31
48	56258.5388	0.0006	0.0012	29
49	56258.6154	0.0006	0.0011	31
50	56258.6913	0.0006	0.0001	28
51	56258.7676	0.0004	−0.0003	31
54	56258.9958	0.0007	−0.0025	97
55	56259.0764	0.0003	0.0014	163
56	56259.1536	0.0003	0.0018	167
57	56259.2301	0.0003	0.0015	170
61	56259.5375	0.0013	0.0019	20
62	56259.6134	0.0009	0.0010	22
63	56259.6928	0.0007	0.0036	21
64	56259.7685	0.0009	0.0025	31
87	56261.5389	0.0010	0.0071	23
88	56261.6171	0.0009	0.0086	23
89	56261.6927	0.0010	0.0073	22
90	56261.7691	0.0008	0.0070	31
100	56262.5368	0.0011	0.0069	23
101	56262.6130	0.0010	0.0063	25
102	56262.6896	0.0008	0.0061	25
103	56262.7649	0.0007	0.0047	36
113	56263.5295	0.0014	0.0015	19
114	56263.6079	0.0010	0.0032	25
115	56263.6839	0.0009	0.0024	24
116	56263.7595	0.0006	0.0012	37
117	56263.8383	0.0024	0.0033	14
119	56263.9904	0.0004	0.0018	127
120	56264.0700	0.0005	0.0047	145
126	56264.5229	0.0046	−0.0031	16
127	56264.6034	0.0010	0.0007	25
128	56264.6806	0.0010	0.0011	24
129	56264.7561	0.0008	−0.0002	38
130	56264.8330	0.0023	−0.0001	17
139	56265.5148	0.0053	−0.0093	15
140	56265.5973	0.0013	−0.0036	25
141	56265.6717	0.0009	−0.0059	25
142	56265.7507	0.0009	−0.0037	37
143	56265.8280	0.0025	−0.0031	22
153	56266.6003	0.0032	0.0013	25
154	56266.6727	0.0018	−0.0030	24
155	56266.7443	0.0015	−0.0081	37
156	56266.8234	0.0078	−0.0059	25
158	56266.9779	0.0100	−0.0049	68
159	56267.0557	0.0011	−0.0039	70

*BJD − 2400000.
†Against max = 2456254.8524 + 0.076774 E.
‡Number of points used to determine the maximum.

Hoffmeister (1949) classified the object as a Mira-type variable (also Kukarkin et al. 1969). Philip (1971) noted its blue color, rapid light variations, and an emission-line spectrum on a low-dispersion objective-prism plate. Kukarkin (1971) suggested that the variable is either a dwarf nova or symbiotic object, not a Mira such as was originally proposed. Fisher et al. (1971) communicated *UBV* and visual observations giving a range (visual and *V*) of 11.5–14.73. The blue color and variation were incompatible with the Mira-type variable. This object has been recognized as a dwarf nova. Splittgerber (1971) also reported on the detection of two outbursts.

Amateur observers (particularly Royal Astronomical Society of New Zealand members) started visual observations in 1971 April. Bateson (1976) suggested the SU UMa-type dwarf nova based on the presence of superoutbursts detected by visual observations. Walker, Marino, and Freeth (1976) reported on the detection of superhumps by photoelectric photometry. The reported period was 0.0783 d based on the two nights' observation. Walker, Marino, and Freeth (1976) also reported on a period of 0.0749 d, and suggested it is the orbital period. Sanduleak (1976) reported on a spectrum showing Balmer lines in emission, which is typical for a dwarf nova. Bailey (1979a) reported on high-speed photometry both in superoutburst and in quiescence. Using observations on four successive nights in 1977 December, Bailey (1979a) derived a superhump period of 0.07737 d. This observation corresponded to the middle part of the superoutburst. In contrast to Walker, Marino, and Freeth (1976), Bailey (1979a) could not detect orbital modulations in quiescence (also J. Bailey 1979 unpublished; see Schoembs & Vogt 1981). Schoembs and Vogt (1981) obtained high time-resolution spectroscopy and determined that the orbital period is 0.0748134(2) d. Pretorius, Warner, and Woudt (2006) reported on the detection of quasi-periodic oscillations (QPOs) in quiescence.

Identifying this object as a dwarf nova led to a suggestion that some SU UMa-type dwarf novae could be misclassified as Mira-type variables (Vogt 1980). DH Aql (Tsesevich 1969; Nogami & Kato 1995), SY Cap (Kato et al. 2009), and FQ Mon (vsnet-chat 3063, 3066; Kato et al. 2009) are indeed such objects. Despite the fact that WX Hyi is a well-known SU UMa-type dwarf nova, the listed set of literature

Table 24. Superhump maxima of VW Hyi (2012) (post-superoutburst).

E	Max*	Error	$O-C^{\dagger}$	$N^{\ddagger}$
0	56268.5388	0.0073	−0.0124	17
1	56268.6241	0.0061	−0.0033	25
2	56268.6976	0.0011	−0.0061	30
3	56268.7775	0.0014	−0.0025	37
19	56269.9944	0.0009	−0.0054	113
20	56270.0744	0.0006	−0.0016	162
21	56270.1533	0.0006	0.0010	164
22	56270.2348	0.0009	0.0062	170
32	56270.9885	0.0004	−0.0025	115
33	56271.0642	0.0006	−0.0030	108
45	56271.9901	0.0006	0.0080	110
46	56272.0576	0.0004	−0.0007	128
52	56272.5238	0.0019	0.0080	15
53	56272.5946	0.0010	0.0026	25
54	56272.6717	0.0013	0.0034	26
55	56272.7439	0.0012	−0.0006	36
56	56272.8264	0.0011	0.0056	21
66	56273.5848	0.0007	0.0016	25
67	56273.6624	0.0007	0.0030	25
68	56273.7367	0.0006	0.0010	37
69	56273.8150	0.0008	0.0031	28
79	56274.5765	0.0016	0.0022	25
80	56274.6526	0.0018	0.0020	24
81	56274.7311	0.0009	0.0043	37
82	56274.8085	0.0015	0.0055	33
92	56275.5669	0.0018	0.0014	25
93	56275.6431	0.0020	0.0013	25
94	56275.7164	0.0010	−0.0015	38
95	56275.7973	0.0013	0.0031	36
105	56276.5613	0.0020	0.0047	15
106	56276.6296	0.0009	−0.0033	23
107	56276.7094	0.0009	0.0003	37
108	56276.7908	0.0011	0.0054	37
125	56278.0760	0.0006	−0.0055	163
126	56278.1569	0.0007	−0.0009	170
127	56278.2315	0.0008	−0.0025	164
132	56278.6073	0.0027	−0.0079	25
133	56278.6847	0.0024	−0.0068	22
134	56278.7632	0.0054	−0.0045	20
148	56279.8325	0.0094	−0.0026	22

*BJD − 2400000.
†Against max = 2456268.5512 + 0.076242 E.
‡Number of points used to determine the maximum.

Table 25. Post-superoutburst superhumps in VW Hyi (2012).

JD*−2400000	Period (d)	Error (d)	Amplitude (mag)
56270–56275	0.07623	0.00001	0.33
56275–56280	0.07584	0.00004	0.36
56280–56285	0.07732	0.00011	0.08
56285–56290	0.07615	0.00014	0.13
56290–56295	0.07600	0.00005	0.15
56295–56300	0.07586	0.00005	0.07
56300–56305	—	—	—
56305–56310	0.07712	0.00013	0.08

*Julian day number.

Table 26. Superhump maxima of WX Hyi (2014).

E	Max*	Error	$O-C^{\dagger}$	$N^{\ddagger}$
0	56687.5605	0.0006	−0.0035	47
13	56688.5721	0.0014	0.0007	28
39	56690.5876	0.0012	0.0012	19
52	56691.5978	0.0016	0.0039	13
90	56694.5404	0.0010	0.0015	21
103	56695.5425	0.0050	−0.0039	21

*BJD − 2400000.
†Against max = 2456687.5640 + 0.077499 E.
‡Number of points used to determine the maximum.

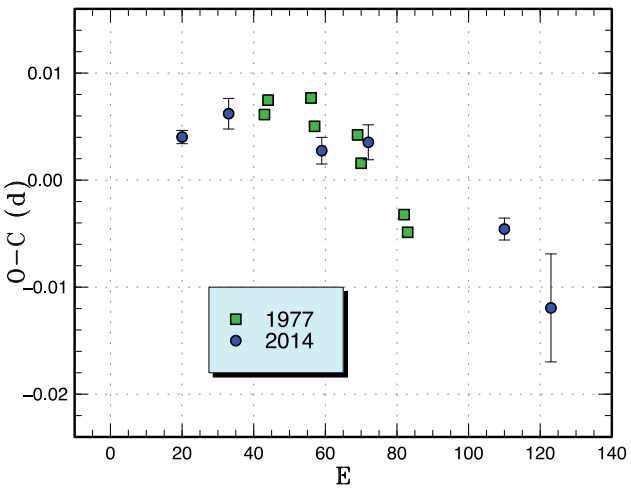

Fig. 23. Comparison of different superoutbursts of WX Hyi in the $O-C$ diagram. A period of 0.07765 d was used to draw this figure. Approximate cycle counts (E) after the maximum of the superoutburst were used.

was probably the last published observation of superhumps before this paper.

Our 2014 January–February observation started after the detection of a bright outburst on January 27 by S. Hovell and R. Stubbings (the start of the outburst was on January 25). From the observations on January 30 fully grown superhumps were detected and the subsequent evolution was observed (vsnet-alert 16851, 16868, 16904). The times of superhump maxima are listed in table 26, which includes post-superoutburst observations.

A comparison of $O-C$ diagrams (figure 23) suggests that Schoembs and Vogt (1981) recorded stage B superhumps on the first two nights and stage C superhumps on the last two nights (since both superoutbursts began with a precursor, we used the maximum which was easier to

Table 27. Superhump maxima of AY Lyr (2013).

E	Max*	Error	$O-C^{\dagger}$	$N^{\ddagger}$
0	56533.0467	0.0007	−0.0000	84
1	56533.1221	0.0005	−0.0007	79
2	56533.1996	0.0008	0.0008	55
14	56534.1116	0.0006	−0.0001	39

*BJD − 2400000.
†Against max = 2456533.0467 + 0.076064 E.
‡Number of points used to determine the maximum.

define). The resultant period of stage B is in agreement with the value of Walker, Marino, and Freeth (1976), who reported on an early part of the superoutburst. We list the periods estimated from this interpretation in table 2.

3.20 AY Lyrae

Observations of this well-known SU UMa-type dwarf nova were performed on only two nights in 2013 August. The times of superhump maxima are listed in table 27.

3.21 AO Octantis

Due to the large outburst amplitude (7.5 mag) listed in Kholopov et al. (1985), this object has long been considered as a candidate for a WZ Sge-type dwarf nova (Downes 1990; Howell & Szkody 1990; O'Donoghue et al. 1991; Kato et al. 2001a). Although Howell et al. (1991) observed this object in quiescence, no orbital modulation was detected. Mason and Howell (2003) obtained a spectrum in quiescence, which was typical of dwarf novae with a low mass-transfer rate but not so extreme as a WZ Sge-type dwarf nova. Patterson et al. (2003) observed the 2000 September outburst and obtained a superhump period of 0.06716(13) d and an orbital period of 0.06557(13) d. Woudt, Warner, and Pretorius (2004) obtained time-resolved photometry in quiescence and detected an orbital modulation with a period of 0.065345(15) d. The presence of the orbital modulation appears to be consistent with the relatively broad emission lines in Mason and Howell (2003).

The 2013 superoutburst of AO Oct was detected by R. Stubbings (vsnet-alert 16376). From subsequent observations superhumps were detected (vsnet-alert 16388, 16396, 16411; figure 24). The times of superhump maxima are listed in table 28. Stages B and C were clearly present. A large $P_{\rm dot}$ of $+19(6) \times 10^{-5}$ for stage B superhumps is typical for this $P_{\rm orb}$.

According to Woudt, Warner, and Pretorius (2004), the maximum magnitude of 13.5 in Kholopov et al. (1985) was probably a typographical error of 15.3 based on the discovery paper (von Gessner & Meinunger 1974). The

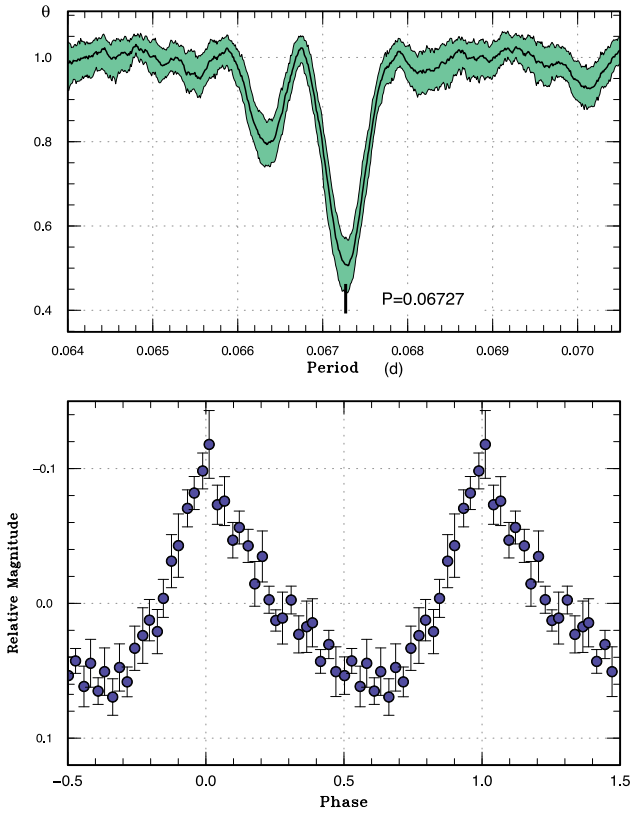

Fig. 24. Superhumps in AO Oct (2013). Upper: PDM analysis. Lower: Phase-averaged profile.

Table 28. Superhump maxima of AO Oct (2013).

E	Max*	Error	$O-C^{\dagger}$	$N^{\ddagger}$
0	56545.5712	0.0006	0.0003	29
1	56545.6371	0.0007	−0.0011	12
2	56545.7043	0.0021	−0.0011	9
3	56545.7744	0.0016	0.0017	8
14	56546.5113	0.0009	−0.0011	22
15	56546.5781	0.0011	−0.0015	28
16	56546.6466	0.0012	−0.0002	15
17	56546.7126	0.0009	−0.0015	15
29	56547.5202	0.0011	−0.0007	26
45	56548.5933	0.0066	−0.0035	10
46	56548.6664	0.0014	0.0024	13
59	56549.5480	0.0011	0.0099	27
75	56550.6161	0.0012	0.0022	25
76	56550.6872	0.0032	0.0061	12
89	56551.5518	0.0020	−0.0035	27
90	56551.6183	0.0052	−0.0043	12
91	56551.6855	0.0019	−0.0042	14

*BJD − 2400000.
†Against max = 2456545.5710 + 0.067240 E.
‡Number of points used to determine the maximum.

Table 29. Superhump maxima of DT Oct (2014).

E	Max*	Error	$O-C$†	N‡
0	56696.7567	0.0008	−0.0020	83
54	56700.7787	0.0006	0.0031	119
65	56701.5969	0.0037	0.0031	35
66	56701.6714	0.0007	0.0032	66
67	56701.7412	0.0006	−0.0014	80
68	56701.8170	0.0014	0.0000	63
81	56702.7779	0.0011	−0.0061	70

*BJD − 2400000.
†Against max = 2456696.7587 + 0.074386 E.
‡Number of points used to determine the maximum.

object, however, has been detected to be as bright as 14.2 (visual magnitude) in outbursts several times. The true range of variability can be regarded as 14.2–20.9, where the minimum magnitude is taken from Woudt, Warner, and Pretorius (2004). Considering the supercycle of ∼300 d, this outburst amplitude is indeed slightly too large for this intermediate length of supercycle. Although TV Crv was reported to have similar parameters (cf. table 1 in Nogami et al. 1997), the maximum magnitude of TV Crv was probably overestimated, since recent magnitudes of superoutbursts only reach 13.0. AO Oct apparently deserves further study for its rather unusual outburst parameters.

3.22 DT Octantis

This object was discovered to be a variable star (= BV 966) with a large amplitude (11.2 to fainter than 15.0 in photographic magnitudes: Knigge & Bauernfeind 1967). Kato et al. (2002c) noticed the identification with a bright ROSAT source and suggested that this object is a cataclysmic variable. Kato et al. (2002c) detected multiple outbursts upon this suggestion. Although Kato et al. (2002c) initially suggested that these may be outbursts in an intermediate polar, Kato et al. (2004c) detected superhumps during the 2003 January outburst. DT Oct was thus recognized as an SU UMa-type dwarf nova. Kato et al. (2009) further studied another superoutburst in 2003 November and a superoutburst in 2008.

The 2014 superoutburst was detected by R. Stubbings (cf. vsnet-alert 16892) and the latter part of the superoutburst was observed. The times of superhump maxima are listed in table 29. The data mostly covered stage C superhumps (figure 25).

Using the near-quiescent data in 2013 (by A. Oksanen, BJD 2456380–2456445), we have obtained a possible orbital signal of 0.072707(5) d with a mean amplitude of 0.16 mag. This period is adopted in table 2. The ε^*value for stage A superhumps—0.050(2)—in 2003 (Kato et al. 2009) corresponds to $q = 0.147(7)$.

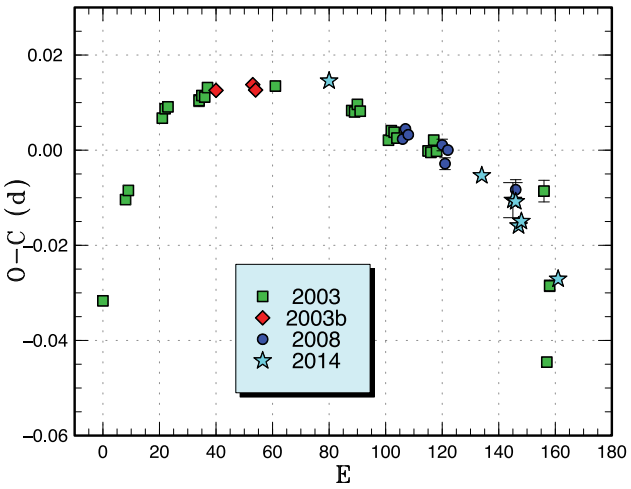

Fig. 25. Comparison of different superoutbursts of DT Oct in the $O-C$ diagram. A period of 0.07485 d was used to draw this figure. Approximate cycle counts (E) after the start of the superoutburst were used. Since the start of the 2014 superoutburst was not well constrained, we shifted the $O-C$ diagram to best fit the others.

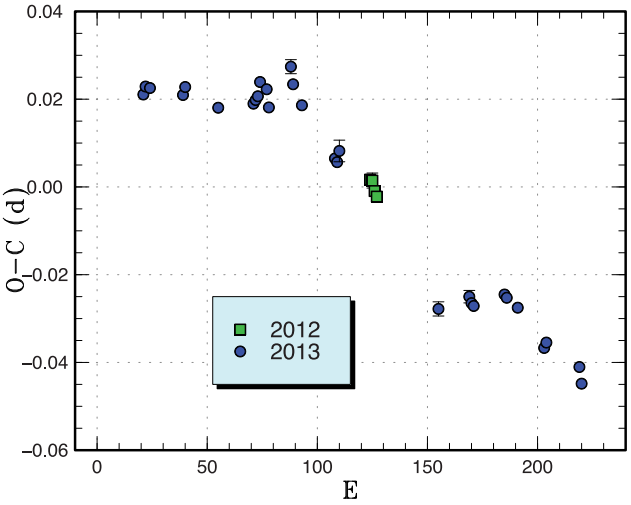

Fig. 26. Comparison of different superoutbursts of V521 Peg in the $O-C$ diagram. A period of 0.06150 d was used to draw this figure. Approximate cycle counts (E) after the start of the superoutburst were used.

3.23 V521 Pegasi

This object (= HS 2219+1824) is a dwarf nova which was reported in Rodríguez-Gil et al. (2005). Although Rodríguez-Gil et al. (2005) reported on the detection of superhumps and a likely orbital modulation, subsequent superoutbursts occurred in seasonally unsuitable conditions, and it was only in 2012 when we succeeded in obtaining the superhump period (Kato et al. 2014a).

The 2013 superoutburst was detected by the ASAS-SN team (vsnet-alert 16093). K. Wenzel also reported on the outburst detection before the ASAS-SN detection. From subsequent observations superhumps were detected (vsnet-alert 16121, 16129, 16134). After rapidly fading from the

Table 30. Superhump maxima of V521 Peg (2013).

E	Max*	Error	$O-C^{\dagger}$	$N^{\ddagger}$
0	56507.0874	0.0009	−0.0139	44
1	56507.1507	0.0006	−0.0118	66
3	56507.2734	0.0005	−0.0114	63
18	56508.1942	0.0007	−0.0074	70
19	56508.2575	0.0007	−0.0052	67
34	56509.1753	0.0006	−0.0043	40
50	56510.1601	0.0004	0.0026	91
51	56510.2223	0.0008	0.0037	86
52	56510.2848	0.0005	0.0050	96
53	56510.3497	0.0011	0.0088	41
56	56510.5325	0.0007	0.0082	66
57	56510.5899	0.0012	0.0045	28
67	56511.2146	0.0016	0.0179	63
68	56511.2718	0.0009	0.0140	62
72	56511.5129	0.0003	0.0106	47
87	56512.4234	0.0008	0.0042	52
88	56512.4840	0.0015	0.0037	159
89	56512.5469	0.0030	0.0055	211
134	56515.2792	0.0016	−0.0128	123
148	56516.1433	0.0014	−0.0044	113
149	56516.2033	0.0009	−0.0055	230
150	56516.2645	0.0012	−0.0054	226
164	56517.1278	0.0006	0.0021	80
165	56517.1885	0.0008	0.0017	128
170	56517.4937	0.0004	0.0013	54
182	56518.2226	0.0006	−0.0034	82
183	56518.2853	0.0006	−0.0018	125
198	56519.2022	0.0011	−0.0017	126
199	56519.2599	0.0012	−0.0051	120

*BJD − 2400000.
†Against max = 2456507.1013 + 0.061124 E.
‡Number of points used to determine the maximum.

Table 31. Superhump maxima of TY Psc (2013).

E	Max*	Error	$O-C^{\dagger}$	$N^{\ddagger}$
0	56635.0415	0.0006	−0.0012	91
1	56635.1110	0.0004	−0.0023	130
2	56635.1812	0.0005	−0.0027	109
27	56636.9499	0.0012	0.0018	25
28	56637.0230	0.0012	0.0043	46
29	56637.0924	0.0006	0.0031	63
30	56637.1630	0.0009	0.0032	47
55	56638.9234	0.0016	−0.0007	52
56	56638.9920	0.0008	−0.0026	52
57	56639.0622	0.0008	−0.0029	101

*BJD − 2400000.
†Against max = 2456635.0428 + 0.070569 E.
‡Number of points used to determine the maximum.

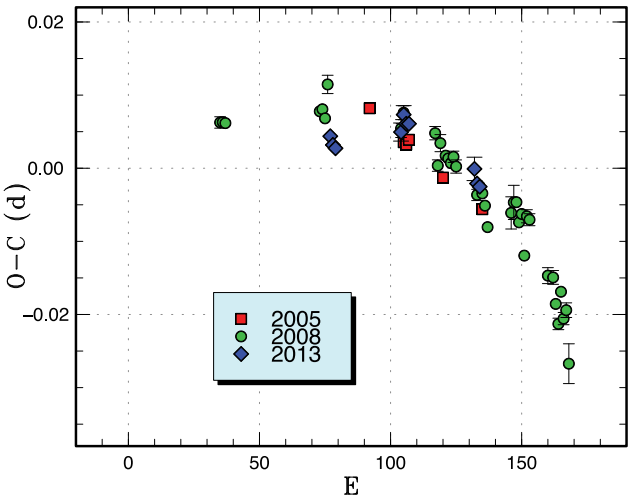

Fig. 27. Comparison of different superoutbursts of TY Psc in the $O-C$ diagram. A period of 0.07066 d was used to draw this figure. Approximate cycle counts (E) after the start of the superoutburst were used. Since the start of the 2013 superoutburst was not well constrained, we shifted the $O-C$ diagram to best fit the others.

superoutburst, the object continued to show superhumps (vsnet-alert 16146, 16149, 16166, 16186). The times of superhumps are listed in table 30, which includes post-superoutburst observations. Stages B and C were observed. During the phase of rapid fading, the superhump profile became doubly humped. The maxima which are on the smooth extension of the rest of the data were selected in the table.

A comparison of the $O-C$ diagram (figure 26) clarified that the 2012 observation covered stage C superhumps, rather than the stage B superhump identified in Kato et al. (2014a).

3.24 TY Piscium

Although the SU UMa-type nature of TY Psc has long been known, the information in the literature was very limited (Szkody & Feinswog 1988; Kunjaya et al. 2001). Kato et al. (2009) was the first to precisely determine the superhump period during the 2005 and 2008 superoutbursts. Thorstensen et al. (1996) determined the orbital period by a radial velocity study.

The 2013 December superoutburst was detected by Kyoto and Kiso Wide-field Survey (KWS; vsnet-alert 16682) and was observed for three nights. The times of superhump maxima are listed in table 31. From the observation stage B–C transition was apparently detected. This identification is confirmed by a comparison of $O-C$ diagrams (figure 27). Also note that the figure in Kato et al. (2009), based on the period of stage C superhumps rather than that of stage B superhumps, may give the reader a different impression from figure 27.

3.25 V893 Scorpii

V893 Sco was discovered to be a variable star (= SVS 1772) by Satyvoldiev (1972). Since this object is located in the region of the Scorpius T1 association, Satyvoldiev (1982) classified this object as a rapid irregular variable of InSF type (object normally in faint states with occasional brightenings up to 3 mag) according to the classification scheme by Filin and Satyvoldiev (1975). This classification corresponded to "RWF" type (RW Aur type in Tsesevich & Dragomiretskaia 1973). Around this time, the RW Aur type or "In" type (irregular, nebular; see Kholopov et al. 1985) referred to pre-main sequence variables. It is apparent that Satyvoldiev (1982) considered this variable as a pre-main sequence variable. In Kholopov et al. (1985), however, the object was reclassified as a dwarf nova, probably based on the published light curve.

The finding chart in this discovery article was interchanged with that of a different star, and this bright dwarf nova remained virtually "lost" for a long time (cf. Downes et al. 1997). The light curves presented in Filin and Satyvoldiev (1975) and Satyvoldiev (1982) were, however, so characteristic of a dwarf nova (and at least two outbursts may be attributed to a superoutburst due to its long duration) that this object has attracted amateur astronomers (particularly VSOLJ members) since the late 1980s. Despite the high potentiality of being a bright SU UMa-type dwarf nova, all attempts (visually watching for the nominal position and photographic searches) to recover this variable were unsuccessful.

In 1998, K. Haseda reported on a detection of on a transient object near the catalog position of V893 Sco, and this object was readily identified as a ROSAT X-ray source. A search for the plate collections at the time of observations of Satyvoldiev (1982) clarified that this outbursting object is indeed V893 Sco. This rediscovery was reported in Kato et al. (1998a).

Thorstensen (1999) spectroscopically confirmed that this object is indeed a dwarf nova, and obtained an orbital period of 0.0760 d. This short orbital period strengthened the suggestion that this object belongs to the SU UMa-type dwarf nova. Thorstensen (1999) also measured a large proper motion, implying a nearby object.

Since 1998, this object has been regularly monitored by amateur observers, and outbursts reaching $\sim$12 mag were recorded. During the observation in 1999, the group led by K. Matsumoto clarified that this object is a grazing eclipsing dwarf nova below the period gap (vsnet-alert 3432, announced on 1999 September 2). Bruch, Steiner, and Gneiding (2000) independently reached the same conclusion and submitted a paper on 1999 September 11. The result of the former research was published as Matsumoto, Mennickent, and Kato (2000).

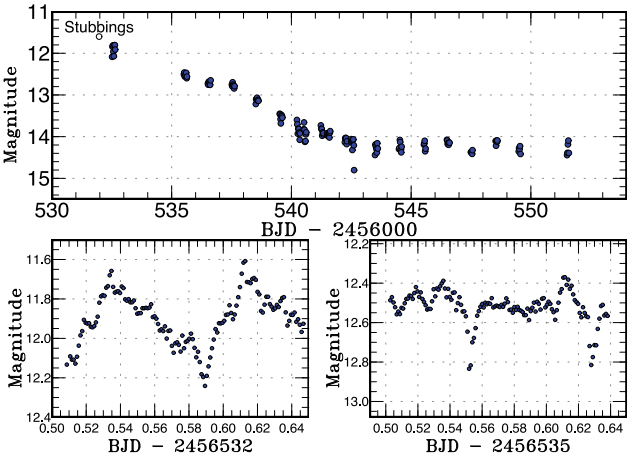

Fig. 28. Light curve of V893 Sco during the 2013 superoutburst. Upper: Overall light curve. Lower: Examples of nightly observations. Both eclipses and superhumps were detected.

Although Bruch, Steiner, and Gneiding (2000) mentioned that V893 Sco cannot be an ER UMa-type dwarf nova, Mason et al. (2001) suggested that it is an ER UMa-type dwarf nova by demonstrating their new Doppler tomograms. Kato, Matsumoto, and Uemura (2002b) explained that this object cannot be an ER UMa-type dwarf nova.

Such a confusion apparently comes from the lack of a definite superoutburst, despite the fact that its existence has been expected for the short orbital period. Although there have been a number of possible detections of "slightly brighter" outbursts, none of them were confirmed to be a genuine superoutburst until 2013.

On 2013 August 27, R. Stubbings reported on a bright (11.6 mag) outburst (vsnet-alert 16276; figure 28). Subsequent observation of this outburst finally confirmed the presence of superhumps (vsnet-alert 16315; figure 29). We observed this superoutburst and report the result here.

Since the eclipse ephemeris by Bruch, Steiner, and Gneiding (2000) was not fitted to modern observations (Mukai et al. 2009), we first refined the eclipse ephemeris. Since the white dwarf is partially eclipsed (Mukai et al. 2009), we used outburst observations in which the central part of the accretion disk is expected to be eclipsed, and the times of minima are expected to be close to the center of eclipse of the white dwarf. We used a combined set of the 2007 data (B. Monard and Osaka Kyoiku Univ. data), 2008 data (G. Bolt data), 2010 data (G. Bolt and Osaka Kyoiku Univ. data), and the present data. All observational data other than the 2013 data were obtained during the normal outbursts. We obtained an ephemeris of

$$\mathrm{Min(BJD)} = 2454173.3030(4) + 0.0759614614(18)E \quad (3)$$

using the MCMC modeling described in Kato et al. (2013b). This orbital period is in agreement with Mukai, Zietsman,

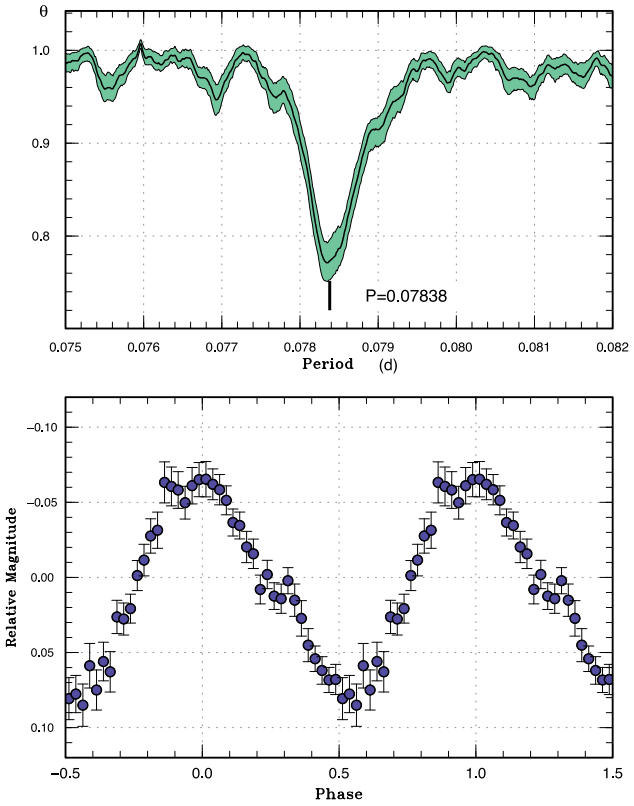

Fig. 29. Superhumps in V893 Sco after subtracting the orbital modulation (2013). Upper: PDM analysis. Lower: Phase-averaged profile.

Table 32. Superhump maxima of V893 Sco (2013).

E	Max*	Error	$O-C$†	phase‡	N§
0	56532.5397	0.0008	−0.0073	0.34	43
1	56532.6179	0.0010	−0.0075	0.37	45
38	56535.5283	0.0013	0.0032	0.68	42
39	56535.6098	0.0028	0.0063	0.76	36
51	56536.5526	0.0007	0.0087	0.17	36
52	56536.6294	0.0012	0.0071	0.18	15
89	56539.5270	0.0016	0.0050	0.32	40
99	56540.3015	0.0009	−0.0041	0.52	136
102	56540.5296	0.0005	−0.0111	0.52	41
128	56542.5793	0.0013	0.0009	0.51	47
140	56543.5208	0.0010	0.0020	0.90	36
141	56543.5975	0.0013	0.0003	0.91	35
153	56544.5343	0.0066	−0.0034	0.24	24

*BJD − 2400000.
†Against max = 2456532.5471 + 0.078370 E.
‡Orbital phase.
§Number of points used to determine the maximum.

and Still (2009), suggesting that the original orbital period derived by Bruch, Steiner, and Gneiding (2000) was systematically too long.

The times of superhump maxima after subtracting the mean orbital modulations were determined outside the eclipses (orbital phase 0.07–0.93; table 32). Although some superhumps were visible in the light curve, some of the times of maxima could not be determined because the superhump maxima coincided with eclipses. These superhumps were not included in table 32. We identified stages B and C and give the measured periods in table 2.

Table 33. Possible superoutbursts of V893 Sco.

JD	Date	Maximum	Duration (d)
2454883	2009 February 20	11.7	>8
2455975	2012 February 17	12.0	>4
2456532	2013 August 27	11.6	>8*

*Confirmed superoutburst.

As mentioned in Bruch, Steiner, and Gneiding (2000), it is surprising that such a bright dwarf nova defied detection of nova searches. This may have been a chance coincidence for superoutbursts occurring in unfavorable seasonal conditions before modern CCD-based search became popular. In table 33, we list the possible superoutbursts in modern observations. Except the 2013 one, all suspected superoutbursts occurred near the solar conjunction. It may be that the supercycle is close to one year, and all superoutbursts in the late 1990s and 2000s could not be observed due to lying near the Sun. The relatively small outburst amplitude is probably a result of the high inclination of the system. It was also likely that the magnitude scale in Satyvoldiev (1982) was ∼1 mag brighter than the modern scale.

3.26 RZ Sagittae

RZ Sge has long been known as a dwarf nova with a long cycle length (e.g., Petit 1956). Bond, Kemper, and Mattei (1982) reported on the detection of superhumps during the 1981 October outburst. Retrospective examination of the past visual observation also clarified a number of superoutbursts in the 1970s (Bond et al. 1982). Kato (1996) and Semeniuk et al. (1997) reported on observations of superhumps during the 1994 and 1996 superoutbursts, respectively. Although both Kato (1996) and Semeniuk et al. (1997) resulted in a global negative $P_{\rm dot}$ of $\sim -10 \times 10^{-5}$, Kato et al. (2009) considered that this is a result of stage B–C transition and that $P_{\rm dot}$ for stage B can be positive. Patterson et al. (2003) also reported on the 1996 superoutburst and the detection of the photometric orbital period in 1999.

We observed the 2013 superoutburst, which was detected in relatively early phase (vsnet-alert 16326). The times of superhump maxima are listed in table 34. The present data suggest a positive $P_{\rm dot}$ (the data for $E = 58$ was better than for $E = 57$, and the positive $O-C$ for $E = 58$ appears to be real). The $O-C$ values of present and past

Table 34. Superhump maxima of RZ Sge (2013).

E	Max*	Error	$O-C^{\dagger}$	$N^{\ddagger}$
0	56539.3871	0.0002	0.0008	90
1	56539.4582	0.0002	0.0013	140
2	56539.5277	0.0002	0.0001	136
3	56539.5978	0.0013	−0.0004	51
29	56541.4335	0.0003	−0.0014	89
42	56542.3523	0.0003	−0.0010	90
43	56542.4227	0.0004	−0.0012	90
44	56542.4930	0.0002	−0.0015	77
57	56543.4121	0.0005	−0.0008	14
58	56543.4879	0.0006	0.0043	22

*BJD − 2400000.
†Against max = 2456539.3863 + 0.070642 E.
‡Number of points used to determine the maximum.

Table 35. Superhump maxima of AW Sge (2013).

E	Max*	Error	$O-C^{\dagger}$	$N^{\ddagger}$
0	56572.6575	0.0003	−0.0068	52
62	56577.3153	0.0004	0.0104	64
63	56577.3892	0.0005	0.0094	64
74	56578.2061	0.0003	0.0029	69
75	56578.2798	0.0004	0.0019	72
76	56578.3544	0.0005	0.0016	72
87	56579.1708	0.0010	−0.0054	45
88	56579.2465	0.0005	−0.0045	71
89	56579.3209	0.0006	−0.0050	69
90	56579.3961	0.0009	−0.0046	48

*BJD − 2400000.
†Against max = 2456572.6642 + 0.074850 E.
‡Number of points used to determine the maximum.

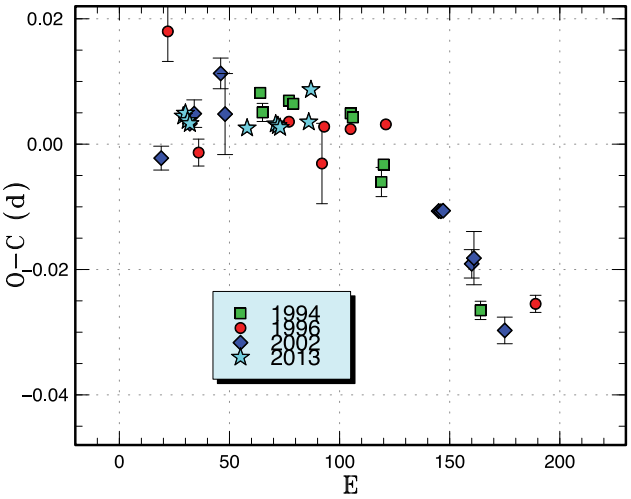

Fig. 30. Comparison of different superoutbursts of RZ Sge in the $O-C$ diagram. A period of 0.07063 d was used to draw this figure. Approximate cycle counts (E) after the start of the superoutburst were used.

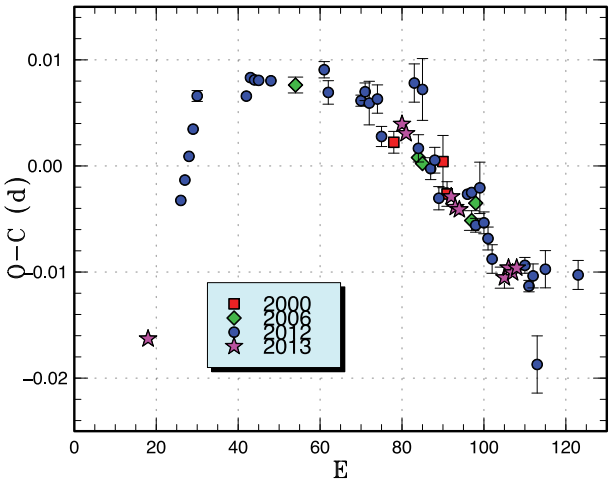

Fig. 31. Comparison of different superoutbursts of AW Sge in the $O-C$ diagram. A period of 0.07480 d was used to draw this figure. Approximate cycle counts (E) after the start of the superoutburst were used. Since the start of the superoutburst was best constrained in 2013, we shifted the $O-C$ diagrams to fit the 2013 one. This made an 18-cycle correction to the figure in Kato et al. (2014a).

superoutbursts can be well described as stage B and stage C (figure 30).

3.27 AW Sagittae

AW Sge was discovered to be a dwarf nova by Wolf and Wolf (1906). The 2000 and 2006 superoutbursts were reported in Kato et al. (2009). Kato et al. (2014a) further reported on the best observed 2012 superoutburst. On 2013 October 6, R. Stubbings detected another likely superoutburst (vsnet-alert 16512). This outburst was independently detected several hours early by AAVSO observers. On the night of this detection, no superhumps were detected. On the next night, a developing superhump was detected. There was a 4 d gap after these observations. The times of superhump maxima are listed in table 35. The epoch $E = 0$ was given a cycle count assuming that this was a stage A superhump with a longer period. A comparison of the period for $E \geq 62$ indicated that they are stage C superhumps. This identification was confirmed by a comparison of $O-C$ diagrams (figure 31). The negative detection of the outburst on 2013 October 3 could constrain the growth time of superhumps 3.5 d at the most.

3.28 V1265 Tauri

V1265 Tau was originally detected to be an optical transient (Skvarc & Palcic 2006). Shafter, Coelho, and Reed (2007) studied this object and detected short-period [0.053394(7) d] superhumps, which has been one of the shortest known superhump periods in classical SU UMa-type dwarf novae.

On 2013 August 4, the ASAS-SN team detected this object again in outburst (vsnet-alert 16120). The outburst

Table 36. Superhump maxima of V1265 Tau (2013).

E	Max*	Error	$O-C^{\dagger}$	$N^{\ddagger}$
0	56509.9538	0.0016	−0.0052	25
1	56510.0132	0.0024	0.0008	11
37	56511.9444	0.0045	0.0100	16
38	56511.9844	0.0004	−0.0034	37
56	56512.9464	0.0025	−0.0024	30
57	56512.9894	0.0025	−0.0128	24
94	56514.9731	0.0008	−0.0046	48
113	56515.9901	0.0012	−0.0019	32
131	56516.9515	0.0013	−0.0016	35
148	56517.8658	0.0031	0.0050	28
149	56517.9275	0.0015	0.0134	8
150	56517.9660	0.0065	−0.0015	49
167	56518.8748	0.0021	−0.0003	28
168	56518.9290	0.0049	0.0005	12
186	56519.8959	0.0028	0.0063	19
187	56519.9481	0.0019	0.0052	31
204	56520.8559	0.0014	0.0053	28
205	56520.9085	0.0056	0.0046	11
206	56520.9582	0.0007	0.0009	45
222	56521.8086	0.0038	−0.0030	14
223	56521.8692	0.0016	0.0042	25
260	56523.8356	0.0033	−0.0048	25
261	56523.8818	0.0013	−0.0120	23
278	56524.7991	0.0096	−0.0024	10
279	56524.8669	0.0023	0.0120	18
297	56525.8170	0.0104	0.0011	13
305	56526.2474	0.0089	0.0044	63
319	56526.9728	0.0041	−0.0177	35

*BJD − 2400000.
†Against max = 2456509.9590 + 0.053390 E.
‡Number of points used to determine the maximum.

was detected sufficiently early to follow the early evolution of the superhumps. On the first night of the observation, superhumps have already been detected (vsnet-alert 16137). This observation has confirmed that V1265 Tau has no characteristics of WZ Sge-type dwarf novae, such as the existence of early superhumps, despite its very short superhump period.

The times of superhump maxima are listed in table 36. Due to the faintness (∼16 mag) of the object, the errors in the time of superhump maxima were relatively large. We could determine a $P_{\rm dot}$ of +1.9(1.9) × 10^{-5} for stage B superhumps. This value is consistent with $P_{\rm dot}$ = +2.1(0.8) × 10^{-5} reported by Skvarc and Palcic (2006). This value of period derivative is small for an ordinary SU UMa-type dwarf nova with a short superhump period. After BJD 2456520, the object apparently showed a stage B–C transition. Since the measured times of superhump maxima during the late stage of the superoutburst were noisy, we determined the period by the PDM method — 0.05309(4) d, which is adopted in table 2.

Table 37. Superhump maxima of SU UMa (2013).

E	Max*	Error	$O-C^{\dagger}$	$N^{\ddagger}$
0	56627.2982	0.0011	0.0051	127
1	56627.3712	0.0029	−0.0007	83
10	56628.0796	0.0013	−0.0013	45
11	56628.1626	0.0007	0.0030	198
12	56628.2401	0.0009	0.0017	85
13	56628.3141	0.0009	−0.0031	85
23	56629.1012	0.0010	−0.0037	13
24	56629.1703	0.0032	−0.0135	8
25	56629.2622	0.0014	−0.0003	86
26	56629.3573	0.0008	0.0160	111
27	56629.4194	0.0009	−0.0007	79
28	56629.4999	0.0007	0.0011	69
29	56629.5701	0.0016	−0.0075	50
38	56630.2856	0.0036	−0.0010	54
51	56631.3153	0.0009	0.0047	86

*BJD − 2400000.
†Against max = 2456627.2931 + 0.078775 E.
‡Number of points used to determine the maximum.

This unusually short-period system is not similar to other systems with a similar short superhump period in which this object has neither WZ Sge-type characteristics nor a large positive $P_{\rm dot}$ as in a non-WZ Sge-type short-period system, V844 Her (Oizumi et al. 2007; Kato et al. 2009, 2013b). The evolution of superhumps was more similar to those in ER UMa-type dwarf novae such as RZ LMi (Olech et al. 2008; Kato et al. 2013b), although this object does not show frequent outbursts such as ER UMa-type dwarf novae do. Further study is needed to clarify the unusual nature of this object.

3.29 SU Ursae Majoris

We observed this "prototype" SU UMa-type dwarf nova (Udalski 1990a) during the late stage of the 2013 November superoutburst. The times of superhump maxima (table 37) also include the first two nights of post-superoutburst state. The resultant period of the stage C superhump is in agreement with the 1989 and 1999 observations (Kato et al. 2009).

3.30 SS Ursae Minoris

SS UMi was originally discovered to be the optical counterpart (dwarf nova) of the X-ray source E 1551+718 (Mason et al. 1982). This object was also selected as a CV by the Palomer Green survey (Green et al. 1982). Andronov (1986) reported on variations with a period of 127 min, which was considered to be the orbital period. Richter (1989) studied the behavior of this object and found that the mean cycle length is 30–48 d. Amateur astronomers also started

Table 38. Superhump maxima of SS UMi (2013).

E	Max*	Error	$O-C^{\dagger}$	$N^{\ddagger}$
0	56540.3119	0.0010	0.0008	53
1	56540.3717	0.0012	−0.0092	77
2	56540.4451	0.0012	−0.0058	78
3	56540.5170	0.0008	−0.0038	77
29	56542.3524	0.0010	0.0132	73
30	56542.4149	0.0008	0.0058	33
31	56542.4847	0.0005	0.0056	77
32	56542.5575	0.0006	0.0085	70
33	56542.6244	0.0012	0.0054	41
43	56543.3123	0.0008	−0.0060	33
44	56543.3922	0.0015	0.0039	37
57	56544.2931	0.0008	−0.0043	38
58	56544.3588	0.0021	−0.0085	35
59	56544.4318	0.0030	−0.0055	22

*BJD − 2400000.
†Against max = 2456540.3111 + 0.069936 E.
‡Number of points used to determine the maximum.

observations of this object in 1987 and recorded frequent outbursts with a cycle length as short as ∼10 d.

Udalski (1990b) observed this object and reported that the orbital period is much longer (probably 6.8 hr) in contrast to Andronov (1986). This contradiction between observations was resolved by the detection of superhumps with a period of 101 min (Chen et al. 1991). Neither Andronov (1986) nor Udalski (1990b) turned out to be correct. Kato et al. (1998b) also reported on observations of superhumps.

This object began to receive attention because of its high frequency of outbursts. Kato et al. (2000) clarified that the supercycle of this object is 84.7 d, one of the shortest known supercycles in ordinary SU UMa-type dwarf novae—note that this object was not classified as an ER UMa-type dwarf nova in this reference; see also Kato et al. (2001b) for the similar case of BF Ara. Olech et al. (2006) reported that the supercycle lengthened to 197 d in 2004. Olech et al. (2006) also reported on the development of superhumps. Kato et al. (2013b) also studied the 2012 superoutburst. A supercycle being as short as 84.7 d has never been recorded convincingly in recent decades.

We observed the final part of the superoutburst in 2003 August–September (the early part of this superoutburst was probably missed). The times of superhump maxima are listed in table 38. The times for $E \geq 29$ were obtained after the rapid fading from the superoutburst. Although these epochs of maxima could be expressed without a phase jump from those for $E \leq 3$, the identification of the phase was not complete due to the gap in the observation.

Table 39. Superhump maxima of CU Vel (2013).

E	Max*	Error	$O-C^{\dagger}$	$N^{\ddagger}$
0	56627.7714	0.0013	0.0004	17
1	56627.8531	0.0052	0.0016	8
12	56628.7378	0.0008	−0.0001	16
13	56628.8223	0.0011	0.0038	17
24	56629.6989	0.0077	−0.0059	6
25	56629.7856	0.0007	0.0003	17
37	56630.7515	0.0015	−0.0007	17
38	56630.8298	0.0017	−0.0029	15
62	56632.7684	0.0010	0.0019	17
63	56632.8488	0.0036	0.0017	10

*BJD − 2400000.
†Against max = 2456627.7710 + 0.080573 E.
‡Number of points used to determine the maximum.

3.31 CU Velorum

Although CU Vel is a well-known SU UMa-type dwarf nova, only a limited amount of information has been published (Vogt 1980; Mennickent & Diaz 1996). We reported on observations of the 2002 superoutburst in Kato et al. (2009).

The 2013 superoutburst was detected on November 25 (vsnet-alert 16648), but the actual start of the superoutburst must have been several days earlier, as later shown in the comparison of the $O-C$ diagrams. The 2013 observation, however, well covered the post-superoutburst state.

The times of superhump maxima during the plateau phase are listed in table 39. These superhumps are likely stage C superhumps since they were observed during the late stage of the superoutburst. A comparison of the $O-C$ diagrams supports this identification (figure 33).

Since orbital modulations are clearly seen in the light curve, we refined the orbital period by using observations around quiescence. The 2013–2014 data after the 2013 November superoutburst yielded a period of 0.078043(5) d. The 2013 January data (P. Nelson and F.-J. Hambsh) yielded a period of 0.07805(4) d. Using the combined data set, we selected a period of 0.0780541(3) d. The resultant profile (figure 32) showed two maxima of different amplitudes. This feature of double maxima is to some extent similar to WZ Sge-type dwarf novae in quiescence (e.g., Patterson et al. 1998; Araujo-Betancor et al. 2005). CU Vel may be intermediate between ordinary SU UMa-type dwarf novae and WZ Sge-type dwarf novae.

We subtracted the mean orbital light curve from the post-superoutburst light curve. A PDM analysis yielded a strong signal at 0.079906(4) d. The times of these post-superoutburst superhumps are listed in table 40. The $O-C$ diagram (figure 34) indicates that the superhump phase was continuous before and after the rapid fading from the superoutburst. There was a decrease in period

after $E = 110$ (after the rapid fading) and this period was almost constant at least until $E = 400$. Both the signals of superhumps and orbital period are clearly seen in the Lasso power spectrum (figure 35). The post-superoutburst superhumps survived at least 30 d after the fading.

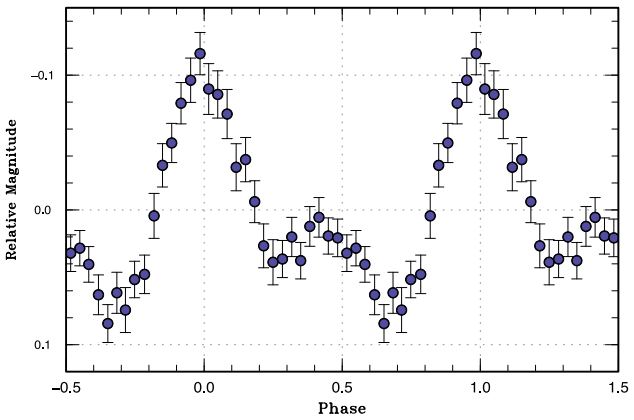

Fig. 32. Orbital variation of CU Vel in quiescence.

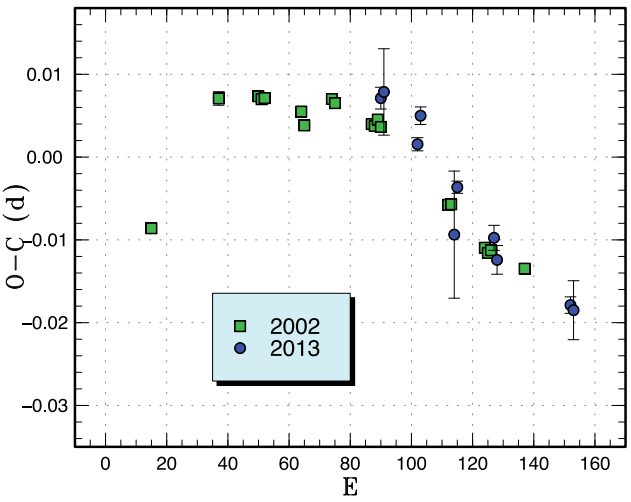

Fig. 33. Comparison of different superoutbursts of CU Vel in the $O-C$ diagram. A period of 0.08100 d was used to draw this figure. Approximate cycle counts (E) after the start of the superoutburst were used. Since the start of the 2013 superoutburst was not well constrained, we shifted the $O-C$ diagram to best fit the 2002 one.

Table 40. Superhump maxima of CU Vel in (2013) (post-superoutburst).

E	Max*	Error	$O-C$†	N‡	E	Max*	Error	$O-C$†	N‡
0	56636.8003	0.0026	−0.0013	17	187	56651.7578	0.0048	0.0118	6
12	56637.7592	0.0021	−0.0014	15	200	56652.7825	0.0016	−0.0024	19
13	56637.8416	0.0023	0.0010	10	201	56652.8650	0.0036	0.0003	11
24	56638.7266	0.0037	0.0070	16	211	56653.6668	0.0017	0.0028	12
25	56638.8052	0.0027	0.0057	16	212	56653.7459	0.0023	0.0020	14
36	56639.6797	0.0160	0.0011	8	213	56653.8269	0.0013	0.0031	19
37	56639.7645	0.0063	0.0060	15	224	56654.7062	0.0020	0.0034	9
38	56639.8600	0.0028	0.0215	7	225	56654.7896	0.0018	0.0068	19
75	56642.7844	0.0106	−0.0109	15	226	56654.8637	0.0027	0.0010	11
87	56643.7411	0.0017	−0.0133	8	236	56655.6604	0.0012	−0.0014	12
88	56643.8264	0.0048	−0.0079	11	237	56655.7420	0.0020	0.0003	14
99	56644.7034	0.0057	−0.0099	13	238	56655.8228	0.0014	0.0011	20
100	56644.7798	0.0033	−0.0134	15	248	56656.6379	0.0061	0.0171	11
111	56645.6772	0.0112	0.0049	10	249	56656.7018	0.0013	0.0011	19
112	56645.7496	0.0016	−0.0026	14	250	56656.7815	0.0019	0.0009	19
113	56645.8343	0.0017	0.0021	15	251	56656.8621	0.0031	0.0015	16
124	56646.7064	0.0039	−0.0048	14	261	56657.6633	0.0038	0.0036	13
125	56646.7885	0.0016	−0.0027	17	262	56657.7400	0.0034	0.0004	16
126	56646.8770	0.0049	0.0059	6	263	56657.8239	0.0028	0.0044	22
136	56647.6679	0.0028	−0.0023	9	274	56658.7006	0.0016	0.0020	15
137	56647.7395	0.0043	−0.0106	13	275	56658.7841	0.0025	0.0055	20
138	56647.8254	0.0021	−0.0047	20	276	56658.8626	0.0027	0.0042	18
149	56648.7093	0.0032	0.0002	14	286	56659.6585	0.0026	0.0008	18
150	56648.7870	0.0016	−0.0020	17	287	56659.7386	0.0030	0.0011	18
151	56648.8610	0.0024	−0.0080	12	288	56659.8242	0.0031	0.0067	22
161	56649.6647	0.0022	−0.0034	9	300	56660.7723	0.0020	−0.0042	32
162	56649.7443	0.0012	−0.0037	13	301	56660.8379	0.0023	−0.0185	34
163	56649.8291	0.0018	0.0012	20	338	56663.7981	0.0028	−0.0152	25

*BJD − 2400000.
†Against max = 2456636.8016 + 0.079916 E.
‡Number of points used to determine the maximum.

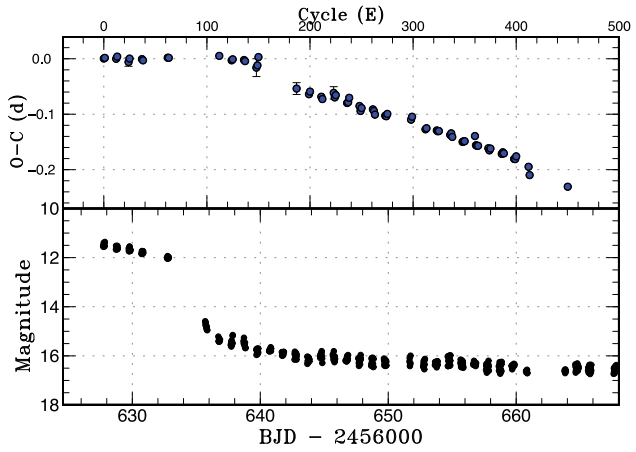

Fig. 34. $O-C$ diagram of superhumps in CU Vel (2013). Upper: $O-C$ diagram. A period of 0.080573 d was used for drawing this figure. Lower: Light curve. The observations were binned to 0.016 d.

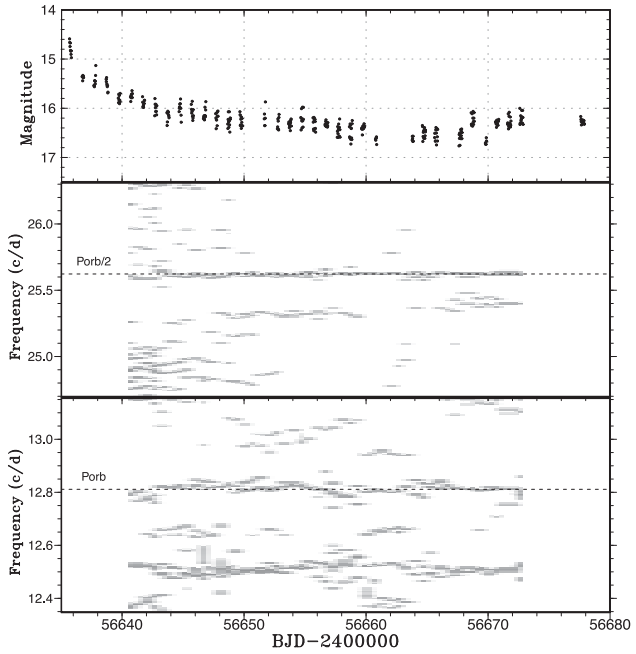

Fig. 35. Two-dimensional Lasso period analysis of CU Vel in the post-superoutburst stage (2013). The superoutburst plateau was excluded from the analysis because it did not yield a meaningful spectrum due to the shortness of the observation. Upper: Light curve. The data were binned to 0.01 d. Middle: First overtones of the superhump and orbital signals. Lower: Fundamentals of the superhump and the orbital signal. The orbital signal was present both in the fundamental and in the first harmonic. The signal of (positive) superhumps with increasing frequency was recorded during the post-superoutburst stage. No indication of a negative superhump was present. $\log\lambda = -8.5$ was used. The width of the sliding window and the time step used are 10 d and 0.4 d, respectively.

3.32 1RXS J231935.0+364705

This object (hereafter 1RXS J231935) was selected as a variable star (= DDE 8, probably a dwarf nova) during the course of identification of the ROSAT sources (Denisenko & Sokolovsky 2011). There was a well-observed superoutburst in 2011 (Kato et al. 2013b). D. Denisenko detected a new outburst on 2013 September 27 (vsnet-alert 16460). This outburst turned out to be a superoutburst. Only a single superhump maximum of BJD 2456565.5851(18) ($N = 19$) was obtained during the observation on two nights.

3.33 ASAS J224349+0809.5

This dwarf nova (hereafter ASAS J224349) was selected by P. Wils (see Shears et al. 2011a). There was one well-recorded outburst (superoutburst) in the ASAS data in 2005 October–November. The outburst in 2009 October was well observed, and superhumps were detected (Kato et al. 2010; Shears et al. 2011a). Although there was another superoutburst in 2011 June, the outburst was observed only for two nights (Kato et al. 2013b).

On 2013 August 14, the ASAS-SN team detected another outburst (vsnet-alert 16197). This outburst turned out to be a superoutburst, and stages B and C were well recorded (table 41). This superoutburst was followed by one post-superoutburst rebrightening 4 d later than the rapid fading from the plateau phase (figure 36). This interval was rather short for an ordinary SU UMa-type dwarf nova. As in the 2009 superoutburst, a definitely positive $P_{\rm dot}$ was recorded during stage B. The $O-C$ diagrams in the two superoutbursts were very similar (figure 37). Although the coincidence in cycle count between two superoutbursts was by chance, the 2013 superoutburst was confirmed to be detected sufficiently early (vsnet-alert 16207, within 3 d of the start of the outburst).

3.34 ASASSN-13cf

This object was discovered by the ASAS-SN survey on 2013 August 24 (vsnet-alert 16261). The coordinates are $21^{\rm h}55^{\rm m}12\overset{\rm s}{.}76$ and $+27^\circ41'18\overset{''}{.}9$. One previous outburst was detected in the CRTS data and another outburst was recorded on a Palomar quick-V plate (D. Denisenko, vsnet-alert 16263). From subsequent observations superhumps were detected (vsnet-alert 16284, 16308; figure 38). The times of superhump maxima are listed in table 42. A positive $P_{\rm dot}$ of $+7.1(1.9) \times 10^{-5}$, characteristic of this short superhump period, was obtained.

3.35 ASASSN-13cg

This object was discovered by the ASAS-SN survey on 2013 August 27. The coordinates are $20^{\rm h}52^{\rm m}52\overset{\rm s}{.}74$ and $-02^\circ39'53\overset{''}{.}0$. This object attracted attention because

Table 41. Superhump maxima of ASAS J224349 (2013).

E	Max*	Error	$O-C^{\dagger}$	$N^{\ddagger}$
0	56521.4291	0.0002	0.0027	116
1	56521.4990	0.0003	0.0028	146
4	56521.7072	0.0007	0.0019	19
5	56521.7753	0.0006	0.0002	24
12	56522.2618	0.0007	−0.0013	45
16	56522.5392	0.0004	−0.0028	123
17	56522.6095	0.0003	−0.0022	142
18	56522.6911	0.0011	0.0097	40
19	56522.7474	0.0014	−0.0037	20
25	56523.1666	0.0006	−0.0028	57
26	56523.2355	0.0004	−0.0036	65
27	56523.3054	0.0003	−0.0034	134
29	56523.4459	0.0003	−0.0024	130
30	56523.5129	0.0006	−0.0050	143
33	56523.7255	0.0008	−0.0016	22
34	56523.7957	0.0012	−0.0011	17
39	56524.1445	0.0003	−0.0009	125
40	56524.2130	0.0009	−0.0021	66
41	56524.2801	0.0006	−0.0048	68
42	56524.3491	0.0022	−0.0055	86
43	56524.4241	0.0005	−0.0002	143
44	56524.4934	0.0004	−0.0006	139
45	56524.5630	0.0004	−0.0007	142
46	56524.6398	0.0008	0.0065	29
47	56524.7039	0.0011	0.0008	33
54	56525.2003	0.0037	0.0092	61
55	56525.2620	0.0024	0.0012	22
87	56527.4994	0.0010	0.0077	49
88	56527.5680	0.0011	0.0066	39
114	56529.3777	0.0004	0.0036	136
115	56529.4478	0.0004	0.0041	158
116	56529.5159	0.0005	0.0025	154
117	56529.5861	0.0006	0.0030	138
129	56530.4187	0.0029	−0.0010	53
130	56530.4886	0.0015	−0.0009	58
131	56530.5579	0.0020	−0.0013	66
132	56530.6269	0.0019	−0.0020	43
133	56530.6970	0.0025	−0.0016	17
134	56530.7656	0.0015	−0.0028	17
147	56531.6697	0.0020	−0.0050	23
149	56531.8106	0.0020	−0.0034	25

*BJD − 2400000.
†Against max = 2456521.4265 + 0.069715 E.
‡Number of points used to determine the maximum.

it has a very blue ($u-g=-0.2$) SDSS color (vsnet-alert 16280). It also has an X-ray counterpart of 1RXS J205252.1−023952. By time-resolved photometry superhumps and possible shallow eclipses were detected (vsnet-alert 16302; figures 39 and 40). These eclipse-like fadings were not recorded on later nights and we could not determine its period. The reality of the eclipses requires future observations. The times of superhump maxima are listed in table 43, which clearly shows a positive $P_{\rm dot}$.

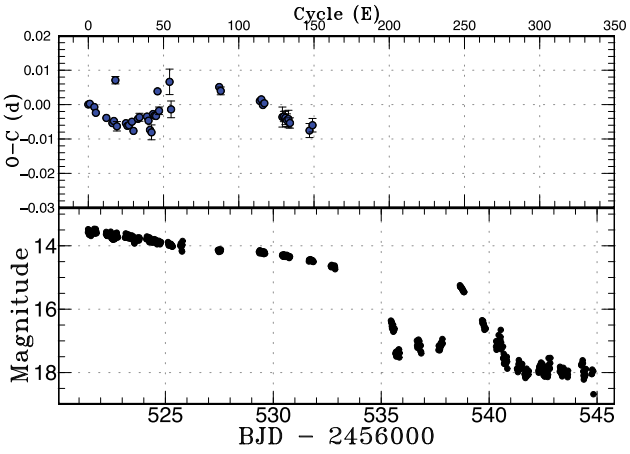

Fig. 36. $O-C$ diagram of superhumps in ASAS J2243 (2013). Upper: $O-C$ diagram. A period of 0.069715 d was used for drawing this figure. Lower: Light curve. The observations were binned to 0.014 d.

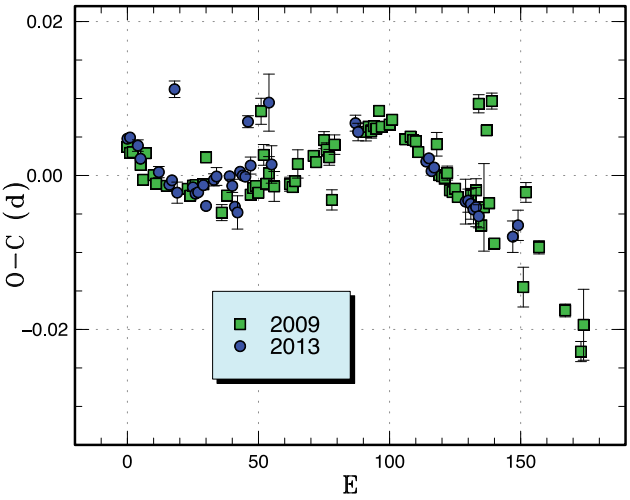

Fig. 37. Comparison of different superoutbursts of ASAS J2243 in the $O-C$ diagram. A period of 0.06975 d was used to draw this figure. Approximate cycle counts (E) after the start of the superoutburst were used. The coincidence in cycle count between two superoutbursts was by chance.

Table 42. Superhump maxima of ASASSN-13cf (2013).

E	Max*	Error	$O-C^{\dagger}$	$N^{\ddagger}$
0	56529.7208	0.0008	0.0007	101
1	56529.7839	0.0013	0.0054	61
2	56529.8388	0.0007	0.0018	96
29	56531.4116	0.0028	−0.0026	27
48	56532.5201	0.0004	−0.0040	100
49	56532.5772	0.0007	−0.0053	65
98	56535.4447	0.0012	−0.0002	52
114	56536.3780	0.0020	−0.0016	40
115	56536.4419	0.0015	0.0039	43
149	56538.4257	0.0015	0.0015	63
150	56538.4828	0.0011	0.0002	64

*BJD − 2400000.
†Against max = 2456529.7201 + 0.058416 E.
‡Number of points used to determine the maximum.

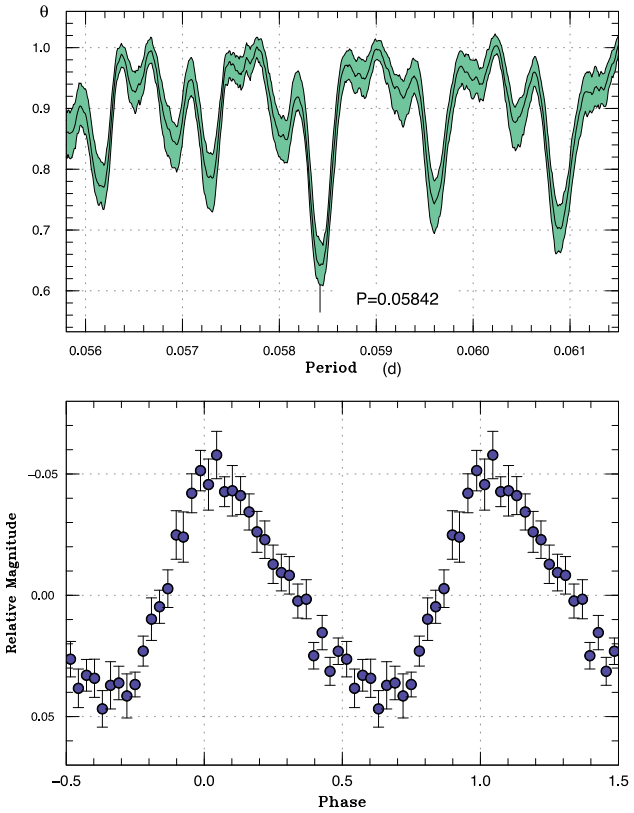

Fig. 38. Superhumps in ASASSN-13cf (2013). Upper: PDM analysis. Lower: Phase-averaged profile.

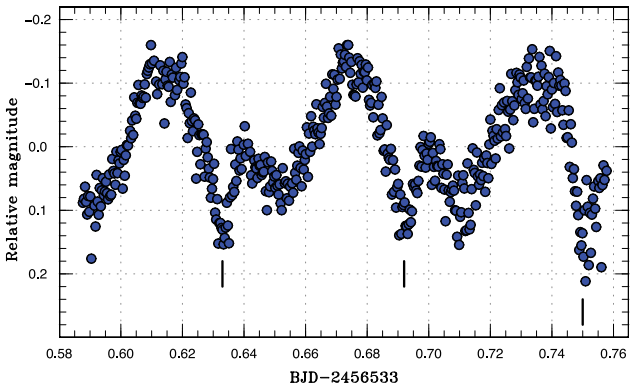

Fig. 39. Superhumps and possible eclipses in ASASSN-13cg on 2013 August 29. The vertical ticks represent possible shallow eclipses.

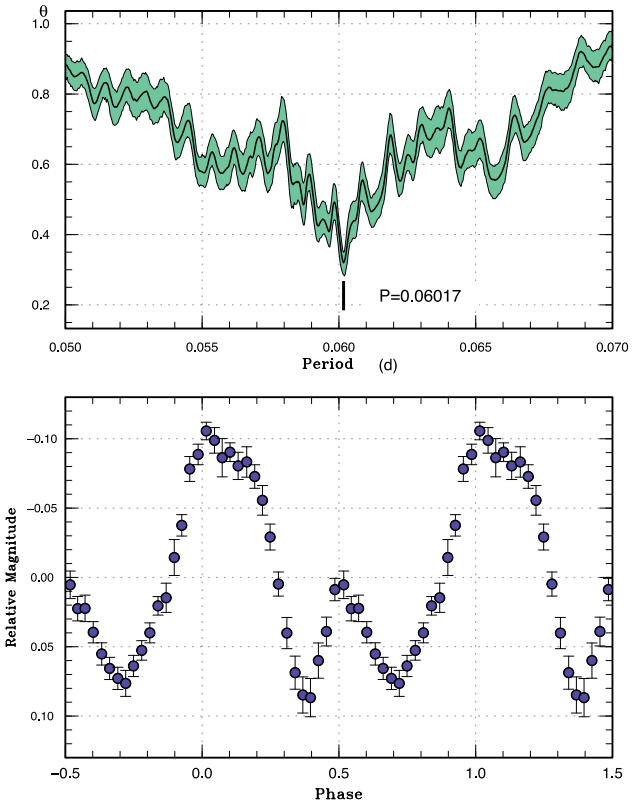

Fig. 40. Superhumps in ASASSN-13cg (2013). Upper: PDM analysis. Lower: Phase-averaged profile. The dip around phase 0.4 is a result of eclipselike feature recorded on the first night.

Table 43. Superhump maxima of ASASSN-13cg (2013).

E	Max*	Error	$O-C^{\dagger}$	$N^{\ddagger}$
0	56533.6131	0.0003	0.0013	132
1	56533.6735	0.0004	0.0015	138
2	56533.7326	0.0005	0.0003	140
12	56534.3338	0.0008	−0.0008	23
13	56534.3939	0.0013	−0.0009	23
46	56536.3759	0.0020	−0.0064	21
61	56537.2850	0.0021	−0.0007	22
62	56537.3490	0.0012	0.0031	23
63	56537.4088	0.0030	0.0026	23

*BJD − 2400000.
†Against max = 2456533.6118 + 0.060228 E.
‡Number of points used to determine the maximum.

3.36 ASASSN-13ck

This object was discovered by the ASAS-SN survey on 2013 August 29 (vsnet-alert 16303). The coordinates are $00^{\rm h}11^{\rm m}33^{\rm s}.71$ and $+04^{\circ}51'23''.0$. The object had a blue SDSS counterpart ($g=20.8$) and its outburst amplitude immediately suggested a WZ Sge-type dwarf nova.

From subsequent observations early superhumps were recorded (vsnet-alert 16307, 16309, 16313, 16314, 16332, 16368; figure 41). Ten days after the outburst detection, ordinary superhumps grew (vsnet-alert 16370, 16374, 16375, 16385; figure 42). Judging from the evolution of superhumps, the outburst of this object was detected sufficiently early.

The times of superhump maxima during the superoutburst plateau are listed in table 44. Clear stages A and B can be recognized as seen in many WZ Sge-type dwarf novae (figure 43). The last point ($E=202$) was obtained during the stage of fading branch of the superoutburst, and its large

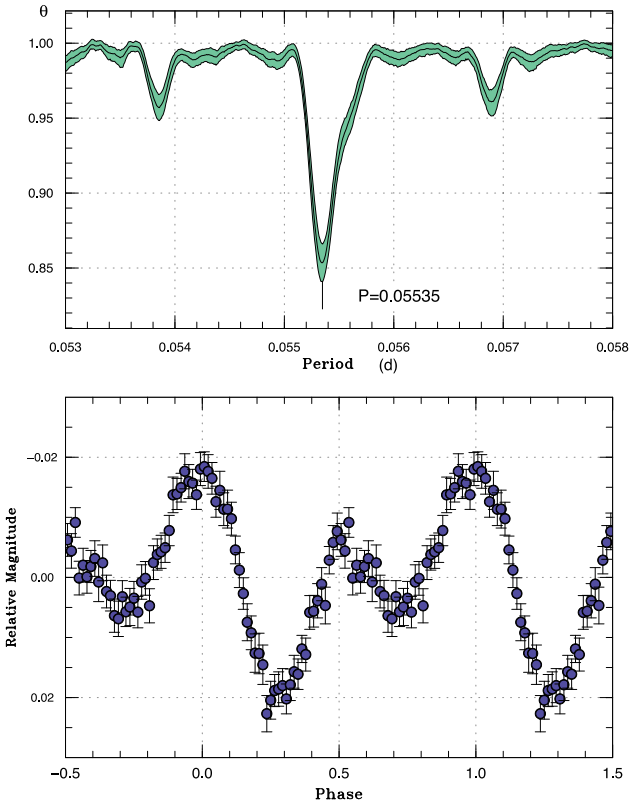

Fig. 41. Early superhumps in ASASSN-13ck (2013). Upper: PDM analysis. Lower: Phase-averaged profile.

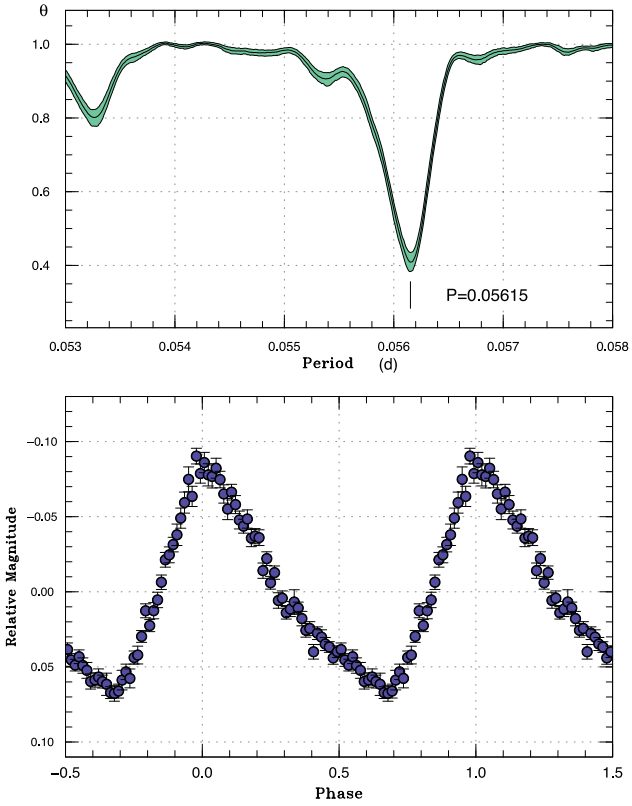

Fig. 42. Ordinary superhumps in ASASSN-13ck (2013). Upper: PDM analysis. Lower: Phase-averaged profile.

positive $O-C$ probably reflects a decrease in pressure effect (cf. Nakata et al. 2013b). This maximum was not used for determining $P_{\rm dot}$ at stage B. As in many WZ Sge-type dwarf novae, this object did not show a marked transition to the stage C superhump.

Five days after the rapid fading, the object showed a short rebrightening (September 23, BJD 2456558.5). The object showed another rebrightening (September 26, BJD 2456561.7), which served as a precursor outburst to the second plateau phase. This second plateau phase lasted 6 d (figure 43). During the second plateau phase, superhumps were also present. The mean superhump period during this phase was 0.056172(14) d, indicating that this precession rate was smaller than that in the main superoutburst. This smaller precession rate can be considered as a result of a smaller disk radius.

The pattern of rebrightening was like a "hybrid" between a long-lasting plateau (type A rebrightening in Kato et al. 2009) and distinct repetitive rebrightenings (type B rebrightening in Kato et al. 2009). There appears to be a smooth transition from one of these types to the other type. The presence of a precursor outburst in the second plateau is also intriguing. Such a precursor was also recorded in AL Com in 1995 (see Nogami et al. 1997; also subsection 3.11 of this paper). It is likely that a normal outburst triggered the second plateau phase (second superoutburst) as in ordinary SU UMa-type dwarf novae (Osaki 1989).

A two-dimensional Lasso analysis is presented in figure 44. The orbital signal was only present during the stage of early superhumps. The signal of (positive) superhumps showed a decrease in frequency (increase in period) during the superoutburst plateau. The superhumps appeared with slightly higher frequencies during the rebrightening plateau.

3.37 ASASSN-13cv

This object was discovered by the ASAS-SN survey on 2013 September 5 (vsnet-alert 16303). The coordinates are $22^{\rm h}10^{\rm m}25^{\rm s}.24$ and $+30^\circ46'06''.9$. Although the quiescent counterpart was not listed in the photometric catalog of SDSS (vsnet-alert 16354), Version 2.3.2 of the Guide Star Catalog (GSC) has an object with 21.4 mag. GALEX (Martin et al. 2005) also has an ultraviolet counterpart within 1″—near-UV and far-UV magnitudes are 22.07(3) and 21.6(4), respectively.

We obtained a single-night observation of this object (vsnet-alert 16364; figure 45). Three superhump maxima were obtained: BJD 2456541.3818(7) ($N=37$), 2456541.4441(2) ($N=66$), and 2456541.5072(6)

Table 44. Superhump maxima of ASASSN-13ck (2013).

E	Max*	Error	$O-C^{\dagger}$	$N^{\ddagger}$	E	Max*	Error	$O-C^{\dagger}$	$N^{\ddagger}$
0	56542.4669	0.0012	−0.0073	50	78	56546.8598	0.0006	−0.0009	53
1	56542.5154	0.0014	−0.0150	57	79	56546.9163	0.0013	−0.0007	31
2	56542.5701	0.0015	−0.0165	58	91	56547.5905	0.0005	−0.0013	45
5	56542.7511	0.0021	−0.0043	15	92	56547.6450	0.0005	−0.0031	66
6	56542.8051	0.0011	−0.0066	70	93	56547.7026	0.0005	−0.0017	69
17	56543.4315	0.0006	0.0013	52	94	56547.7597	0.0005	−0.0009	55
18	56543.4866	0.0003	0.0001	111	95	56547.8142	0.0008	−0.0026	18
19	56543.5404	0.0002	−0.0023	104	96	56547.8698	0.0011	−0.0032	22
20	56543.5987	0.0006	−0.0003	55	97	56547.9275	0.0006	−0.0017	58
22	56543.7172	0.0030	0.0058	21	98	56547.9803	0.0007	−0.0052	57
23	56543.7713	0.0002	0.0036	54	110	56548.6569	0.0015	−0.0034	13
24	56543.8288	0.0003	0.0049	64	111	56548.7124	0.0005	−0.0041	48
25	56543.8842	0.0005	0.0041	30	112	56548.7701	0.0005	−0.0028	48
35	56544.4499	0.0006	0.0074	33	113	56548.8248	0.0009	−0.0042	35
36	56544.5069	0.0002	0.0081	82	114	56548.8829	0.0005	−0.0024	51
37	56544.5627	0.0002	0.0077	73	115	56548.9387	0.0006	−0.0028	76
38	56544.6208	0.0010	0.0096	37	116	56548.9933	0.0009	−0.0045	52
40	56544.7287	0.0006	0.0050	26	124	56549.4440	0.0004	−0.0036	59
41	56544.7856	0.0003	0.0056	70	125	56549.5005	0.0004	−0.0034	53
42	56544.8417	0.0004	0.0055	65	126	56549.5619	0.0016	0.0017	18
43	56544.8983	0.0015	0.0059	20	131	56549.8364	0.0009	−0.0050	50
47	56545.1232	0.0002	0.0058	73	132	56549.8950	0.0009	−0.0025	40
48	56545.1788	0.0004	0.0052	76	141	56550.4006	0.0007	−0.0031	33
54	56545.5132	0.0020	0.0022	26	142	56550.4577	0.0015	−0.0022	18
55	56545.5717	0.0003	0.0045	106	145	56550.6239	0.0037	−0.0047	15
56	56545.6260	0.0003	0.0025	115	146	56550.6776	0.0035	−0.0073	17
57	56545.6820	0.0003	0.0022	99	162	56551.5857	0.0024	0.0010	53
58	56545.7383	0.0004	0.0024	63	163	56551.6396	0.0024	−0.0013	59
59	56545.7945	0.0003	0.0022	73	164	56551.6921	0.0031	−0.0051	12
60	56545.8498	0.0004	0.0014	76	165	56551.7559	0.0079	0.0025	42
61	56545.9062	0.0007	0.0016	36	166	56551.8122	0.0021	0.0025	71
73	56546.5797	0.0004	0.0002	58	167	56551.8684	0.0012	0.0026	64
74	56546.6343	0.0005	−0.0015	69	184	56552.8218	0.0013	−0.0001	28
75	56546.6915	0.0005	−0.0005	74	185	56552.8827	0.0025	0.0046	26
76	56546.7476	0.0005	−0.0007	62	202	56553.8532	0.0038	0.0190	61
77	56546.8046	0.0003	0.0001	77					

*BJD − 2400000.
†Against max = 2456542.4742 + 0.056238 E.
‡Number of points used to determine the maximum.

($N = 36$). The best period by the PDM method is 0.0607(2) d.

3.38 ASASSN-13cz

This object was discovered by the ASAS-SN survey on 2013 September 14 (vsnet-alert 16401). The coordinates are $15^{\rm h}27^{\rm m}55^{\rm s}.3$ and $+63^{\circ}27'53''.4$. From subsequent observations superhumps were detected (vsnet-alert 16405; figure 46). The times of superhump maxima are listed in table 45. The period shown in table 2 is a result of the PDM analysis.

3.39 ASASSN-13da

This object was discovered by the ASAS-SN survey on 2013 September 20 (vsnet-alert 16426). The coordinates are $19^{\rm h}59^{\rm m}18^{\rm s}.03$ and $-18^{\circ}33'31''.4$. The quiescent counterpart is a 21 mag object in CRTS. On the first three nights, only low-amplitude modulations were detected. Four days after the detection, fully grown superhumps appeared (vsnet-alert 16494; figure 47). This growth of superhumps was associated with an increase in the system's brightness. The times of superhump maxima are listed in table 46. The times for $E \leq 29$ were those for superhumps in the growing stage—they are likely stage A superhumps. Cycle counts

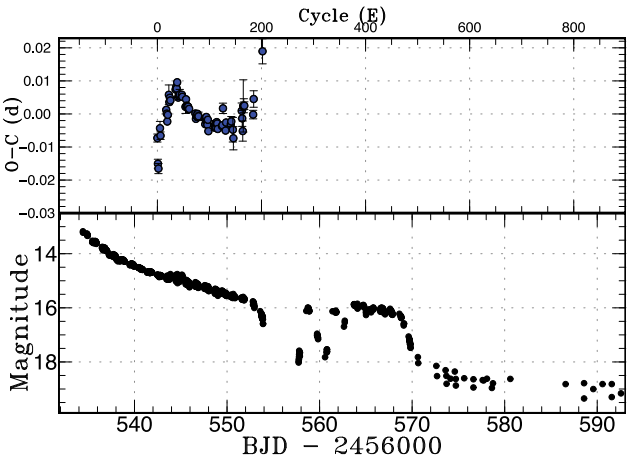

Fig. 43. $O-C$ diagram of superhumps in ASASSN-13ck (2013). Upper: $O-C$ diagram. A period of 0.056238 d was used for drawing this figure. Lower: Light curve. The observations were binned to 0.012 d.

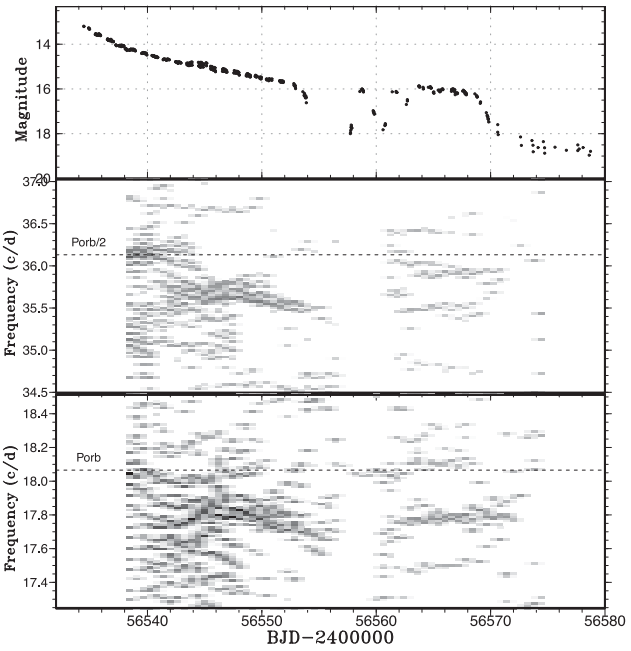

Fig. 44. Lasso analysis of ASASSN-13ck (2013). Upper: Light curve. The data were binned to 0.02 d. Middle: First overtones of the superhump and orbital signals. Lower: Fundamentals of the superhump and the orbital signal. The orbital signal was present both in the fundamental and in the first overtone during the earliest phase (early superhumps). The signal of (positive) superhumps with a variable frequency was recorded during the superoutburst plateau. No indication of negative superhump was present. The parameter $\log\lambda = -8.8$ was used. The width of the sliding window and the time step used are 8 d and 0.6 d, respectively.

for these maxima are uncertain. Although a PDM analysis of this segment yielded a possible period of 0.07300(5) d, this value was not included in table 2 due to its uncertainty. The decrease in $O-C$ for $E \geq 153$ suggests a stage B–C transition.

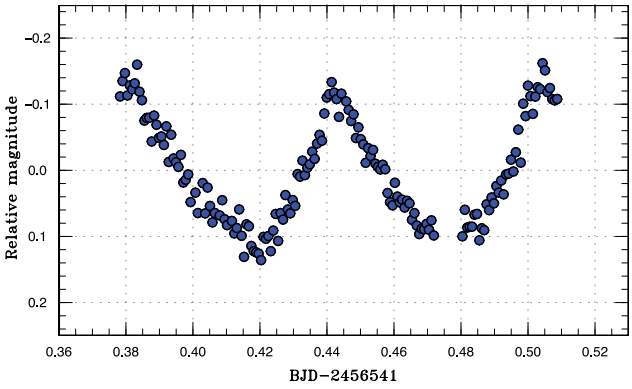

Fig. 45. Superhumps in ASASSN-13cv on 2013 September 5.

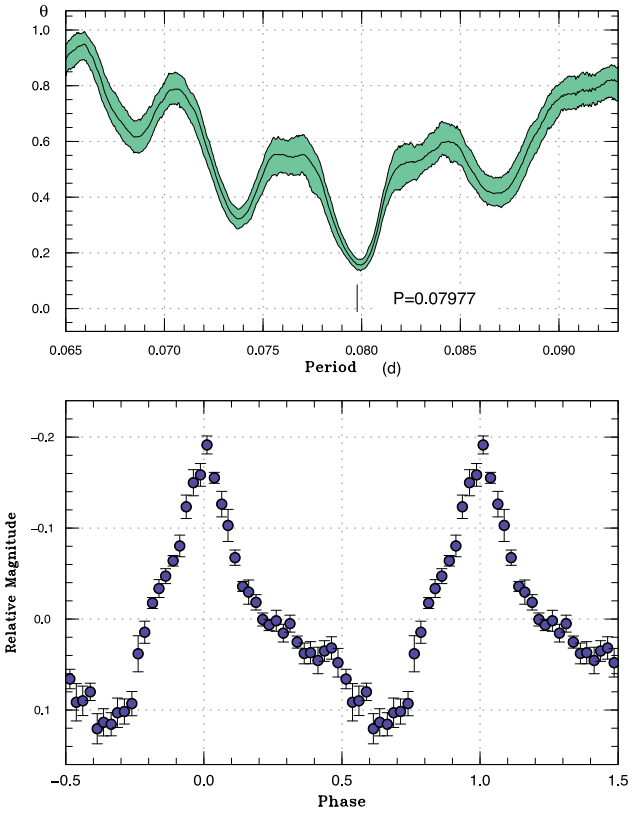

Fig. 46. Superhumps in ASASSN-13cz (2013). Upper: PDM analysis. Lower: Phase-averaged profile.

Table 45. Superhump maxima of ASASSN-13cz (2013).

E	Max*	Error	$O-C^{\dagger}$	$N^{\ddagger}$
0	56550.3610	0.0004	0.0003	86
1	56550.4407	0.0004	0.0002	81
2	56550.5198	0.0005	−0.0006	82
13	56551.3986	0.0006	0.0001	50

*BJD − 2400000.
†Against max = 2456550.3607 + 0.079834 E.
‡Number of points used to determine the maximum.

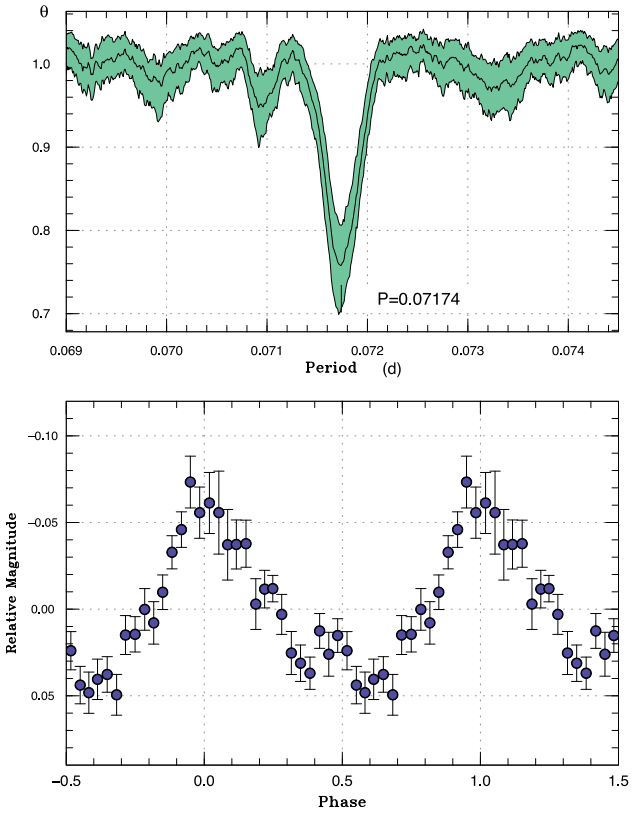

Fig. 47. Superhumps in ASASSN-13da (2013). Upper: PDM analysis. Lower: Phase-averaged profile.

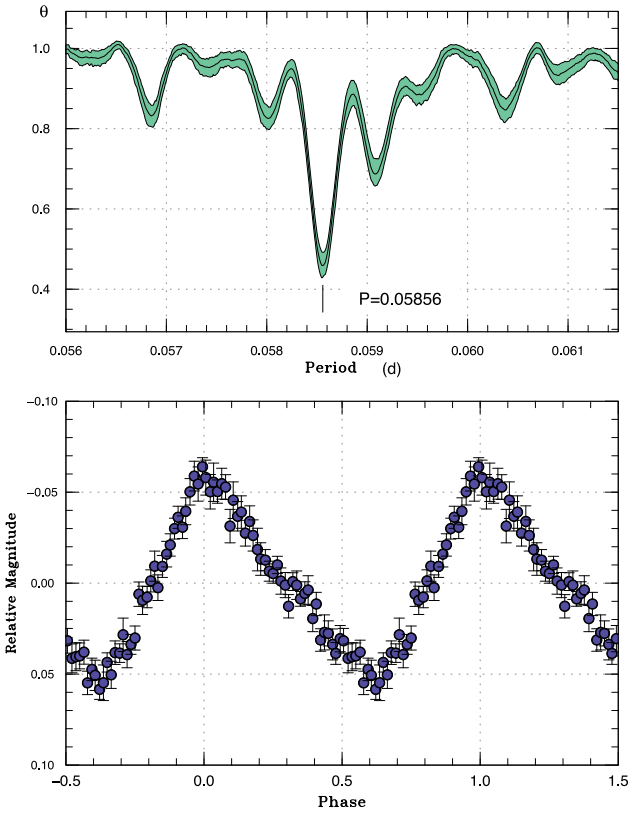

Fig. 48. Superhumps in ASASSN-14ac (2014). Upper: PDM analysis for the interval BJD 2456692–2456701. Lower: Phase-averaged profile.

Table 46. Superhump maxima of ASASSN-13da (2013).

E	Max*	Error	$O-C^{\dagger}$	$N^{\ddagger}$
0	56556.5090	0.0025	0.0017	19
1	56556.5711	0.0047	−0.0079	20
29	56558.5871	0.0048	−0.0002	17
56	56560.5208	0.0010	−0.0032	19
57	56560.5976	0.0012	0.0019	20
70	56561.5317	0.0009	0.0036	19
71	56561.6015	0.0007	0.0016	19
98	56563.5360	0.0015	−0.0006	19
99	56563.6082	0.0014	−0.0001	15
112	56564.5350	0.0011	−0.0057	24
113	56564.6136	0.0021	0.0011	17
126	56565.5511	0.0016	0.0062	21
139	56566.4829	0.0111	0.0055	9
140	56566.5555	0.0018	0.0065	25
153	56567.4878	0.0212	0.0062	10
154	56567.5563	0.0010	0.0031	25
168	56568.5571	0.0014	−0.0004	26
181	56569.4737	0.0046	−0.0162	6
182	56569.5585	0.0024	−0.0031	26

*BJD − 2400000.

†Against max = 2456556.5072 + 0.071728 E.

‡Number of points used to determine the maximum.

3.40 ASASSN-14ac

This object was discovered by the ASAS-SN survey on 2014 January 18 (Shappee et al. 2014b). The coordinates are $07^{\rm h}52^{\rm m}54^{\rm s}.9$ and $+53^{\circ}05'31''.2$. The large outburst amplitude ($\sim$7 mag) and the blue SDSS counterpart ($u-g=-0.3$) was suggestive of a WZ Sge-type dwarf nova (vsnet-alert 16794). Although subsequent observations showed some low-amplitude modulations (vsnet-alert 16823, 16830), no distinct period was obtained. The object started to show ordinary superhumps 14 d after the discovery (vsnet-alert 16880, 16895; figure 48).

The times of superhump maxima are listed in table 47. The early part of the observation clearly revealed stage A superhumps. The global light curve showed systematic brightening associated with the appearance of superhumps (see also figure 49). Although the latter part of the superoutburst was not very well recorded, the $P_{\rm dot}$ of stage B superhumps was not strongly positive. The object started rapidly fading from the plateau stage on February 17 (30 d after the discovery).

On March 1, E. Muyllaert recorded the object at 17.2 mag (unfiltered CCD magnitude), which appeared to be a post-superoutburst rebrightening. The type of the rebrightening, however, could not be determined.

Table 47. Superhump maxima of ASASSN-14ac (2014).

E	Max*	Error	$O-C$†	N‡
0	56689.1105	0.0023	−0.0364	43
1	56689.1686	0.0016	−0.0370	42
15	56690.0034	0.0006	−0.0245	32
52	56692.2034	0.0029	0.0023	17
53	56692.2656	0.0006	0.0058	31
54	56692.3279	0.0010	0.0094	31
55	56692.3847	0.0003	0.0074	24
56	56692.4400	0.0010	0.0040	23
57	56692.5074	0.0006	0.0127	31
58	56692.5630	0.0006	0.0096	30
68	56693.1495	0.0007	0.0087	25
69	56693.2077	0.0014	0.0081	39
70	56693.2673	0.0008	0.0090	47
71	56693.3261	0.0005	0.0091	31
72	56693.3863	0.0004	0.0106	32
83	56694.0294	0.0004	0.0076	42
84	56694.0876	0.0006	0.0071	42
85	56694.1463	0.0004	0.0070	42
86	56694.2066	0.0007	0.0086	50
87	56694.2665	0.0010	0.0098	42
88	56694.3246	0.0006	0.0091	31
89	56694.3837	0.0007	0.0095	31
90	56694.4382	0.0007	0.0053	18
151	56698.0078	0.0008	−0.0079	56
152	56698.0692	0.0010	−0.0052	50
153	56698.1300	0.0018	−0.0032	56
185	56700.0049	0.0009	−0.0077	38
186	56700.0588	0.0008	−0.0126	61
187	56700.1190	0.0016	−0.0111	61
188	56700.1737	0.0012	−0.0151	60

*BJD − 2400000.
†Against max = 2456689.1469 + 0.058734 E.
‡Number of points used to determine the maximum.

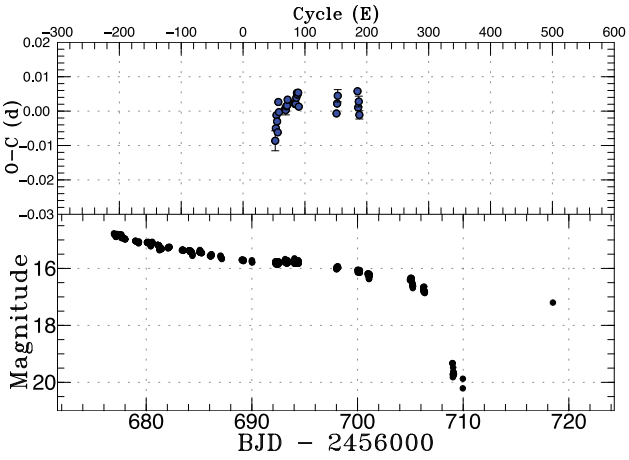

Fig. 49. $O-C$ diagram of superhumps in ASASSN-14ac (2014). Upper: $O-C$ diagram. A period of 0.05855 d was used for drawing this figure. Lower: Light curve. The observations were binned to 0.012 d.

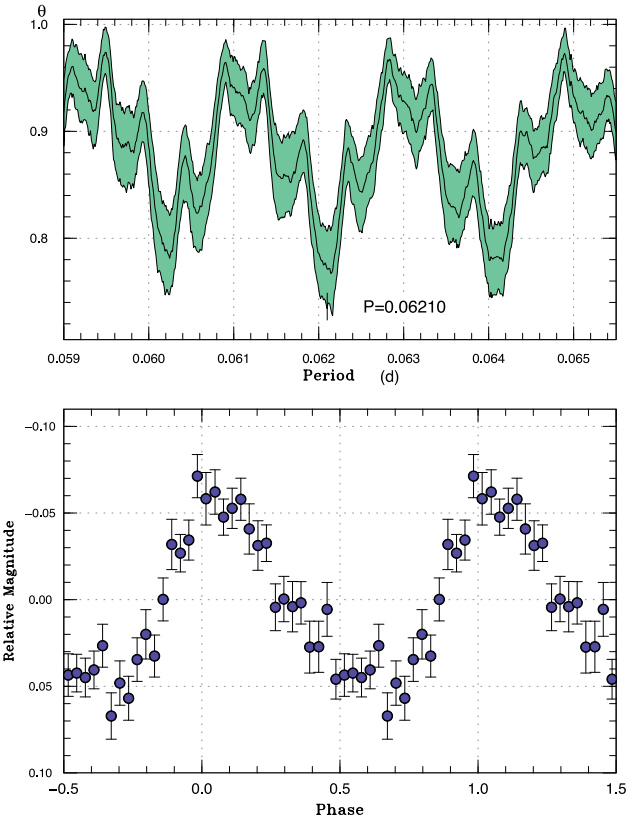

Fig. 50. Superhumps in CSS J024354 (2013). Upper: PDM analysis. Lower: Phase-averaged profile.

Table 48. Superhump maxima of CSS J024354 (2013).

E	Max*	Error	$O-C$†	N‡
0	56594.5208	0.0033	0.0094	143
1	56594.5645	0.0024	−0.0089	140
94	56600.3445	0.0009	−0.0020	80
126	56602.3336	0.0007	0.0007	121
127	56602.3953	0.0008	0.0003	143
128	56602.4548	0.0011	−0.0022	142
129	56602.5220	0.0093	0.0028	50

*BJD − 2400000.
†Against max = 2456594.5114 + 0.062076 E.
‡Number of points used to determine the maximum.

Since the stage A superhumps of this object are well established, determination of the orbital period in quiescence is desired to estimate the mass ratio.

3.41 CSS J024354.0−160314

This object (= CSS131026:024354−160314, hereafter CSS J024354) was detected to be a large-amplitude dwarf nova by CRTS on 2013 October 26 (vsnet-alert 16564). From subsequent observations superhumps were detected (vsnet-alert 16600; figure 50). The times of superhump maxima are listed in table 48.

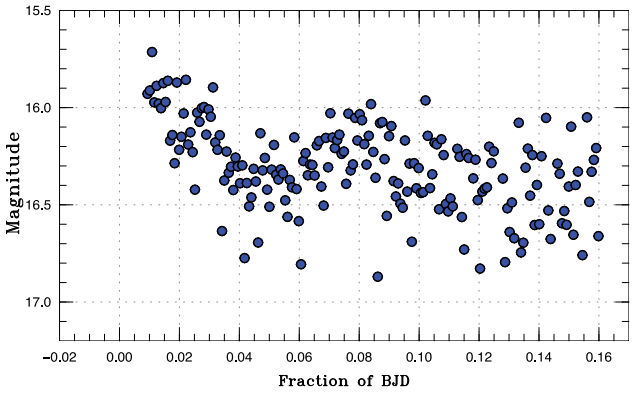

Fig. 51. Possible superhumps in DDE 31.

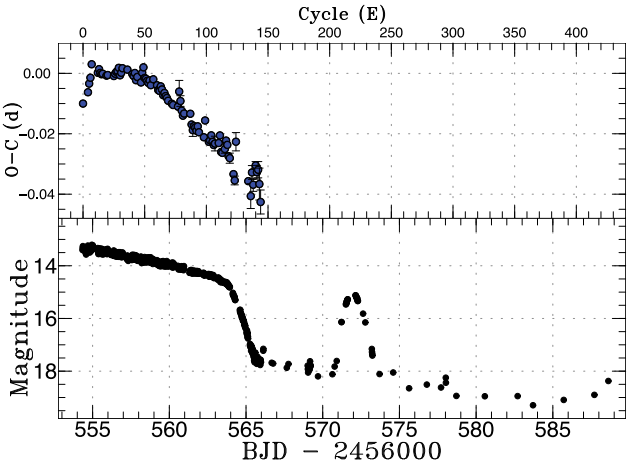

Fig. 52. $O-C$ diagram of superhumps in MASTER J004527 (2013). Upper: $O-C$ diagram. A period of 0.08039 d was used to draw this figure. Lower: Light curve. The observations were binned to 0.016 d.

3.42 DDE 31

This dwarf nova was discovered by D. Denisenko in outburst (16.3 mag; all magnitudes for this object are unfiltered CCD magnitudes) on 2012 October 15 (vsnet-alert 15007). The coordinates are $02^{\rm h}13^{\rm m}17\overset{\rm s}{.}18$ and $+46^\circ06'03\overset{''}{.}4$. On the next night, the object faded to 17.7 mag (B. Staels). On 2012 December 15, D. Denisenko again detected this object in outburst (16.2 mag) and reported on a previous outburst on 2012 September 14 (17.0 mag, vsnet-alert 15170).

On 2014 January 4, D. Denisenko reported on a brighter outburst (15.3 mag, vsnet-alert 16757). From time-resolved observations modulations resembling a superoutburst were detected (figure 51). Although a period of 0.073(3) d was inferred, the outburst faded rapidly (~ 1 mag d^{-1}) and the object was not detected to be brighter than 18.2 mag five nights later. This behavior was unusual for a superoutburst. Furthermore, an analysis of the SDSS colors (Kato et al. 2012a) yielded an expected orbital period longer than 0.1 d (it is also likely that these SDSS observations were not obtained in true quiescence, cf. vsnet-alert 15170). We should therefore await another outburst to clarify the classification of this object.

3.43 MASTER OT J004527.52+503213.8

This object (hereafter MASTER J004527) was detected to be a bright (12.5 mag) transient by the MASTER network (Gorbovskoy et al. 2013) on 2013 September 17 (Denisenko et al. 2013c). The object has an 18–19 mag quiescent counterpart and its large outburst amplitude suggested a WZ Sge-type dwarf nova. The last non-detection observation prior to the outburst was announced on September 13 (fainter than 18.5; vsnet-alert 16422).

From subsequent observations superhumps were immediately detected (vsnet-alert 16423). The long (~ 0.081 d) superhump period, however, was not compatible with the suggested WZ Sge-type classification (vsnet-alert 16425). Later observations yielded a slightly shorter superhump period (vsnet-alert 16433, 16434, 16459). A further decrease in the superhump period was announced on September 22 (vsnet-alert 16463, 16497). The object showed a single post-superoutburst rebrightening on October 6 (vsnet-alert 16513; figure 52).

The times of superhump maxima are listed in table 49. The decrease in period around September 22 ($E \sim 50$; figure 52) may be attributed to either stage B–C transition (such as is observed in ordinary SU UMa-type dwarf novae) or stage A–B transition [such as are reported in likely period bouncers: SSS J122221.7−311523 (Kato et al. 2013a) and OT J075418.7+381225 and OT J230425.8+062546 (Nakata et al. 2014)]. Since the large outburst amplitude of MASTER J004527 suggested the WZ Sge-type dwarf nova, the second possibility would deserve consideration. We consider that the former interpretation is more probable for several reasons: (1) The difference between periods before and after the transition was 0.5%, which is typical of stage B–C transition (e.g., Kato et al. 2009), but is smaller than in stage A–B transition (1.0%–1.5%, cf. Nakata et al. 2013b). (2) There was a phase with a longer superhump period ($E \leq 7$), which can be considered as stage A. (3) The amplitudes of superhumps were much larger (0.2–0.3 mag; figure 53) than those in likely period bouncers (e.g., Kato et al. 2013a). We list the periods based on the former interpretation in table 2.

Following this interpretation of the superhump stages, the object can be recognized as an SU UMa-type dwarf nova (not a period bouncer) with a long orbital period and infrequent, large-amplitude outbursts. The object may resemble V1251 Cyg (Kato 1995a; Kato et al. 2009) or QY Per (Kato et al. 2009). Future monitoring of outbursts would be helpful in identifying the supercycle.

Table 49. Superhump maxima of MASTER J004527 (2013).

E	Max*	Error	$O-C^{\dagger}$	$N^{\ddagger}$	E	Max*	Error	$O-C^{\dagger}$	$N^{\ddagger}$
0	56554.3649	0.0003	−0.0181	95	72	56560.1529	0.0003	0.0023	120
4	56554.6902	0.0002	−0.0132	226	73	56560.2329	0.0002	0.0021	137
5	56554.7735	0.0002	−0.0101	147	77	56560.5539	0.0006	0.0027	56
6	56554.8558	0.0002	−0.0079	124	78	56560.6393	0.0037	0.0080	42
7	56554.9406	0.0008	−0.0031	73	79	56560.7165	0.0018	0.0051	28
12	56555.3398	0.0002	−0.0045	197	80	56560.7938	0.0007	0.0023	61
13	56555.4214	0.0001	−0.0030	292	81	56560.8725	0.0006	0.0009	69
14	56555.5005	0.0001	−0.0040	386	82	56560.9536	0.0009	0.0019	37
15	56555.5804	0.0001	−0.0042	305	87	56561.3555	0.0009	0.0032	104
16	56555.6610	0.0002	−0.0037	310	88	56561.4323	0.0003	−0.0001	108
19	56555.9016	0.0004	−0.0035	63	89	56561.5108	0.0021	−0.0017	30
20	56555.9821	0.0003	−0.0030	59	90	56561.5925	0.0008	−0.0000	70
25	56556.3838	0.0002	−0.0019	279	91	56561.6724	0.0005	−0.0002	69
26	56556.4649	0.0002	−0.0009	279	92	56561.7518	0.0008	−0.0010	57
27	56556.5459	0.0002	0.0000	171	93	56561.8336	0.0007	0.0007	72
28	56556.6266	0.0002	0.0006	202	94	56561.9121	0.0008	−0.0009	68
29	56556.7080	0.0003	0.0019	190	98	56562.2320	0.0004	−0.0015	154
30	56556.7859	0.0004	−0.0003	186	99	56562.3179	0.0006	0.0044	113
31	56556.8672	0.0003	0.0009	197	102	56562.5520	0.0008	−0.0018	61
32	56556.9491	0.0006	0.0027	52	103	56562.6329	0.0008	−0.0010	65
36	56557.2702	0.0003	0.0033	312	104	56562.7149	0.0008	0.0009	52
40	56557.5902	0.0006	0.0030	62	105	56562.7932	0.0009	−0.0010	63
41	56557.6700	0.0004	0.0026	69	106	56562.8725	0.0006	−0.0018	70
42	56557.7514	0.0005	0.0039	61	107	56562.9534	0.0024	−0.0010	21
43	56557.8294	0.0005	0.0018	71	110	56563.1947	0.0005	0.0001	75
44	56557.9109	0.0005	0.0032	71	111	56563.2776	0.0007	0.0028	81
47	56558.1502	0.0004	0.0022	125	112	56563.3525	0.0006	−0.0024	149
48	56558.2338	0.0003	0.0057	212	113	56563.4326	0.0005	−0.0024	93
49	56558.3160	0.0003	0.0078	227	115	56563.5947	0.0014	−0.0005	64
50	56558.3929	0.0003	0.0046	187	116	56563.6779	0.0010	0.0026	124
51	56558.4730	0.0003	0.0046	196	117	56563.7569	0.0009	0.0014	87
52	56558.5527	0.0003	0.0041	225	118	56563.8335	0.0011	−0.0020	71
53	56558.6324	0.0003	0.0037	256	119	56563.9132	0.0017	−0.0024	66
54	56558.7136	0.0004	0.0049	130	122	56564.1491	0.0004	−0.0068	63
55	56558.7924	0.0005	0.0036	61	123	56564.2274	0.0014	−0.0087	84
57	56558.9552	0.0011	0.0061	24	124	56564.3206	0.0030	0.0045	17
60	56559.1944	0.0002	0.0050	209	134	56565.1115	0.0011	−0.0058	58
61	56559.2731	0.0002	0.0037	263	136	56565.2673	0.0041	−0.0101	27
62	56559.3533	0.0002	0.0037	144	137	56565.3555	0.0023	−0.0020	36
63	56559.4352	0.0003	0.0055	128	138	56565.4319	0.0022	−0.0058	35
64	56559.5145	0.0003	0.0047	169	140	56565.5990	0.0013	0.0012	71
65	56559.5930	0.0004	0.0031	66	141	56565.6772	0.0023	−0.0008	72
66	56559.6741	0.0003	0.0041	206	142	56565.7584	0.0027	0.0003	69
67	56559.7535	0.0002	0.0034	188	143	56565.8340	0.0053	−0.0042	73
68	56559.8333	0.0003	0.0030	68	144	56565.9085	0.0040	−0.0098	67
69	56559.9127	0.0005	0.0024	70					

*BJD − 2400000.

†Against max = 2456554.3830 + 0.080106 E.

‡Number of points used to determine the maximum.

3.44 MASTER OT J005740.99+443101.5

This object (hereafter MASTER J005740) was detected to be a transient by the MASTER network on 2013 November 6 (Balanutsa et al. 2013a). From subsequent observations early superhumps were immediately detected (vsnet-alert 16603, 16606, 16609). The large amplitude (0.4 mag) of early superhumps suggested a high inclination. There was also an eclipse-like feature in the light curve

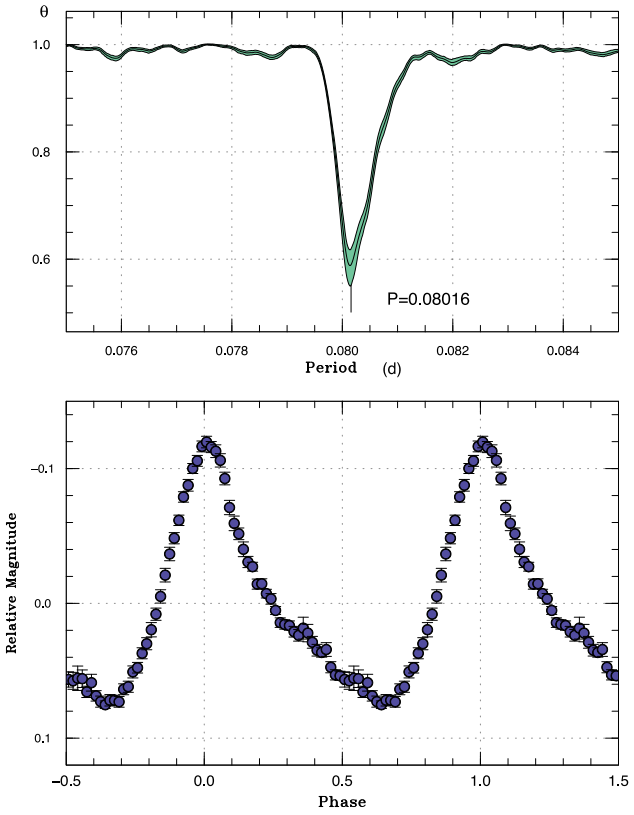

Fig. 53. Superhumps in MASTER J004527 (2013). Upper: PDM analysis. Lower: Phase-averaged profile.

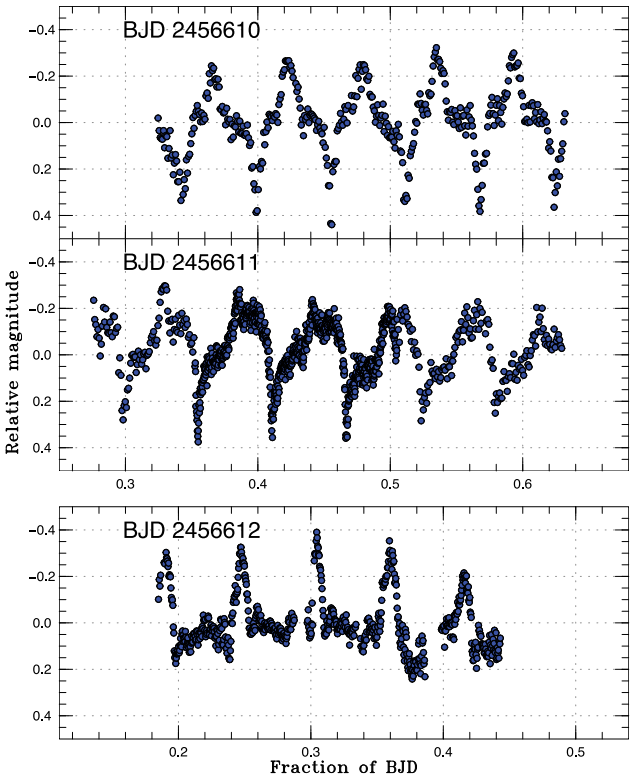

Fig. 54. Superhumps and eclipses in MASTER J005740 (2013). On the first night, eclipses were sharply detected. On the second night, eclipses became less apparent as the superhump maximum approached the eclipses. On the third night, eclipses were not apparent.

(vsnet-alert 16614; see also vsnet-alert 16603). On November 12–13, ordinary superhumps began to appear, and were accompanied by eclipses (vsnet-alert 16624; figure 54). After the light curve faded away on the plateau, the eclipses became deeper ($\sim$1 mag, vsnet-alert 16640), implying that the white dwarf is eclipsed. This object became the first candidate for the WZ Sge-type dwarf nova showing the eclipse of the white dwarf.

We first obtained the eclipse ephemeris using the observations in the phases other than early superhumps, since the profile of early superhumps is similar to, but known to be different from, that of the eclipse (cf. Uemura et al. 2012). We obtained the following ephemeris:

$$\mathrm{Min(BJD)} = 2456617.36772(4) + 0.0561904(3)E, \qquad (4)$$

by using MCMC modeling the some as in V893 Sco. Note that this ephemeris is not intended as a long-term prediction of eclipses, in contrast to other eclipsing dwarf novae treated in this paper, since the eclipse profile is strongly affected by the varying superhumps and systematic variations in relation to the system brightness. The errors given in equation (4) are formal statistic ones, and the actual errors are expected to be larger due to the systematic error.

The times of superhump maxima, determined after removing the data within 0.07 orbital phases of eclipse, are listed in table 50. The $O-C$ diagram is presented in figure 57. The maxima for $E < 14$ are stage A superhumps with growing amplitude. The maxima for $14 \leq E \leq 144$ are stage B superhumps. The times for $144 < E < 245$ were not well determined because the amplitude of superhumps became smaller and the profile was difficult of detection due to the orbital modulation. After $E = 245$, the amplitude of superhumps grew again. These superhumps can be identified as stage C superhumps, which are not usually seen in WZ Sge-type dwarf novae (see Kato et al. 2009).

The period of early superhump by the PDM method was 0.056169(3) d (figure 55), which is 0.04% shorter than the orbital period. A summary of the comparison between periods of early superhumps and orbital periods in various WZ Sge-type dwarf novae is given in subsection 4.4. The zero epoch in this figure is based on the ephemeris equation (4). Since the period of early superhumps and the orbital period are very slightly different, we used the eclipse center nearest to the center of observation of early superhumps. The period used for phase-averaging is that of early superhumps. The profile of these early superhumps and its implication are discussed in subsection 4.5.

Table 50. Superhump maxima of MASTER J005740 (2013).

E	Max*	Error	$O-C$†	Phase‡	N§	E	Max*	Error	$O-C$†	Phase‡	N§
0	56609.3288	0.0012	−0.0089	0.93	70	86	56614.2438	0.0066	0.0011	0.40	25
1	56609.3910	0.0008	−0.0036	0.04	71	87	56614.2953	0.0023	−0.0044	0.32	24
2	56609.4467	0.0014	−0.0050	0.03	64	90	56614.4781	0.0025	0.0073	0.57	27
3	56609.5028	0.0008	−0.0060	0.03	54	92	56614.5781	0.0034	−0.0067	0.35	8
4	56609.5642	0.0008	−0.0016	0.12	46	93	56614.6390	0.0010	−0.0030	0.44	40
14	56610.1370	0.0013	0.0008	0.32	35	94	56614.6940	0.0010	−0.0049	0.42	73
15	56610.1940	0.0007	0.0008	0.33	35	95	56614.7516	0.0015	−0.0044	0.44	63
18	56610.3661	0.0005	0.0019	0.40	50	101	56615.0939	0.0027	−0.0043	0.53	83
19	56610.4235	0.0005	0.0022	0.42	50	109	56615.5609	0.0026	0.0064	0.84	27
20	56610.4785	0.0005	0.0002	0.40	48	110	56615.6153	0.0015	0.0038	0.81	63
21	56610.5352	0.0005	−0.0001	0.40	51	111	56615.6708	0.0014	0.0022	0.80	65
22	56610.5930	0.0007	0.0006	0.43	53	112	56615.7257	0.0025	0.0001	0.78	31
35	56611.3323	0.0007	−0.0016	0.59	51	113	56615.7905	0.0035	0.0079	0.93	26
36	56611.3915	0.0003	0.0006	0.64	193	121	56616.2415	0.0020	0.0026	0.96	17
37	56611.4489	0.0005	0.0009	0.66	198	122	56616.2984	0.0012	0.0024	0.97	69
38	56611.5045	0.0005	−0.0005	0.65	139	123	56616.3527	0.0014	−0.0002	0.94	85
39	56611.5629	0.0008	0.0009	0.69	45	124	56616.4136	0.0012	0.0036	0.02	69
40	56611.6163	0.0008	−0.0028	0.64	44	125	56616.4687	0.0012	0.0016	1.00	37
43	56611.7909	0.0010	0.0008	0.75	37	126	56616.5280	0.0010	0.0039	0.06	37
44	56611.8472	0.0022	0.0000	0.75	35	139	56617.2709	0.0082	0.0054	0.28	19
47	56612.0208	0.0016	0.0025	0.84	31	140	56617.3255	0.0009	0.0030	0.25	38
48	56612.0773	0.0013	0.0019	0.85	25	141	56617.3837	0.0009	0.0041	0.28	47
50	56612.1907	0.0006	0.0013	0.87	46	142	56617.4435	0.0012	0.0069	0.35	45
51	56612.2512	0.0005	0.0048	0.94	103	143	56617.4995	0.0006	0.0058	0.34	47
52	56612.3071	0.0012	0.0037	0.94	75	144	56617.5561	0.0010	0.0053	0.35	33
53	56612.3583	0.0006	−0.0022	0.85	95	154	56618.1461	0.0043	0.0251	0.85	23
54	56612.4155	0.0005	−0.0020	0.87	86	158	56618.3666	0.0036	0.0174	0.78	24
57	56612.5832	0.0016	−0.0055	0.85	30	195	56620.4539	0.0076	−0.0056	0.92	45
59	56612.6998	0.0017	−0.0029	0.93	28	197	56620.5633	0.0040	−0.0103	0.87	34
60	56612.7562	0.0022	−0.0035	0.93	30	213	56621.4701	0.0011	−0.0161	0.01	23
61	56612.8176	0.0025	0.0009	0.02	17	233	56622.6231	0.0040	−0.0038	0.53	26
65	56613.0396	0.0016	−0.0053	0.97	28	245	56623.3129	0.0029	0.0016	0.80	45
75	56613.6132	0.0072	−0.0021	0.18	29	246	56623.3660	0.0022	−0.0023	0.75	53
76	56613.6682	0.0016	−0.0041	0.16	50	247	56623.4269	0.0020	0.0016	0.83	84
77	56613.7265	0.0009	−0.0028	0.20	50	248	56623.4778	0.0013	−0.0046	0.74	65
78	56613.7852	0.0013	−0.0012	0.24	50	249	56623.5386	0.0025	−0.0008	0.82	46
79	56613.8396	0.0036	−0.0038	0.21	50	264	56624.3887	0.0015	−0.0063	0.95	46
85	56614.1919	0.0012	0.0062	0.48	31	265	56624.4452	0.0017	−0.0068	0.96	45

*BJD − 2400000.
†Against max = 2456609.3377 + 0.057035 E.
‡Orbital phase.
§Number of points used for determine the maximum.

The mean profile of stage B superhumps is shown in figure 56. Since the times of superhumps during the growing stage (stage A) were difficult of determination due to the orbital modulation, we also measured the period for the interval BJD 2456608–2456610 by PDM. The resultant period was 0.05783(3) d. This value is slightly different from that of the $O-C$ analysis [0.05758(19) d, $E \leq 14$], which was probably more affected by the shorter period close to stage B. We therefore chose the former period as the representative period of stage A. The resultant ε^* of 0.028(5) corresponds to $q = 0.076(16)$.

A two-dimensional Lasso analysis is presented in figure 58. As in the eclipsing WZ Sge-type dwarf nova WZ Sge (Kato et al. 2014a), the orbital signal was continuously seen. The superhump signal with a decreasing frequency (increasing period) during the plateau phase of the superoutburst is also clearly visible.

3.45 MASTER OT J024847.86+501239.7

This object (hereafter MASTER J024847) was detected to be a transient by the MASTER network on 2013

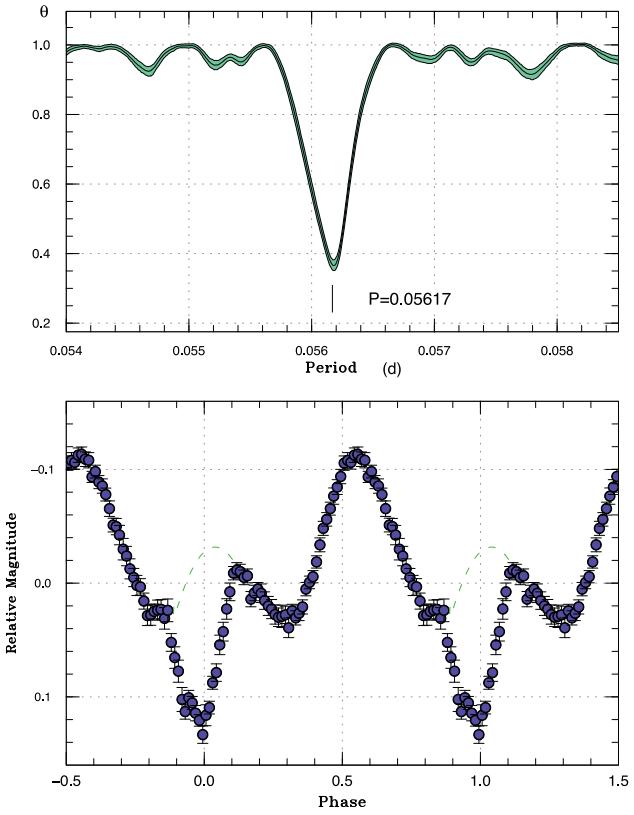

Fig. 55. Early superhumps in MASTER J005740 (2013). Upper: PDM analysis. Lower: Phase-averaged profile. The phase is relative to the eclipse ephemeris (see text for details). The dashed line represents a hypothetical hump maximum without an eclipse.

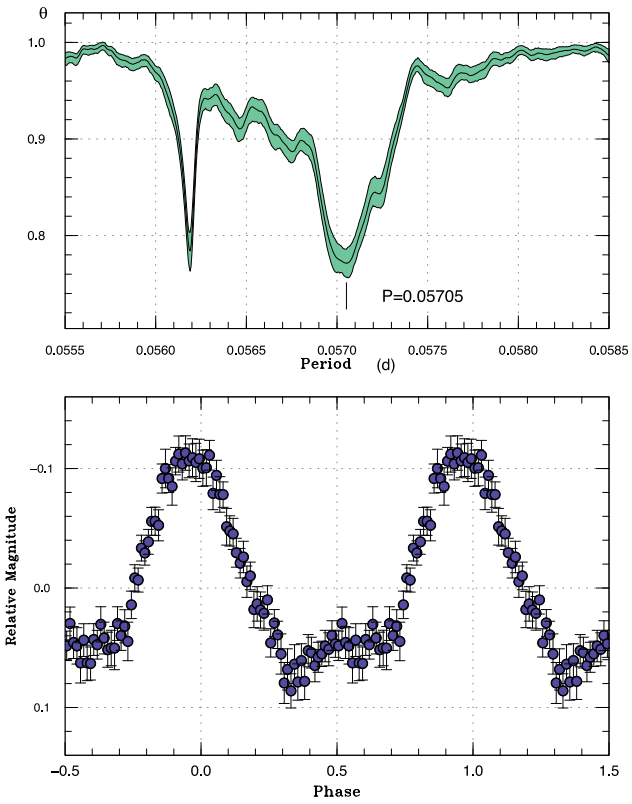

Fig. 56. Ordinary superhumps in MASTER J005740 (2013). The segment of stage B superhumps was used. Upper: PDM analysis. Lower: Phase-averaged profile. The sharp signal at 0.05619 d is the orbital period.

November 11 (Denisenko et al. 2013a). From subsequent observations superhumps were detected immediately (vsnet-alert 16619; figure 59). A single-night observation yielded the following times of superhump maxima: BJD 2456609.3402(7) ($E = 62$), 2456609.4043(8) ($E = 62$), and 2456609.4683(12) ($E = 65$). A PDM analysis yielded a period of 0.0644(3) d.

3.46 MASTER OT J061335.30+395714.7

This object (hereafter MASTER J061335) was detected to be a bright (14.2 mag) transient by the MASTER network on 2013 October 15 (Vladimirov et al. 2013). After a period without strong modulations, growing superhumps were detected (vsnet-alert 16554, 16555, 16556, 16563, 16567; figure 60). The times of superhump maxima are listed in table 51. There are well-defined stages A–B–C (figure 61), although the period of stage A superhumps was not determined. Although early superhumps were potentially present for the first two nights, we could not detect their period due to the shortness of the observation. There was significant brightening around the stage B–C transition (figure 61).

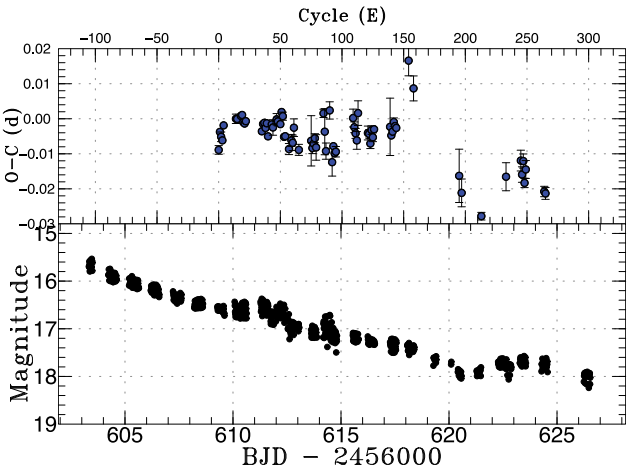

Fig. 57. $O-C$ diagram of superhumps in MASTER J005740 (2013). Upper: $O-C$ diagram. A period of 0.05709 d was used to draw this figure. Lower: Light curve. The observations were binned to 0.011 d.

3.47 MASTER OT J073208.11+064149.5

This object (hereafter MASTER J073208) was detected to be a large-amplitude (~ 7 mag) transient by the MASTER network on 2013 December 29 (Balanutsa et al. 2013b). The object indeed showed short-period superhumps (vsnet-alert 16747, 16756). The times of superhump maxima are listed in table 52. Although a PDM analysis favors a

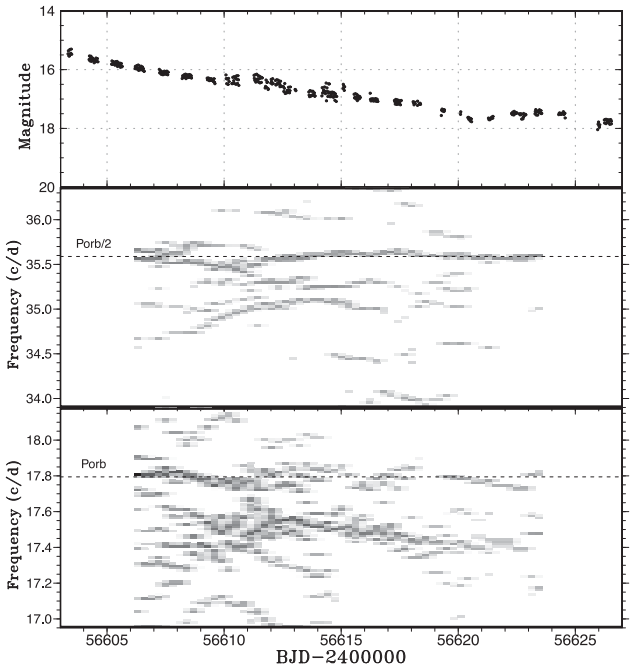

Fig. 58. Lasso analysis of MASTER J005740 (2013). Upper: Light curve. The data were binned to 0.02 d. Middle: First overtones of the superhump and orbital signals. Lower: Fundamentals of the superhump and the orbital signal. The orbital signal was present both in the fundamental and in the first overtone. The signal of (positive) superhumps with variable frequency was recorded during the superoutburst plateau. No indication of negative superhump was present. The parameter $\log\lambda = -8.7$ was used. The width of the sliding window and the time step used were 6 d and 0.3 d, respectively.

period of 0.05878(2) d, a shorter alias of 0.05722(2) d is not excluded (figure 62).

3.48 MASTER OT J095018.04−063921.9

This object (hereafter MASTER J095018) was detected to be a 14.1 mag transient by the MASTER network on 2013 November 11 (Rufanov et al. 2013). From subsequent observations superhumps were detected immediately (vsnet-alert 16631, 16659; figure 63). Although a period of 0.06681(3) d was initially reported, a reanalysis of the data clarified that this is double the value of the true variation (see also figure 63). A PDM analysis of all data yielded a period of 0.033409(4) d (figure 64). The profile, however, is not similar to that of ordinary superhumps, but resembles that of early superhumps with double maxima (cf. Kato 2002). An $O-C$ analysis did not show significant period variation.

The period suggests a system with a compact, evolved secondary such as SBS 1108+574 (Kato et al. 2013b; Littlefield et al. 2013; Carter et al. 2013). If the present variation is indeed due to early superhumps, data from the present observation are the first to reveal early superhumps in such

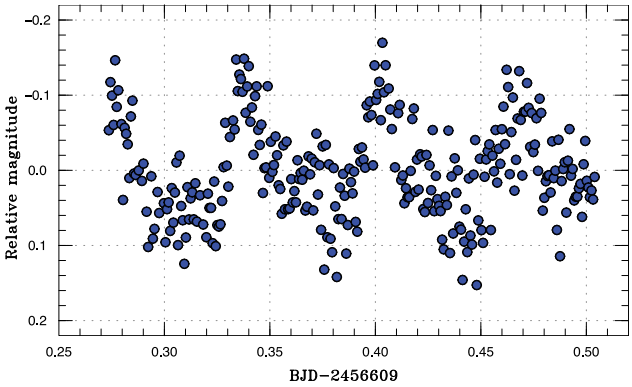

Fig. 59. Superhumps in MASTER J024847.

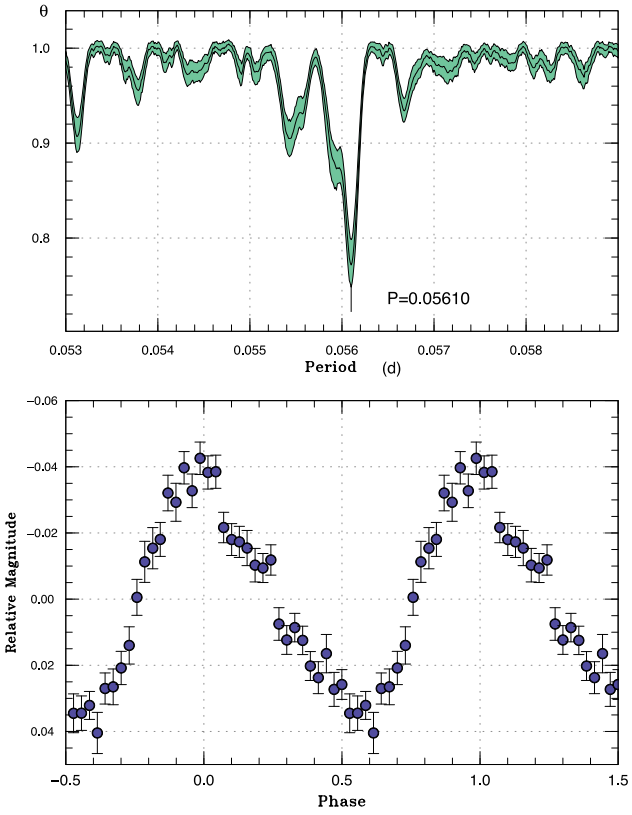

Fig. 60. Possible early superhumps in MASTER J061335 (2013). Upper: PDM analysis. Lower: Phase-averaged profile.

systems. We preserve this possibility for future observations since we could not follow the latter stage, when its ordinary superhumps were expected. On the last two nights (November 24 and 25), the double-wave modulation became less apparent and waves with a period of $\sim$0.08 d seemed to appear. We, however, were not confident of presence of this periodicity due to the limited signal-to-noise ratio of this faint object.

Table 51. Superhump maxima of MASTER J061335 (2013).

E	Max*	Error	$O-C^{\dagger}$	$N^{\ddagger}$
0	56587.2100	0.0013	0.0042	119
1	56587.2635	0.0007	0.0016	167
61	56590.6387	0.0007	0.0099	56
62	56590.6942	0.0009	0.0094	37
76	56591.4781	0.0015	0.0076	32
77	56591.5312	0.0010	0.0047	31
78	56591.5864	0.0009	0.0038	30
79	56591.6400	0.0013	0.0012	21
90	56592.2572	0.0008	0.0012	41
91	56592.3116	0.0008	−0.0006	41
93	56592.4240	0.0007	−0.0004	35
94	56592.4804	0.0007	−0.0001	90
95	56592.5368	0.0007	0.0002	74
96	56592.5916	0.0015	−0.0011	30
108	56593.2630	0.0009	−0.0031	46
109	56593.3207	0.0006	−0.0015	101
110	56593.3777	0.0004	−0.0006	51
143	56595.2393	0.0080	0.0093	36
144	56595.2768	0.0053	−0.0094	33
146	56595.3958	0.0019	−0.0026	31
162	56596.2882	0.0012	−0.0080	58
163	56596.3477	0.0008	−0.0046	95
164	56596.3997	0.0065	−0.0087	27
165	56596.4576	0.0006	−0.0069	67
166	56596.5147	0.0005	−0.0060	77
167	56596.5675	0.0010	−0.0092	39
179	56597.2461	0.0026	−0.0040	35
180	56597.3000	0.0025	−0.0063	41
181	56597.3606	0.0106	−0.0018	20
185	56597.5773	0.0025	−0.0095	23
186	56597.6408	0.0019	−0.0021	19
197	56598.2544	0.0037	−0.0057	50
268	56602.2595	0.0067	0.0153	41
269	56602.3072	0.0057	0.0068	40
303	56604.2153	0.0027	0.0071	36
304	56604.2665	0.0014	0.0022	41
305	56604.3244	0.0023	0.0040	41
321	56605.2218	0.0054	0.0036	44

*BJD − 2400000.
†Against max = 2456587.2058 + 0.056114 E.
‡Number of points used to determine the maximum.

3.49 MASTER OT J141143.46+262051.5

This object (hereafter MASTER J141143) was detected to be a transient (15.4 mag) by the MASTER network on 2013 February 13 (Shumkov et al. 2013). The object was again detected in outburst on 2014 January 30. The outburst was caught in the early stage (vsnet-alert 16852). The only available observation on February 5 showed superhumps with an amplitude of 0.15 mag (vsnet-alert 16881; figure 65). The period was determined by the PDM method—0.064(1) d. The times of superhump maxima were BJD 2456693.5806(9) ($N = 35$) and 2456693.6466(9) ($N = 33$).

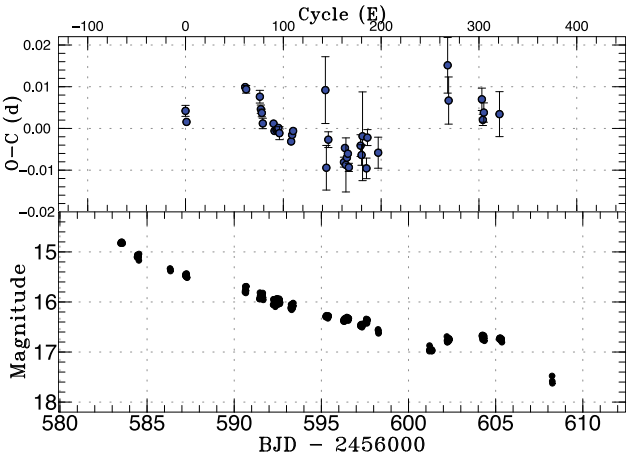

Fig. 61. $O-C$ diagram of superhumps in MASTER J061335 (2013). Upper: $O-C$ diagram. A period of 0.056114 d was used for drawing this figure. Lower: Light curve. The observations were binned to 0.011 d.

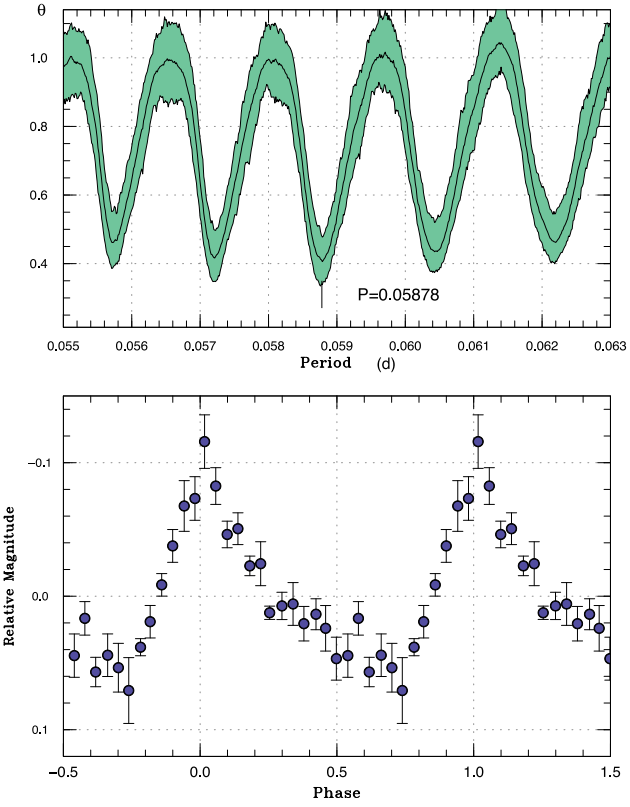

Fig. 62. (Early?) superhumps in MASTER J073208 (2013). Upper: PDM analysis. Lower: Phase-averaged profile.

3.50 MASTER OT J162323.48+782603.3

This object (hereafter MASTER J162323) was detected to be a bright (13.0 mag) transient by the MASTER network on 2013 December 9 (Denisenko et al. 2013b). There were a number of past ROSAT chance observations, showing a relatively soft source with variable intensity (vsnet-alert 16698). From subsequent observations modurations were detected immediately modulations were

Table 52. Superhump maxima of MASTER J073208 (2013).

E	Max*	Error	$O-C$†	N‡
0	56658.3918	0.0018	−0.0028	15
1	56658.4553	0.0006	0.0018	40
2	56658.5134	0.0007	0.0010	23
37	56660.5747	0.0007	0.0031	20
38	56660.6273	0.0011	−0.0031	42

*BJD − 2400000.
†Against max = 2456658.3947 + 0.058836 E.
‡Number of points used to determine the maximum.

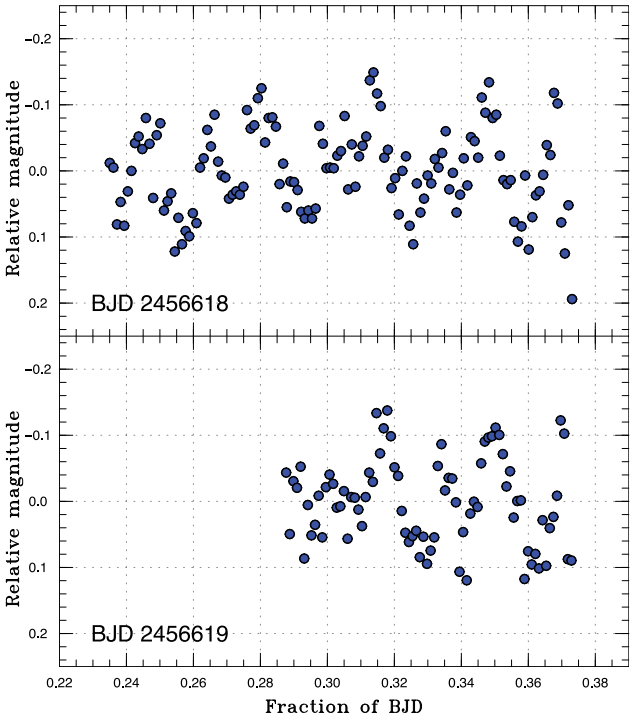

Fig. 63. Example of (early?) superhumps in MASTER J095018 on two nights.

detected immediately (vsnet-alert 16703) and were followed by growing superhumps (vsnet-alert 16706, 16716, 16717, 16723; figure 66). The times of superhump maxima are listed in table 53. There were clear stages A and B. There was no variation of the superhump period around the rapid fading. There was an apparent decrease in period 5 d after the fading (around $E = 200$). We interpret the superhumps up to $E = 192$ as stage B superhumps and list the period in table 2. The resultant $P_{\rm dot}$ of $+3.9(9) \times 10^{-5}$ for stage B again offers another example of the positive $P_{\rm dot}$ in the long-$P_{\rm orb}$ system—such examples include GX Cas (Kato et al. 2012b), V1239 Her, OT J145921.8+354806, OT J214738.4+244553 (Kato et al. 2013b), V444 Peg, CSS J203937.7−042907, and MASTER OT J212624.16+253827.2 (Kato et al. 2014a).

The quiescent SDSS colors suggest an orbital period of 0.072 d based on Kato, Maehara, and Uemura (2012a).

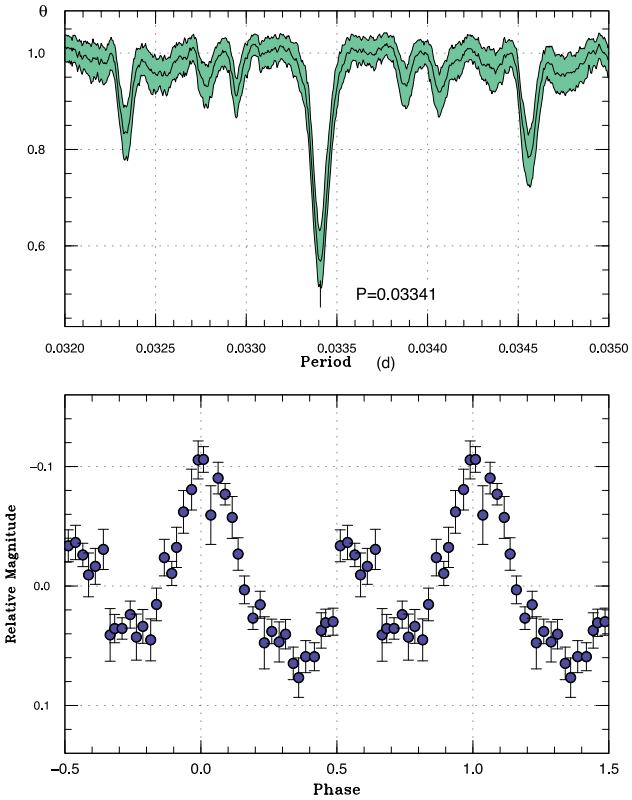

Fig. 64. (Early?) superhumps in MASTER J095018 (2013). Upper: PDM analysis. Lower: Phase-averaged profile.

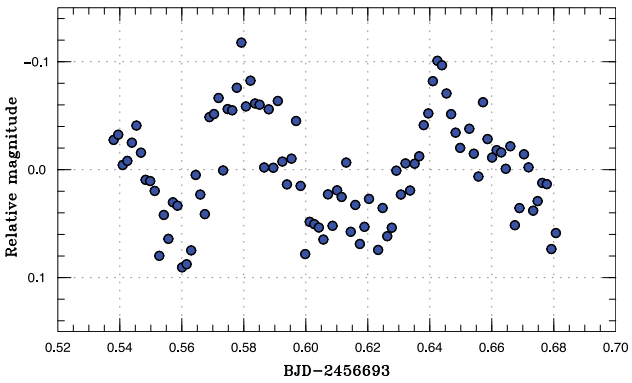

Fig. 65. Superhumps in MASTER J141143 on 2014 February 5.

This relatively long orbital period for an SU UMa-type dwarf nova is in agreement with the present observation. The object was twice detected in outburst in 2012 by the MASTER network (Denisenko et al. 2013b). The supercycle appears to be less than 1 yr. Since the object is bright and frequently outbursting, future observations, including the determination of the orbital period, will be promising.

3.51 MASTER OT J234843.23+250250.4

This object (hereafter MASTER J234843) was detected to be a 14.4 mag transient by the MASTER network on 2013

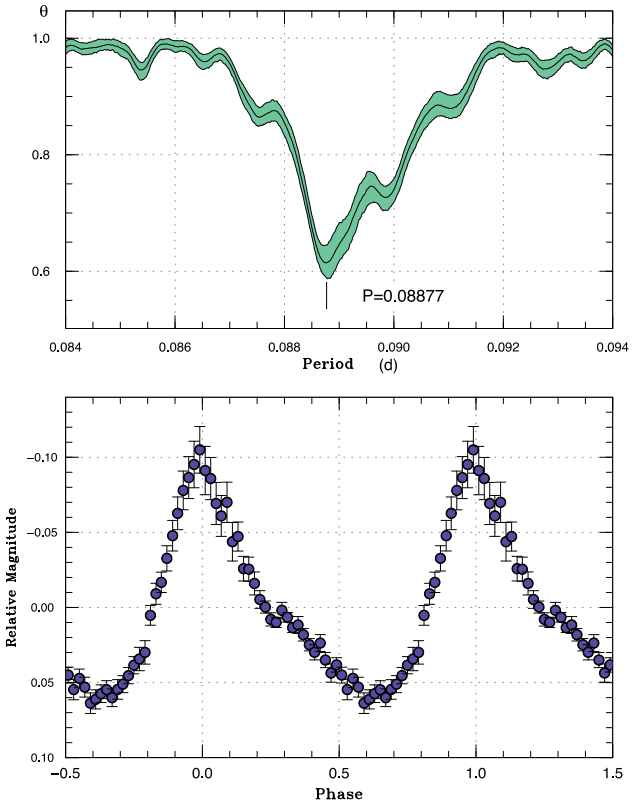

Fig. 66. Superhumps in MASTER J162323 during the superoutburst plateau (2013). Upper: PDM analysis. Lower: Phase-averaged profile.

October 29 (Shurpakov et al. 2013). The object has a faint, blue ($g = 20.2$, $g - r = -0.1$) SDSS counterpart. Five previous outbursts were recorded by CRTS.

From subsequent observations modulations resembling early superhumps were detected (vsnet-alert 16577, 16578). Later observations, however, indicated that their period was half what was initially suggested (figure 67), and the object was recognized as a CV below the period minimum (vsnet-alert 16608; the superhump profile is shown in figure 68). The times of superhump maxima based on this interpretation are listed in table 54. Although the data were not sufficient, the $O - C$ values suggest that there was a stage B–C transition around $E = 252$ as in SBS 1108+574, a similar ultrashort-$P_{\rm orb}$ dwarf nova (Kato et al. 2013b). The outburst light curve and $O - C$ diagram are shown in figure 69.

Although spectroscopic observation is needed to see whether this object is hydrogen-rich or not, we suspect that this object is a binary containing hydrogen in the secondary with an evolved core rather than a hydrogen-depleted AM CVn-type binary, since the known AM CVn-type objects with this $P_{\rm orb}$ do not show outbursts (cf. Solheim 2010; Ramsay et al. 2012). Further detailed observations will clarify the nature of this object.

Table 53. Superhump maxima of MASTER J162323 (2013).

E	Max*	Error	$O - C^{\dagger}$	$N^{\ddagger}$
0	56637.5690	0.0011	−0.0542	94
1	56637.6655	0.0020	−0.0464	86
2	56637.7684	0.0012	−0.0323	46
19	56639.3104	0.0006	0.0021	40
20	56639.3987	0.0002	0.0017	177
21	56639.4874	0.0003	0.0017	157
22	56639.5749	0.0008	0.0005	12
23	56639.6642	0.0007	0.0011	12
30	56640.2879	0.0010	0.0040	17
31	56640.3795	0.0002	0.0069	159
32	56640.4681	0.0003	0.0068	165
33	56640.5578	0.0003	0.0078	112
35	56640.7456	0.0014	0.0182	9
42	56641.3661	0.0028	0.0179	24
44	56641.5352	0.0003	0.0096	66
45	56641.6238	0.0008	0.0095	25
46	56641.7088	0.0009	0.0059	12
56	56642.6015	0.0007	0.0116	56
57	56642.6897	0.0015	0.0112	16
67	56643.5716	0.0012	0.0062	10
68	56643.6643	0.0019	0.0102	15
79	56644.6320	0.0031	0.0023	15
98	56646.3168	0.0005	0.0020	73
99	56646.4037	0.0005	0.0003	112
101	56646.5840	0.0018	0.0032	12
102	56646.6708	0.0010	0.0012	15
135	56649.5986	0.0057	0.0024	16
136	56649.6894	0.0021	0.0044	16
143	56650.3106	0.0012	0.0048	44
153	56651.2012	0.0055	0.0086	28
154	56651.2825	0.0012	0.0012	50
155	56651.3732	0.0011	0.0031	50
156	56651.4641	0.0063	0.0053	13
180	56653.5948	0.0027	0.0075	13
181	56653.6807	0.0100	0.0047	13
187	56654.2236	0.0044	0.0155	18
188	56654.3132	0.0028	0.0164	13
192	56654.6519	0.0030	0.0004	21
223	56657.3771	0.0015	−0.0238	30
224	56657.4603	0.0018	−0.0293	28
244	56659.2330	0.0013	−0.0304	14

*BJD − 2400000.
†Against max = 2456637.6232 + 0.088689 E.
‡Number of points used to determine the maximum.

3.52 OT J013741.1+220312

This object was detected to be an unknown type of transient by CRTS (= CSS140104:013741+220312, hereafter OT J013741) on 2014 January 4. There was no previous outburst detection in CRTS. From subsequent observations double-wave early superhumps with a mean period of 0.05854(2) d were detected (vsnet-alert 16765,

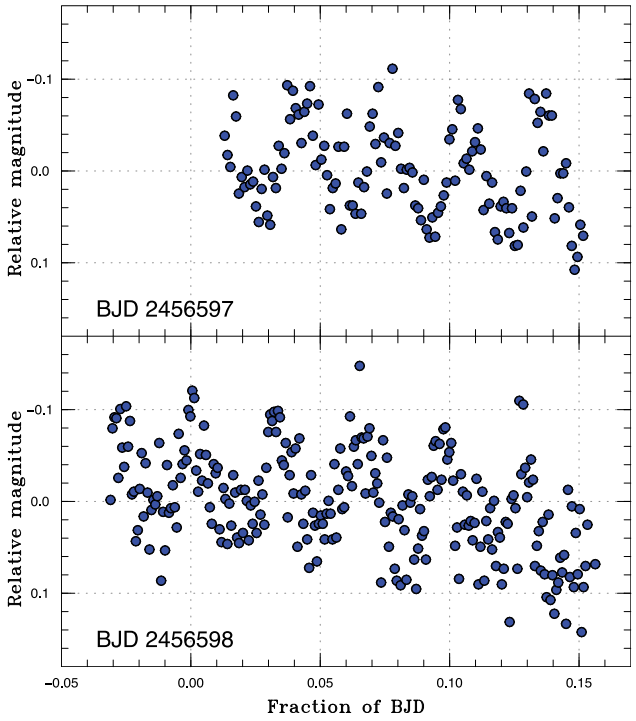

Fig. 67. Example of superhumps in MASTER J234843 on two nights.

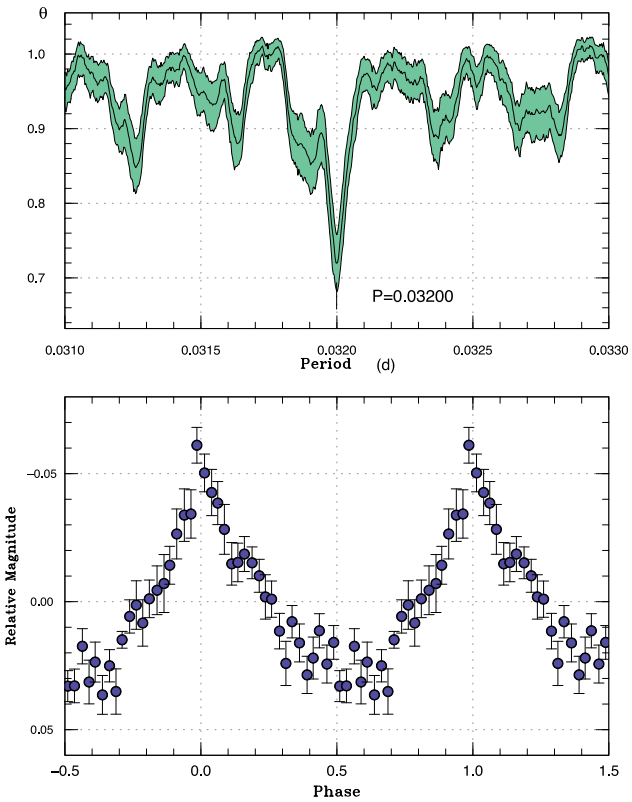

Fig. 68. Superhumps in MASTER J234843 during the superoutburst plateau (2013). Upper: PDM analysis. Lower: Phase-averaged profile.

16769; figure 70). Only the stage of early superhumps was observed.

3.53 OT J210016.0−024258

This object was detected to be a transient by CRTS (= CSS130905:210016−024258, hereafter OT J210016) on 2013 September 5. The quiescent counterpart has an SDSS magnitude of $g = 19.9$, implying a dwarf nova with a large outburst amplitude (vsnet-alert 16347).

Low-amplitude modulations resembling early superhumps were recorded until September 12 (vsnet-alert 16362; figure 71). From September 16, ordinary superhumps appeared (vsnet-alert 16420, 16430; figure 72). The times of ordinary superhumps are listed in table 55. Although observational data at the earliest epochs may contain stage A superhumps, we could not convincingly detect stage A. Since $E = 0$ and $E = 1$ were probably obtained during the growing stage of superhumps, we excluded these epochs when determining $P_{\rm dot}$ of stage B superhumps.

The object rapidly faded on the superoutburst plateau on September 29. It showed a post-superoutburst rebrightening on October 6 (around 17.4 mag—all magnitudes during this rebrightening were unfiltered CCD ones; vsnet-alert 16525). The snapshot CCD observations indicate that this object was already bright on October 1 (16.86 mag) and October 4 (17.55 mag). These observations indicate that the faint state following the superoutburst plateau lasted less than 2 d. This fading was probably a "dip" type between the main superoutburst and long rebrightening as seen in the WZ Sge-type dwarf nova AL Com (1995, cf. Nogami et al. 1997). The WZ Sge-type nature is supported by the likely presence of early superhumps, the large outburst amplitude, and the lack of past outburst detections in the CRTS data.

3.54 PNV J19150199+0719471

This object (hereafter PNV J191501) was detected to be a possible nova of 10.8 mag on 2013 May 31.5974 UT (Itagaki et al. 2013).[6] The object was detected at 9.8 mag on May 30.721 UT by T. Kojima. The object was identified as an Hα emission object IPHAS J191502.09+071947.6 ($r = 18.503$, Drew et al. 2005), and its color and large proper motion suggested the object as a dwarf nova rather than a classical nova (vsnet-alert 15768). The object was then regarded as a likely candidate for a WZ Sge-type dwarf nova (vsnet-alert 15776). Although data of subsequent observations revealed small variations suggesting early superhumps (vsnet-alert 15778, 15785, 15788), the period was difficult of determination due to the low amplitude. We will deal with this issue later.

[6] See also ⟨http://www.cbat.eps.harvard.edu/unconf/followups/J19150199+0719471.html⟩.

Table 54. Superhump maxima of MASTER J234843 (2013).

E	Max*	Error	$O-C$†	N‡
0	56595.2868	0.0025	0.0032	13
1	56595.3167	0.0005	0.0011	33
2	56595.3480	0.0004	0.0005	26
3	56595.3803	0.0004	0.0008	34
4	56595.4106	0.0005	−0.0009	29
5	56595.4431	0.0005	−0.0004	26
54	56597.0157	0.0019	0.0043	15
55	56597.0420	0.0007	−0.0014	23
56	56597.0747	0.0010	−0.0007	23
57	56597.1052	0.0007	−0.0021	23
58	56597.1358	0.0007	−0.0036	23
84	56597.9728	0.0012	0.0015	22
85	56598.0007	0.0006	−0.0026	34
86	56598.0335	0.0007	−0.0018	34
87	56598.0651	0.0009	−0.0021	34
88	56598.0978	0.0008	−0.0015	35
89	56598.1285	0.0009	−0.0028	34
249	56603.2517	0.0009	0.0009	22
250	56603.2836	0.0017	0.0007	28
251	56603.3156	0.0019	0.0008	28
252	56603.3543	0.0014	0.0075	19
253	56603.3825	0.0016	0.0037	26
254	56603.4137	0.0019	0.0028	28
255	56603.4427	0.0018	−0.0001	28
275	56604.0826	0.0017	−0.0002	23
276	56604.1165	0.0038	0.0017	22
277	56604.1430	0.0011	−0.0038	24
436	56609.2325	0.0018	−0.0018	15
437	56609.2655	0.0053	−0.0008	17
438	56609.2952	0.0034	−0.0030	16

*BJD − 2400000.
†Against max = 2456595.2835 + 0.031997 E.
‡Number of points used to determine the maximum.

In the meantime, low-resolution spectra confirmed that the object is classified as a type of dwarf nova (vsnet-alert 15779). The spectrum showed double-peak Hβ emission line and a C III/N III emission line, suggesting that this object is a WZ Sge-type dwarf nova with a moderate inclination (vsnet-alert 15782). Further spectroscopic observations were also reported (vsnet-alert 15787, 15800). The latter spectrum showed Balmer series in absorption with emission cores in Hα and Hβ. Nakata et al. (2013a) also reported on a UV spectrum taken by the Swift satellite.

Six days after the discovery, modulations suggesting growing superhumps appeared (vsnet-alert 15815; the actual variations could be detected two days before). The times of superhump maxima during the superoutburst plateau are listed in table 56. The profile is shown in figure 73. There were remarkably well-sampled stages B and C. The existence of stage C in a WZ Sge-type dwarf nova is rather exceptional. Although stage A was detected,

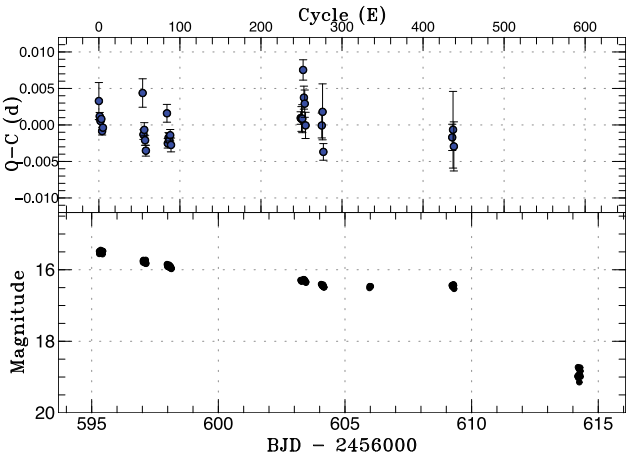

Fig. 69. $O-C$ diagram of superhumps in MASTER J234843 (2013). Upper: $O-C$ diagram. A period of 0.031997 d was used for drawing this figure. Lower: Light curve. The observations were binned to 0.010 d.

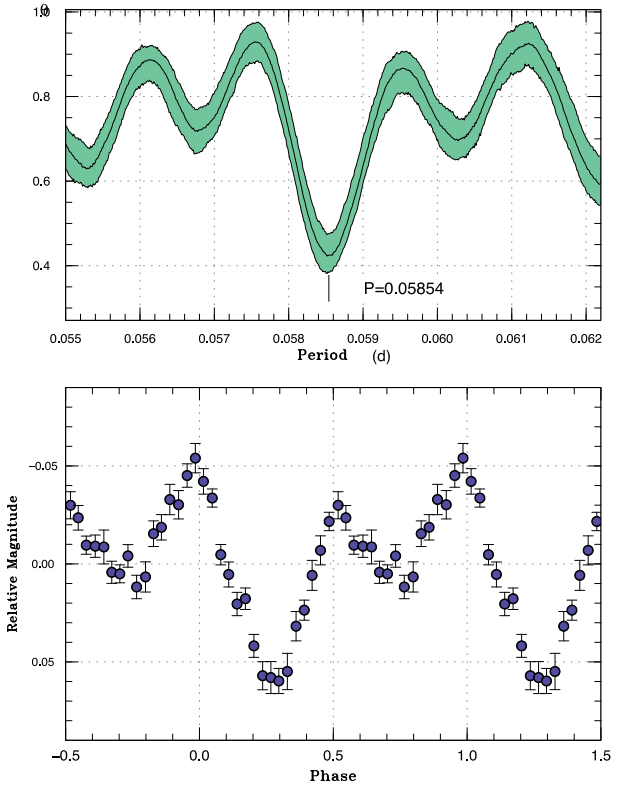

Fig. 70. Early superhumps in OT J013741 (2013). Upper: PDM analysis. Lower: Phase-averaged profile.

a lack of observations for 1 d due to bad weather hindered us from measuring the period of stage A superhumps from the $O-C$ analysis. A PDM analysis during the interval of BJD 2456449–2456452 yielded a period of 0.05883(6) d with an amplitude of 0.015 mag.

After the superoutburst rapidly faded, the superhump signal became strong again. The times of these post-superoutburst superhumps are listed in table 57. The data indicate that there was a phase jump of $\sim$0.5 between

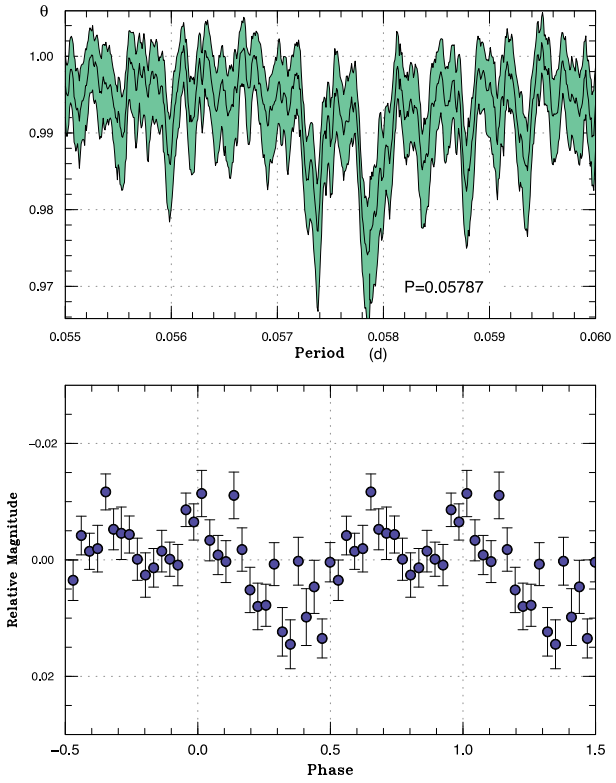

Fig. 71. Possible early superhumps in OT J210016 (2013). Upper: PDM analysis. The rejection rate for bootstraping was reduced to 0.3. Lower: Phase-averaged profile.

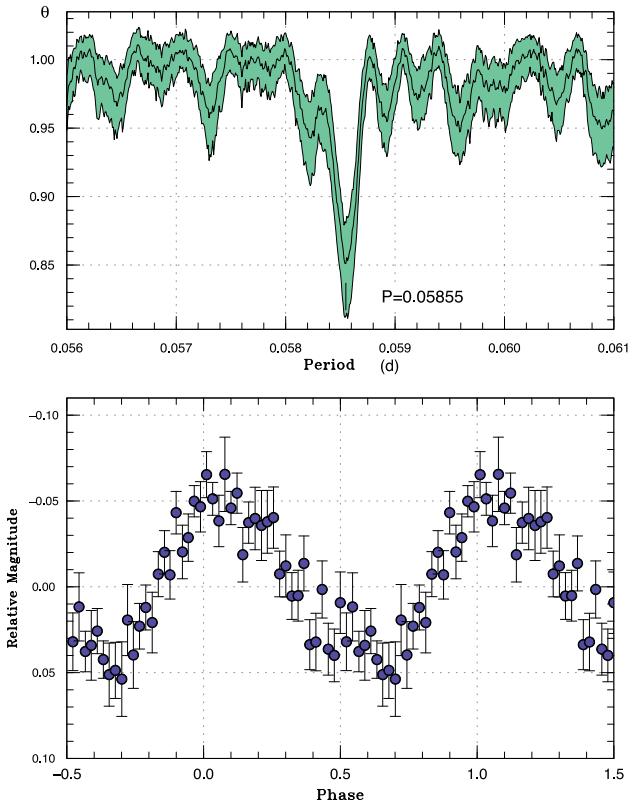

Fig. 72. Ordinary superhumps in OT J210016 (2013). Upper: PDM analysis. Lower: Phase-averaged profile.

Table 55. Superhump maxima of OT J210016 (2013).

E	Max*	Error	$O-C^{\dagger}$	$N^{\ddagger}$
0	56552.0076	0.0014	−0.0070	40
1	56552.0764	0.0018	0.0033	61
17	56553.0093	0.0007	−0.0001	60
18	56553.0705	0.0006	0.0027	61
34	56554.0039	0.0014	−0.0002	47
35	56554.0678	0.0014	0.0052	47
57	56555.3469	0.0013	−0.0030	47
58	56555.4057	0.0010	−0.0027	46
59	56555.4675	0.0015	0.0006	47
60	56555.5296	0.0030	0.0042	17
108	56558.3312	0.0109	−0.0030	17
109	56558.3908	0.0008	−0.0019	44
110	56558.4503	0.0010	−0.0008	45
160	56561.3796	0.0012	0.0027	31

*BJD − 2400000.
†Against max = 2456552.0146 + 0.058514 E.
‡Number of points used to determine the maximum.

BJD 2456472.295 and BJD 2456472.688. A combined $O-C$ diagram (figure 74), however, indicates that the superhumps in the post-superoutburst stage are on a smooth extension of stage C superhumps. The signal of reversed phases (likely corresponding to "traditional" late superhumps) appeared only briefly near the rapid fading.

The signal of early superhumps was very weak and the period of 0.05706(2) d is the only candidate in the region of the period of early superhumps expected from the superhump period (figure 75). Although the fractional excess of stage A superhumps based on the $O-C$ analysis corresponds to $q = 0.095(4)$, this measurement suffers from uncertainties arising from the low amplitudes of both early superhumps and stage A superhumps. Future determination of the orbital period will be necessary for confirming this value.

A two-dimensional Lasso analysis is presented in figure 76. The superhumps with increasing frequencies (decreasing periods) after the superoutburst are clearly seen. The overall behavior resembles that of an SU UMa-type dwarf nova rather than an extreme WZ Sge-type dwarf nova (cf. WZ Sge in Kato et al. 2014a), except for the possible presence of early superhumps.

3.55 SSS J094327.3−272038

This object (= SSS111226:094327−272039, hereafter SSS J094327) was discovered to be a transient object by the CRTS Siding Spring Survey (SSS) on 2011 December 26 at an unfiltered CCD magnitude of 16.6. The object, however, showed several outbursts reaching $V = 12.8$ mag in ASAS-3 data (vsnet-alert 14013). There is also an X-ray

Table 56. Superhump maxima of PNV J191501 (2013).

E	Max*	Error	$O-C^{\dagger}$	$N^{\ddagger}$	E	Max*	Error	$O-C^{\dagger}$	$N^{\ddagger}$
0	56449.3764	0.0010	−0.0056	221	167	56459.1236	0.0025	−0.0094	83
1	56449.4229	0.0025	−0.0175	222	168	56459.1862	0.0002	−0.0051	199
2	56449.4826	0.0010	−0.0162	211	169	56459.2426	0.0002	−0.0071	204
7	56449.7761	0.0018	−0.0146	64	170	56459.3015	0.0002	−0.0066	202
8	56449.8298	0.0012	−0.0193	313	171	56459.3604	0.0003	−0.0061	201
24	56450.7898	0.0009	0.0064	124	172	56459.4240	0.0007	−0.0009	72
25	56450.8453	0.0019	0.0035	154	173	56459.4773	0.0003	−0.0059	172
30	56451.1402	0.0006	0.0065	784	174	56459.5371	0.0003	−0.0046	181
48	56452.1993	0.0005	0.0146	98	175	56459.5924	0.0002	−0.0077	183
49	56452.2646	0.0009	0.0215	126	176	56459.6519	0.0009	−0.0066	71
58	56452.7916	0.0005	0.0230	32	177	56459.7101	0.0010	−0.0067	15
59	56452.8486	0.0002	0.0217	51	178	56459.7702	0.0006	−0.0051	142
71	56453.5446	0.0002	0.0170	63	179	56459.8276	0.0004	−0.0060	147
74	56453.7190	0.0003	0.0162	38	180	56459.8857	0.0004	−0.0063	147
75	56453.7754	0.0003	0.0142	53	181	56459.9445	0.0005	−0.0059	129
76	56453.8347	0.0003	0.0151	89	183	56460.0628	0.0004	−0.0043	81
77	56453.8929	0.0002	0.0150	99	184	56460.1196	0.0003	−0.0059	94
104	56455.4592	0.0014	0.0048	45	185	56460.1869	0.0008	0.0030	421
105	56455.5171	0.0002	0.0042	92	186	56460.2359	0.0005	−0.0065	614
106	56455.5754	0.0002	0.0042	92	187	56460.2919	0.0010	−0.0088	370
107	56455.6345	0.0003	0.0049	108	190	56460.4692	0.0002	−0.0067	228
109	56455.7499	0.0002	0.0035	97	191	56460.5278	0.0003	−0.0064	208
110	56455.8079	0.0002	0.0031	114	192	56460.5861	0.0003	−0.0065	176
111	56455.8665	0.0001	0.0033	113	193	56460.6474	0.0008	−0.0036	108
112	56455.9241	0.0002	0.0025	113	195	56460.7645	0.0005	−0.0033	91
116	56456.1595	0.0003	0.0044	651	196	56460.8177	0.0007	−0.0085	232
122	56456.5059	0.0003	0.0005	181	197	56460.8783	0.0005	−0.0063	241
123	56456.5645	0.0003	0.0006	101	198	56460.9369	0.0006	−0.0061	79
124	56456.6218	0.0003	−0.0004	89	199	56460.9989	0.0006	−0.0025	22
132	56457.0887	0.0002	−0.0007	238	205	56461.3464	0.0009	−0.0053	70
133	56457.1520	0.0030	0.0043	183	206	56461.4080	0.0023	−0.0021	176
134	56457.2050	0.0001	−0.0011	586	207	56461.4647	0.0004	−0.0038	207
135	56457.2618	0.0001	−0.0027	566	208	56461.5200	0.0005	−0.0069	196
136	56457.3217	0.0002	−0.0012	97	211	56461.7135	0.0024	0.0114	72
137	56457.3803	0.0003	−0.0010	192	212	56461.7574	0.0006	−0.0031	161
138	56457.4391	0.0003	−0.0006	221	213	56461.8138	0.0009	−0.0050	179
139	56457.4958	0.0002	−0.0022	303	214	56461.8763	0.0013	−0.0009	247
140	56457.5550	0.0003	−0.0015	121	215	56461.9288	0.0019	−0.0068	146
141	56457.6122	0.0002	−0.0026	105	224	56462.4541	0.0014	−0.0070	76
143	56457.7287	0.0003	−0.0029	132	225	56462.5174	0.0010	−0.0021	92
144	56457.7872	0.0002	−0.0028	156	226	56462.5758	0.0011	−0.0021	87
145	56457.8450	0.0002	−0.0034	163	227	56462.6359	0.0012	−0.0004	120
146	56457.9028	0.0002	−0.0040	124	229	56462.7502	0.0007	−0.0029	153
150	56458.1365	0.0004	−0.0039	234	230	56462.8088	0.0008	−0.0026	195
151	56458.1950	0.0004	−0.0037	394	231	56462.8654	0.0004	−0.0045	251
152	56458.2567	0.0009	−0.0004	77	232	56462.9244	0.0010	−0.0038	89
155	56458.4271	0.0003	−0.0052	44	236	56463.1602	0.0005	−0.0016	208
156	56458.4866	0.0005	−0.0041	33	237	56463.2184	0.0006	−0.0018	210
157	56458.5451	0.0003	−0.0039	66	238	56463.2811	0.0012	0.0026	208
161	56458.7791	0.0003	−0.0035	137	239	56463.3324	0.0009	−0.0045	257
162	56458.8365	0.0003	−0.0045	183	240	56463.3952	0.0008	−0.0001	251
163	56458.8933	0.0003	−0.0061	180	241	56463.4557	0.0011	0.0020	84
164	56458.9516	0.0003	−0.0062	98	242	56463.5102	0.0007	−0.0019	63

Table 56. (Continued)

E	Max*	Error	$O-C^{\dagger}$	$N^{\ddagger}$	E	Max*	Error	$O-C^{\dagger}$	$N^{\ddagger}$
243	56463.5670	0.0007	−0.0035	61	295	56466.6151	0.0004	0.0085	118
244	56463.6315	0.0020	0.0026	102	297	56466.7380	0.0028	0.0145	16
246	56463.7500	0.0014	0.0043	64	308	56467.3717	0.0008	0.0060	111
247	56463.8061	0.0018	0.0020	59	309	56467.4320	0.0012	0.0079	136
248	56463.8603	0.0010	−0.0021	112	310	56467.4883	0.0007	0.0058	88
249	56463.9201	0.0018	−0.0007	43	311	56467.5487	0.0009	0.0078	63
253	56464.1579	0.0007	0.0035	206	313	56467.6581	0.0006	0.0004	34
254	56464.2148	0.0008	0.0020	206	326	56468.4267	0.0007	0.0100	62
255	56464.2735	0.0007	0.0024	204	327	56468.4734	0.0006	−0.0017	124
256	56464.3298	0.0006	0.0002	209	328	56468.5401	0.0010	0.0066	87
257	56464.3869	0.0008	−0.0011	248	329	56468.5915	0.0009	−0.0004	60
258	56464.4514	0.0010	0.0051	151	330	56468.6457	0.0008	−0.0046	66
259	56464.5034	0.0023	−0.0013	131	331	56468.7059	0.0041	−0.0028	15
260	56464.5692	0.0012	0.0061	61	332	56468.7609	0.0020	−0.0062	17
261	56464.6256	0.0011	0.0041	98	342	56469.3528	0.0013	0.0019	79
262	56464.6899	0.0040	0.0100	65	343	56469.4120	0.0008	0.0027	194
263	56464.7471	0.0014	0.0089	104	344	56469.4674	0.0008	−0.0003	224
264	56464.8025	0.0028	0.0058	162	345	56469.5263	0.0005	0.0002	151
265	56464.8564	0.0008	0.0014	191	346	56469.5906	0.0009	0.0061	151
266	56464.9168	0.0015	0.0033	84	347	56469.6476	0.0015	0.0047	64
267	56464.9753	0.0009	0.0035	76	348	56469.7037	0.0013	0.0024	96
270	56465.1522	0.0011	0.0053	117	349	56469.7592	0.0007	−0.0005	127
271	56465.2116	0.0012	0.0062	115	350	56469.8181	0.0008	0.0000	172
272	56465.2715	0.0008	0.0078	121	351	56469.8773	0.0010	0.0009	161
273	56465.3290	0.0015	0.0069	226	352	56469.9307	0.0016	−0.0041	64
274	56465.3880	0.0016	0.0075	112	355	56470.1060	0.0009	−0.0041	77
275	56465.4417	0.0014	0.0028	112	361	56470.4542	0.0013	−0.0062	63
280	56465.7386	0.0033	0.0077	15	362	56470.5139	0.0015	−0.0049	61
281	56465.7884	0.0019	−0.0008	15	363	56470.5683	0.0009	−0.0088	59
292	56466.4363	0.0010	0.0048	135	364	56470.6282	0.0035	−0.0073	64
293	56466.4991	0.0005	0.0092	156	365	56470.6935	0.0014	−0.0004	93
294	56466.5604	0.0006	0.0121	136	366	56470.7348	0.0012	−0.0175	180

*BJD − 2400000.
†Against max = 2456449.3820 + 0.058389 E.
‡Number of points used to determine the maximum.

counterpart 1RXS J094326.1−272035. The past outburst behavior suggested an SU UMa-type dwarf nova. The 2011 December outburst brightened up to 14.7 mag (unfiltered CCD) and was observed for one night when the object possibly showed superhumps (vsnet-alert 14034).

The 2014 outburst was visually detected by A. Pearce on January 29. The bright magnitude (13.1 mag) immediately suggested a superoutburst (vsnet-alert 16842). From subsequent observations superhumps were indeed detected (vsnet-alert 16853, 16859, 16867; figure 77). The times of superhump maxima are listed in table 59. The epochs for $E \leq 2$ were likely stage A superhumps. There were probably stages B and C. Although the object rapidly faded in the superoutburst, no phase jump (corresponding to "traditional" late superhumps) was observed.

Although the period could not be determined, the 2011 observation was compatible with a period of ~ 0.07 d.

In table 58 we summarize the past outbursts from the ASAS-3 data. Many of the detected outbursts were superoutbursts and the shortest interval between two superoutbursts was ~ 390 d.

3.56 TCP J23382254−2049518

This object (hereafter TCP J233822) was discovered to be a transient object by K. Itagaki on 2013 September 28 at an unfiltered CCD magnitude of 13.6.[7] The object is identical with a blue SDSS object ($g = 21.5$, $g - r = -0.2$) and a GALEX ultraviolet source, GALEX J233822.5−204951 (vsnet-alert 16468). The large outburst amplitude already suggested a WZ Sge-type dwarf nova.

[7] ⟨http://www.cbat.eps.harvard.edu/unconf/followups/J23382254-2049518.html⟩.

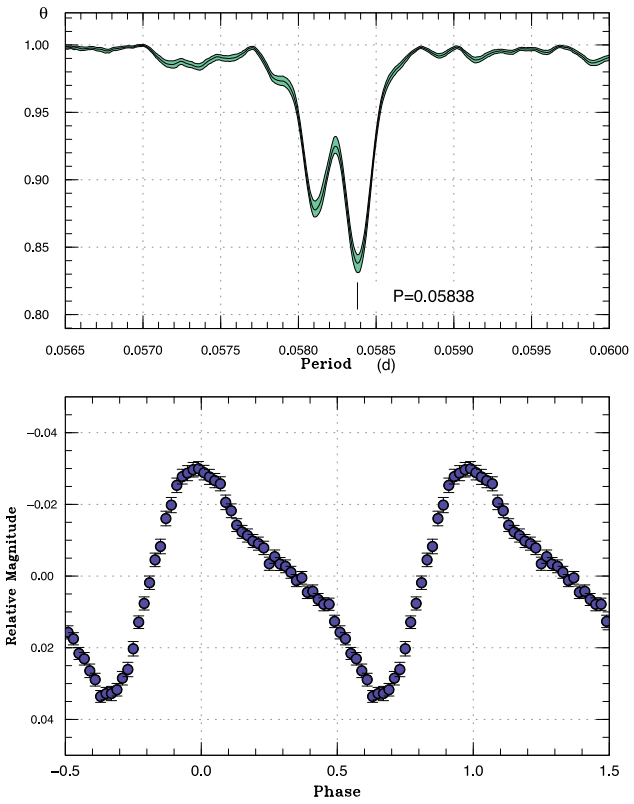

Fig. 73. Ordinary superhumps in PNV J191501 (2013). Upper: PDM analysis. Lower: Phase-averaged profile.

The object initially showed early superhumps (vsnet-alert 16486, 16489, 16496, 16528; figure 78). Twelve days after the discovery, the object started to show ordinary superhumps (vsnet-alert 16520, 16529, 16532, 16536; figure 79). The times of superhump maxima are listed in table 60, in which the stage A–B transition is clearly seen (also figure 80). For the epochs $E \geq 222$, there was some evidence that its period shortened. This part may correspond to stage C superhumps.

The fractional superhump excess (in frequency) for stage A superhumps was $\varepsilon^* = 0.0231(14)$. This value corresponds to $q = 0.061(4)$, suggesting that the object is near the period minimum or somewhat past the period minimum.

The object showed two post-superoutburst rebrightenings (figure 80). It is rare to observe multiple post-superoutburst rebrightenings in such a short-$P_{\rm orb}$ system (cf. Nakata et al. 2013b).

4 Discussion

We first report in this section general statistical properties of the sample together with the earlier sample the same as in Kato et al. (2014a), and then deal with new topics which arose in this paper.

4.1 Period derivatives during stage B

Figure 81 represents the updated relation between $P_{\rm dot}$ during stage B and $P_{\rm orb}$. Most of the objects with $P_{\rm orb} < 0.085$ d followed the general trend reported in Kato et al. (2013b). Some objects with $P_{\rm orb}$ longer than 0.085 d show a negative $P_{\rm dot}$, while some others show a large positive $P_{\rm dot}$ (as we see in subsection 4.7, some of them may have been contaminated by stage A superhumps). We could add a new sample, MASTER J162323, to the latter group. We can say that most of objects $P_{\rm orb} < 0.080$ d have a positive $P_{\rm dot}$ during stage B.

4.2 Mass ratios from stage A superhumps

It has been proposed that the binary's mass ratio superhumps can be estimated from the stage A superhumps, which are considered to reflect the dynamical precession rate at the radius of the 3:1 resonance (Kato & Osaki 2013b). Stage A superhumps recorded in the present study are listed in table 61. In table 62, we list the new estimates of mass ratios from this paper. An updated summary of q estimates is shown in figure 82, in which measurements in Nakata et al. (2013b) are also included. The Kepler DNe shown in this figure are V516 Lyr (Kato & Osaki 2013a), KIC 7524178 (Kato & Osaki 2013c), and the unusual short-$P_{\rm orb}$ object GALEX J194419.33+491257.0 in the field of KIC 11412044 (Kato & Osaki 2014)—located at $P_{\rm orb}$=0.05282 d, $q = 0.14$.

4.3 WZ Sge-type stars

The WZ Sge-type dwarf novae in this study are listed in table 63. In figure 83, we show the relation between $P_{\rm dot}$ and $P_{\rm orb}$ for the entire set of WZ Sge-type dwarf novae. This figure is an updated version of figure 86 of Kato et al. (2014a). We use here the types of superoutburst in terms of rebrightenings as introduced in Imada et al. (2006) and Kato et al. (2009): type-A outburst (a long-duration rebrightening), type-B outburst (multiple discrete rebrightenings), type-C outburst (a single rebrightening), and type-D outburst (no rebrightening) (see, e.g., figure 35 in Kato et al. 2009). The type-E outburst (superoutburst with early superhumps and another superoutburst with ordinary superhumps) has been introduced since Kato et al. (2014a). The new data have confirmed the trend that each subtype of rebrightening pattern appears in a cluster in this diagram. Objects with type-B outburst have a high concentration around $P_{\rm orb} = 0.060$ d. Nakata et al. (2013b) indicated that at least two objects with type-B outburst are not period bouncers but lie on the ordinary track of CV evolution before the period minimum. If this interpretation is

Table 57. Superhump maxima of PNV J191501 (2013) (post-superoutburst).

E	Max*	Error	$O-C^{\dagger}$	$N^{\ddagger}$	E	Max*	Error	$O-C^{\dagger}$	$N^{\ddagger}$
0	56471.7401	0.0018	−0.0068	185	115	56478.4241	0.0006	0.0048	102
1	56471.8019	0.0026	−0.0030	210	116	56478.4828	0.0008	0.0054	85
7	56472.1209	0.0024	−0.0322	61	117	56478.5384	0.0009	0.0030	83
8	56472.1853	0.0086	−0.0258	62	118	56478.5980	0.0007	0.0046	85
9	56472.2412	0.0021	−0.0280	62	119	56478.6540	0.0006	0.0025	44
10	56472.2953	0.0011	−0.0319	77	120	56478.7177	0.0006	0.0082	54
16	56472.6877	0.0090	0.0124	23	121	56478.7671	0.0008	−0.0004	91
17	56472.7242	0.0029	−0.0091	84	130	56479.3000	0.0016	0.0104	26
18	56472.7908	0.0019	−0.0005	224	131	56479.3469	0.0006	−0.0007	39
19	56472.8465	0.0006	−0.0029	202	132	56479.4057	0.0005	0.0000	99
24	56473.1319	0.0020	−0.0076	59	133	56479.4658	0.0006	0.0021	97
25	56473.1993	0.0004	0.0018	123	134	56479.5271	0.0018	0.0054	83
26	56473.2578	0.0008	0.0023	119	135	56479.5821	0.0005	0.0023	85
32	56473.6053	0.0069	0.0017	27	136	56479.6407	0.0013	0.0029	74
33	56473.6628	0.0014	0.0012	50	137	56479.6981	0.0021	0.0023	28
34	56473.7212	0.0013	0.0015	56	138	56479.7548	0.0008	0.0010	68
35	56473.7793	0.0004	0.0016	125	144	56480.1060	0.0010	0.0041	60
46	56474.4220	0.0005	0.0061	84	145	56480.1632	0.0006	0.0032	61
47	56474.4768	0.0006	0.0028	104	146	56480.2200	0.0005	0.0020	62
48	56474.5360	0.0004	0.0041	108	147	56480.2746	0.0005	−0.0014	60
49	56474.5906	0.0009	0.0006	116	148	56480.3384	0.0024	0.0044	31
50	56474.6537	0.0022	0.0057	86	149	56480.3968	0.0006	0.0047	50
51	56474.7087	0.0006	0.0027	104	150	56480.4486	0.0012	−0.0015	67
52	56474.7671	0.0004	0.0031	161	151	56480.5103	0.0005	0.0022	71
54	56474.8831	0.0004	0.0030	184	152	56480.5700	0.0006	0.0039	64
63	56475.4060	0.0006	0.0038	28	153	56480.6232	0.0007	−0.0009	63
64	56475.4634	0.0003	0.0031	77	154	56480.6828	0.0008	0.0007	20
65	56475.5192	0.0004	0.0009	65	155	56480.7413	0.0006	0.0011	79
67	56475.6335	0.0044	−0.0009	20	161	56481.0886	0.0007	0.0003	61
68	56475.6953	0.0015	0.0030	51	162	56481.1461	0.0008	−0.0002	63
69	56475.7551	0.0006	0.0047	103	163	56481.2036	0.0009	−0.0007	62
70	56475.8115	0.0004	0.0030	133	164	56481.2606	0.0010	−0.0017	60
71	56475.8702	0.0003	0.0037	138	165	56481.3203	0.0007	−0.0001	52
80	56476.3910	0.0013	0.0024	20	166	56481.3779	0.0011	−0.0005	23
81	56476.4493	0.0004	0.0027	63	167	56481.4387	0.0006	0.0022	51
82	56476.5068	0.0005	0.0022	54	168	56481.4971	0.0005	0.0027	69
85	56476.6795	0.0015	0.0008	18	169	56481.5559	0.0008	0.0035	47
86	56476.7401	0.0005	0.0034	73	170	56481.6079	0.0007	−0.0026	43
87	56476.7928	0.0008	−0.0020	135	171	56481.6654	0.0020	−0.0031	46
88	56476.8527	0.0009	−0.0000	128	172	56481.7281	0.0010	0.0016	58
97	56477.3801	0.0007	0.0052	42	173	56481.7872	0.0015	0.0027	63
98	56477.4338	0.0005	0.0008	63	174	56481.8456	0.0008	0.0030	65
99	56477.4919	0.0014	0.0009	69	175	56481.9040	0.0011	0.0034	67
100	56477.5498	0.0004	0.0008	45	179	56482.1338	0.0006	0.0011	77
101	56477.6096	0.0006	0.0026	62	180	56482.1938	0.0006	0.0031	109
102	56477.6669	0.0003	0.0018	95	181	56482.2501	0.0008	0.0014	125
103	56477.7214	0.0009	−0.0017	125	183	56482.3686	0.0010	0.0038	69
104	56477.7859	0.0005	0.0048	97	184	56482.4235	0.0007	0.0007	111
109	56478.0779	0.0013	0.0066	44	185	56482.4814	0.0007	0.0006	108
110	56478.1357	0.0009	0.0064	60	186	56482.5375	0.0006	−0.0013	57
111	56478.1905	0.0006	0.0032	62	187	56482.5969	0.0009	0.0001	38
112	56478.2476	0.0008	0.0023	63	188	56482.6550	0.0011	0.0001	28
113	56478.3054	0.0007	0.0021	62	191	56482.8280	0.0003	−0.0009	100

Table 57. (Continued)

E	Max*	Error	$O-C^{\dagger}$	$N^{\ddagger}$	E	Max*	Error	$O-C^{\dagger}$	$N^{\ddagger}$
194	56483.0056	0.0016	0.0026	35	271	56487.4680	0.0017	−0.0026	25
195	56483.0595	0.0014	−0.0015	27	275	56487.6911	0.0012	−0.0115	60
198	56483.2330	0.0007	−0.0021	117	276	56487.7617	0.0005	0.0010	110
199	56483.2923	0.0026	−0.0008	66	287	56488.3981	0.0010	−0.0008	42
200	56483.3513	0.0009	0.0002	39	288	56488.4516	0.0005	−0.0053	41
201	56483.4062	0.0007	−0.0029	108	289	56488.5159	0.0006	0.0009	45
202	56483.4676	0.0004	0.0005	108	290	56488.5721	0.0006	−0.0008	45
203	56483.5236	0.0017	−0.0016	61	293	56488.7439	0.0006	−0.0031	93
204	56483.5855	0.0006	0.0023	39	294	56488.7993	0.0007	−0.0057	88
205	56483.6442	0.0025	0.0030	25	304	56489.3905	0.0017	0.0053	70
207	56483.7573	0.0006	0.0000	94	305	56489.4405	0.0012	−0.0027	70
215	56484.2213	0.0024	−0.0001	111	306	56489.4985	0.0006	−0.0028	45
216	56484.2824	0.0046	0.0030	55	307	56489.5569	0.0004	−0.0024	46
218	56484.4016	0.0014	0.0061	21	308	56489.6166	0.0007	−0.0007	46
219	56484.4556	0.0015	0.0021	24	322	56490.4293	0.0012	−0.0003	44
220	56484.5078	0.0013	−0.0037	24	323	56490.4799	0.0018	−0.0077	48
229	56485.0381	0.0019	0.0044	55	324	56490.5430	0.0008	−0.0026	46
230	56485.0901	0.0011	−0.0016	56	325	56490.6023	0.0007	−0.0014	47
232	56485.2041	0.0027	−0.0036	99	326	56490.6620	0.0042	0.0003	30
234	56485.3237	0.0010	−0.0001	38	339	56491.4113	0.0008	−0.0046	46
242	56485.7879	0.0005	−0.0001	110	340	56491.4717	0.0005	−0.0023	45
243	56485.8401	0.0010	−0.0059	108	341	56491.5352	0.0009	0.0032	45
269	56487.3480	0.0019	−0.0065	24	343	56491.6406	0.0010	−0.0075	43
270	56487.4103	0.0006	−0.0022	40	408	56495.4172	0.0025	−0.0022	40

*BJD − 2400000.

†Against max = 2456471.7470 + 0.058021 E.

‡Number of points used to determine the maximum.

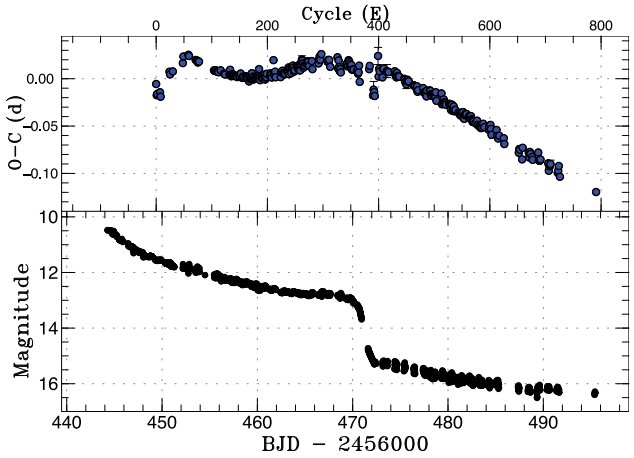

Fig. 74. $O-C$ diagram of superhumps in PNV J191501 (2013). Upper: $O-C$ diagram. A period of 0.05835 d was used for drawing this figure. Lower: Light curve. The observations were binned to 0.010 d.

applied to the majority of the objects with type-B outburst, these objects may be in a stage of CV evolution from short-period SU UMa-type dwarf novae to extreme WZ Sge-type dwarf novae near the period minimum.

4.4 A comparison between periods of early superhumps and orbital periods

Although early superhumps have been reported (e.g., Kato et al. 1996b, 2001a; Patterson et al. 1996, 2002; Ishioka et al. 2002; Kato 2002) as double-wave modulations having a period very close to the orbital period, there has been no summary of comparisons between the period of early superhumps and the orbital period. We therefore make a study of the WZ Sge-type dwarf novae with a well-established orbital period.

The periods of early superhumps of AL Com (2001) and HV Vir (2008) were estimated from the data in Ishioka et al. (2002) and Kato et al. (2009), respectively. The orbital period of BW Scl has been refined by using quiescent observations (B. Monard, F.-J. Hambsch, P. Starr, and AAVSO data during the period from 2004 September to 2013 September, 14070 measurements). The orbital period of EZ Lyn is a revised one by using post-superoutburst eclipses reported in Kato et al. (2012b). The orbital period of AL Com is an updated one using observations of early superhumps in three superoutbursts (subsection 3.11).

The result is summarized in table 64. Although all the objects showed statistically significant negative ε for early

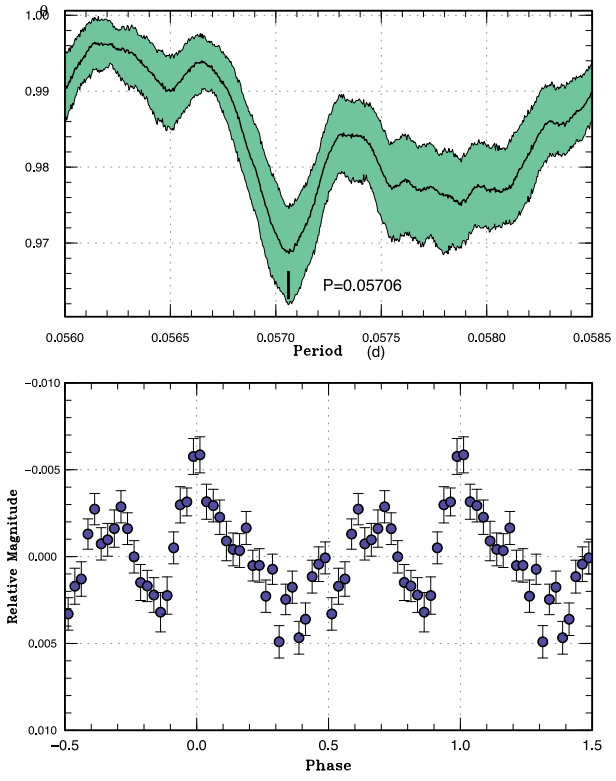

Fig. 75. Possible early superhumps in PNV J191501 (2013). Upper: PDM analysis. Lower: Phase-averaged profile.

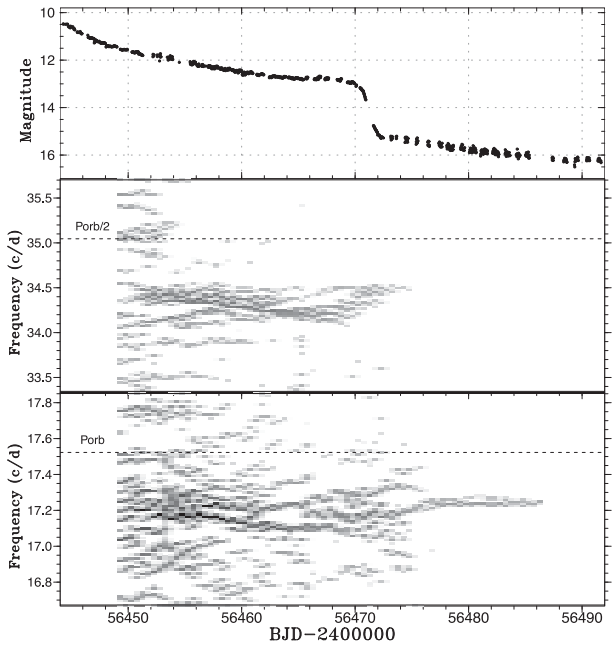

Fig. 76. Lasso analysis of PNV J191501 (2013). Upper: Light curve. The data were binned to 0.02 d. Middle: First overtones of the superhump and possible orbital signals. Lower: Fundamentals of the superhump and the possible orbital signal. The orbital signal was present only in the initial part of the outburst. The signal of (positive) superhumps with variable frequency was recorded during the superoutburst plateau and post-superoutburst stage. No indication of negative superhump was present. The parameter $\log\lambda = -8.0$ was used. The width of the sliding window and the time step used are 10 d and 0.5 d, respectively.

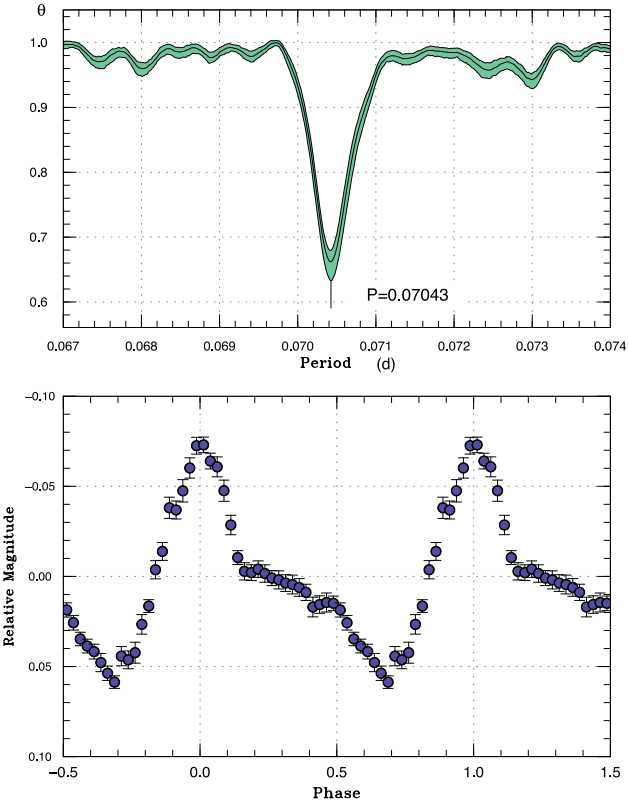

Fig. 77. Superhumps in SSS J094327 (2014). Upper: PDM analysis. Lower: Phase-averaged profile.

Table 58. Outbursts of SSS J094327.

JD−2400000	Maximum (V)	Duration	Type
51926	l3.1	12	Super
52440	12.8	>3	Super?
53005	13.8	1*	Normal?
53385	12.8	11	Super
53776	13.0	>7	Super
54182	13.1	>8	Super
54667	13.6	2	Normal
54796	13.3	1*	Normal?

*Single detection.

superhumps, the period deficit is very small (of the order of 0.05%). This result has confirmed the finding in Ishioka et al. (2002). Since the period deficit is very small, the period of early superhumps can be considered as the orbital period with accuracy of 0.1%. If more accuracy is needed and the orbital period is not known, we propose to estimate the orbital period by assuming ε of −0.05%.

4.5 Eclipses during the phase of early superhumps

In the light curve of early superhumps in MASTER J005740 (figure 55), there are sharp structures (kinks in the light

Table 59. Superhump maxima of SSS J094327 (2014).

E	Max*	Error	$O-C^{\dagger}$	$N^{\ddagger}$
0	56689.0954	0.0013	−0.0073	123
1	56689.1697	0.0010	−0.0036	112
14	56690.0889	0.0003	0.0000	140
15	56690.1581	0.0003	−0.0012	142
16	56690.2310	0.0003	0.0012	142
17	56690.3007	0.0003	0.0005	140
18	56690.3716	0.0005	0.0009	81
28	56691.0753	0.0004	0.0002	136
29	56691.1462	0.0003	0.0006	141
43	56692.1327	0.0003	0.0010	142
44	56692.2032	0.0005	0.0010	142
45	56692.2741	0.0004	0.0015	141
46	56692.3434	0.0005	0.0004	138
50	56692.6270	0.0009	0.0023	22
51	56692.6971	0.0007	0.0019	24
52	56692.7674	0.0009	0.0018	19
53	56692.8385	0.0015	0.0024	22
57	56693.1213	0.0006	0.0035	142
58	56693.1913	0.0006	0.0030	143
59	56693.2610	0.0010	0.0022	141
60	56693.3325	0.0006	0.0034	132
65	56693.6825	0.0009	0.0012	23
66	56693.7536	0.0009	0.0018	19
72	56694.1758	0.0031	0.0014	76
78	56694.5904	0.0052	−0.0067	11
79	56694.6640	0.0011	−0.0036	23
80	56694.7388	0.0013	0.0008	20
81	56694.8097	0.0016	0.0013	21
82	56694.8773	0.0021	−0.0016	16
85	56695.0884	0.0012	−0.0018	137
86	56695.1567	0.0012	−0.0039	141
87	56695.2272	0.0011	−0.0038	142
88	56695.3007	0.0016	−0.0008	78

*BJD − 2400000.
†Against max = 2456689.1028 + 0.070440 E.
‡Number of points used to determine the maximum.

curve) around orbital phases of −0.15 and 0.15. They suggest that the phases between −0.15 and 0.15 were affected by the eclipse. We can propose a hypothetical uneclipsed hump structure (assuming that larger and smaller humps are separated equally) as the dashed line in figure 55.

It has been a mystery why eclipses are not evident during the stage of early superhumps in such a high-inclination system as WZ Sge (Patterson et al. 2002), despite the fact that eclipses appear more strongly after the appearance of ordinary superhumps. While Patterson et al. (2002) suggested the enhanced hot spot as the origin of eclipses during the phase of ordinary superhumps, Osaki and Meyer (2003) suggested that what is eclipsed is the superhump light source rather than the enhanced hot spot. In the interpretation of Osaki and Meyer (2003), the source of early superhumps, which Osaki and Meyer (2002) interpret as the two-armed

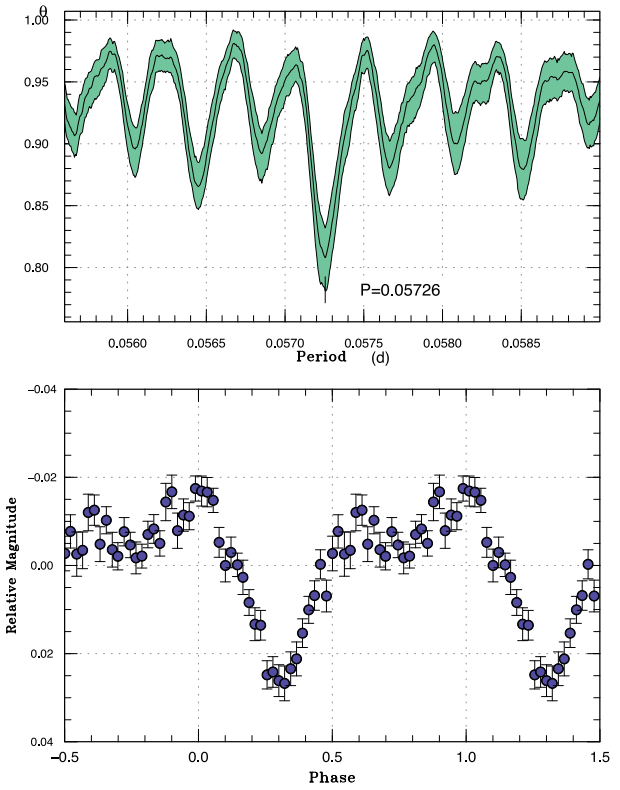

Fig. 78. Early superhumps in TCP J233822 (2013). Upper: PDM analysis. Lower: Phase-averaged profile.

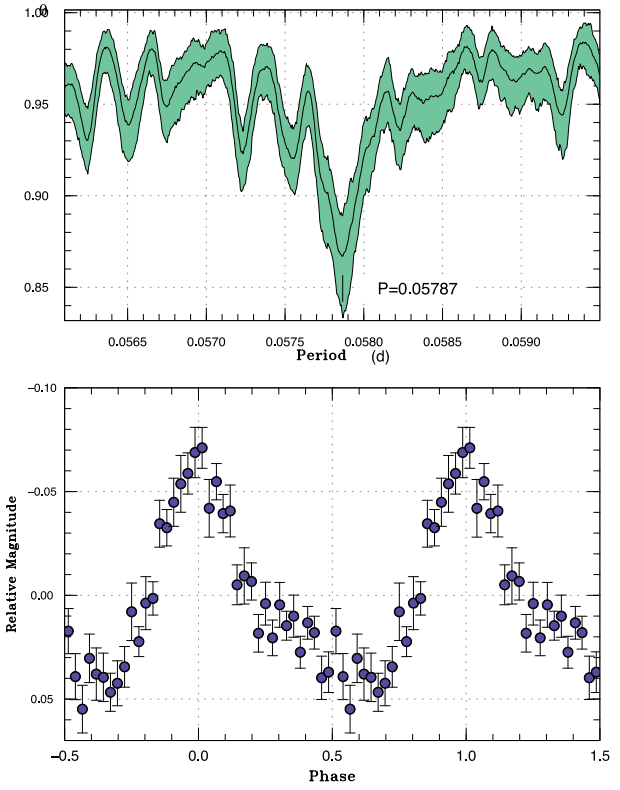

Fig. 79. Ordinary superhumps in TCP J233822 (2013). The data of BJD 2456577.6–2456593 was used. Upper: PDM analysis. Lower: Phase-averaged profile.

Table 60. Superhump maxima of TCP J233822 (2013).

E	Max*	Error	$O-C^{\dagger}$	$N^{\ddagger}$	E	Max*	Error	$O-C^{\dagger}$	$N^{\ddagger}$
0	56575.7668	0.0016	−0.0178	28	103	56581.7476	0.0011	−0.0020	28
15	56576.6453	0.0017	−0.0079	14	118	56582.6154	0.0063	−0.0029	12
16	56576.7008	0.0017	−0.0103	15	119	56582.6782	0.0017	0.0020	13
17	56576.7607	0.0010	−0.0083	28	120	56582.7293	0.0014	−0.0048	21
22	56577.0564	0.0007	−0.0023	27	153	56584.6426	0.0024	−0.0027	19
23	56577.1140	0.0009	−0.0026	37	154	56584.7083	0.0028	0.0051	29
24	56577.1786	0.0028	0.0041	15	155	56584.7562	0.0013	−0.0049	72
32	56577.6414	0.0006	0.0037	13	159	56584.9939	0.0022	0.0012	12
33	56577.6995	0.0007	0.0038	14	160	56585.0535	0.0022	0.0029	15
34	56577.7575	0.0005	0.0039	27	161	56585.1065	0.0045	−0.0021	11
39	56578.0499	0.0008	0.0068	20	162	56585.1671	0.0027	0.0006	15
50	56578.6861	0.0008	0.0058	18	170	56585.6263	0.0024	−0.0035	15
51	56578.7437	0.0006	0.0056	25	172	56585.7438	0.0015	−0.0018	31
60	56579.2642	0.0004	0.0048	124	187	56586.6078	0.0019	−0.0065	14
61	56579.3229	0.0006	0.0056	123	188	56586.6706	0.0023	−0.0017	13
62	56579.3795	0.0004	0.0043	133	189	56586.7244	0.0017	−0.0058	22
63	56579.4388	0.0007	0.0057	134	206	56587.7241	0.0030	0.0094	23
64	56579.4949	0.0008	0.0039	133	222	56588.6437	0.0016	0.0024	13
65	56579.5520	0.0007	0.0030	133	223	56588.6979	0.0028	−0.0013	17
86	56580.7644	0.0017	−0.0007	30	224	56588.7606	0.0019	0.0034	19
91	56581.0576	0.0007	0.0030	11	233	56589.2765	0.0027	−0.0018	133
92	56581.1159	0.0010	0.0034	15	234	56589.3336	0.0016	−0.0027	134
101	56581.6412	0.0022	0.0074	13	235	56589.3905	0.0024	−0.0037	132
102	56581.6880	0.0021	−0.0037	14					

*BJD − 2400000.

†Against max = 2456575.7845 + 0.057913 E.

†Number of points used to determine the maximum.

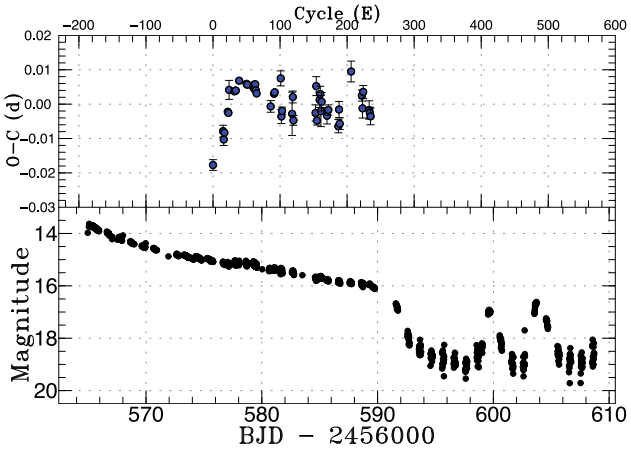

Fig. 80. $O-C$ diagram of superhumps in TCP J233822 (2013). Upper: $O-C$ diagram. A period of 0.057913 d was used for drawing this figure. Lower: Light curve. The observations were binned to 0.011 d.

dissipation pattern of the 2:1 Lindblad resonance, cannot be eclipsed because this pattern is located azimuthally far away from the secondary star. The present observation indicates that the broad eclipse was located close to the expected eclipse center, which suggests that (the axisymmetric component of) the bright disk, rather than the enhanced hot spot, is eclipsed. This picture smoothly fits in with the interpretation by Osaki and Meyer (2003), and the mystery of the apparent absence of the eclipse during the phase of early superhumps is solved.

In Uemura et al. (2012), the eclipse of the disk was considered in the model. This effect, however, was not so large in the model parameters of V455 And, which apparently has a lower inclination than MASTER J005740, and it was difficult to distinguish its effect from the uneclipsed light curve of early superhumps. Our new observation in a system of higher inclination now presents more convincing evidence against the greatly increased mass-transfer in the WZ Sge-type outburst.

4.6 Model of the eclipse during early superhumps

We further studied whether or not a simple model can reproduce the depth of the eclipse in MASTER J005740 during the phase of early superhumps. We adopted $q = 0.076$ from our measurement using stage A superhumps (it is well known that there is a strong relation in modeling the eclipse light curve between its q and inclination, and the

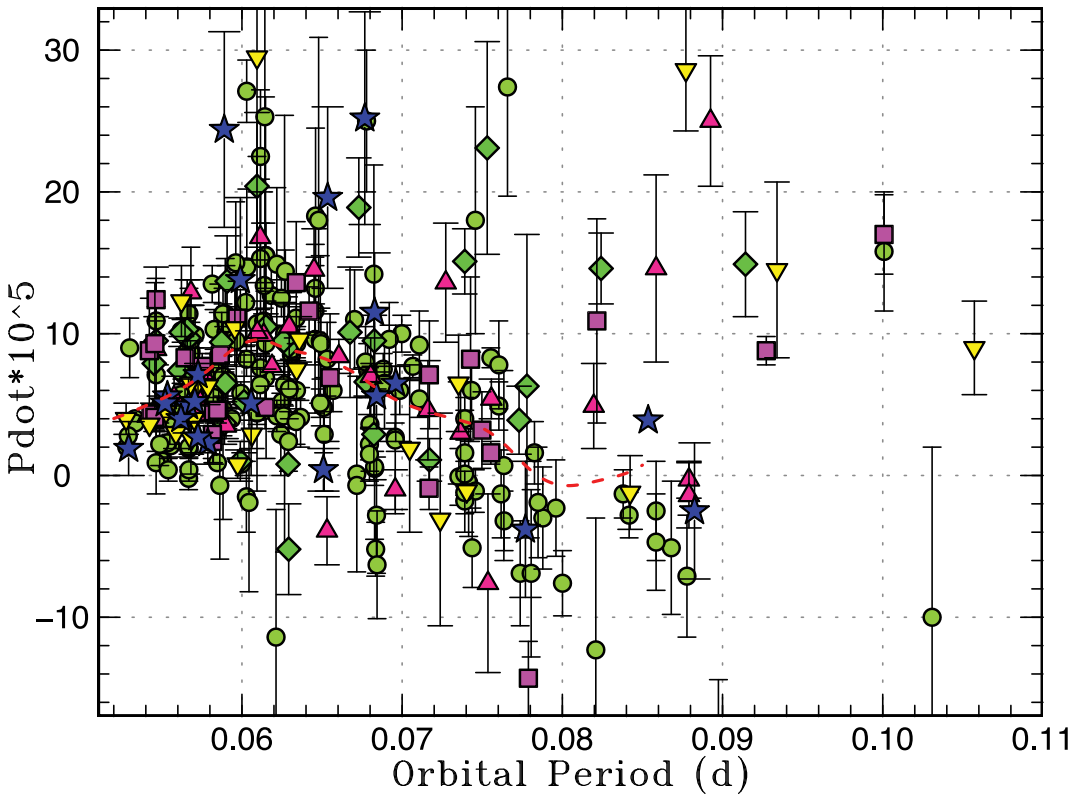

Fig. 81. $P_{\rm dot}$ for stage B versus $P_{\rm orb}$. The filled circles, filled diamonds, filled triangles, filled squares, filled lower-pointed triangles, and filled stars represent samples in Kato et al. (2009, 2010, 2012b, 2013b, 2014a), and this paper, respectively. The curve represents the spline-smoothed global trend.

Table 61. New estimates for the binary's mass ratio from stage A superhumps.

Object	ε^* (stage A)	q from stage A
GZ Cnc	0.089(7)	0.30(2)
MN Dra (2012, 2013)	0.078, 0.092	0.29(5)
DT Oct	0.050(2)	0.147(7)
MASTER J005740	0.028(5)	0.076(16)
PNV J191501	0.0344(12)	0.095(4)
TCP J233822	0.0231(14)	0.061(4)

Table 62. Superhump periods during stage A.

Object	Year	Period (d)	Error
UZ Boo	2013	0.06210	0.00005
GZ Cnc	2014	0.09690	0.00030
AL Com	2013	0.05859	0.00009
MN Dra	2012	0.10993	0.00009
MN Dra	2013	0.10822	0.00013
DT Oct	2014	0.07271	—
ASASSN-13ck	2013	0.05700	0.00010
ASASSN-14ac	2014	0.05952	0.00003
MASTER J004527	2013	0.08210	0.00035
MASTER J005740	2013	0.05783	0.00034
MASTER J162323	2013	0.09134	0.00055
PNV J191501	2013	0.05909	0.00008
TCP J233822	2013	0.05861	0.00008

uncertainty in q can be reasonably neglected by allowing a free selection of the inclination). We assumed that the disk radius is the radius of the 2:1 resonance ($0.615A$ in the case of $q = 0.076$). We assumed flat and axisymmetric geometry and a standard disk having a surface luminosity with a radial dependence $\propto r^{-3/4}$ (assuming that we observed the Rayleigh–Jeans tail of the emission from the hot disk). Although all of these assumptions are rough, they will not seriously affect the results. We constructed the eclipse light curve using the Roche geometry. We could reproduce the eclipse depth of 0.16 mag from the assumed secondary maximum of early superhumps and the bottom of the eclipse (as seen from figure 55) by assuming an inclination of $81^\circ.5 \pm 0^\circ.5$. The total duration of the eclipse was 0.28 binary phase, which is in agreement with the observation. Under these parameters, the white dwarf is marginally eclipsed, which is also in agreement with the observational suggestion.

The model light curve is shown in figure 84. In this model, it is assumed that the standard disk is eclipsed by the secondary and the light source of early superhumps is simply added to the light curve (i.e., we assume that the light source of early superhumps is not eclipsed). The two maxima of early superhumps are approximated by

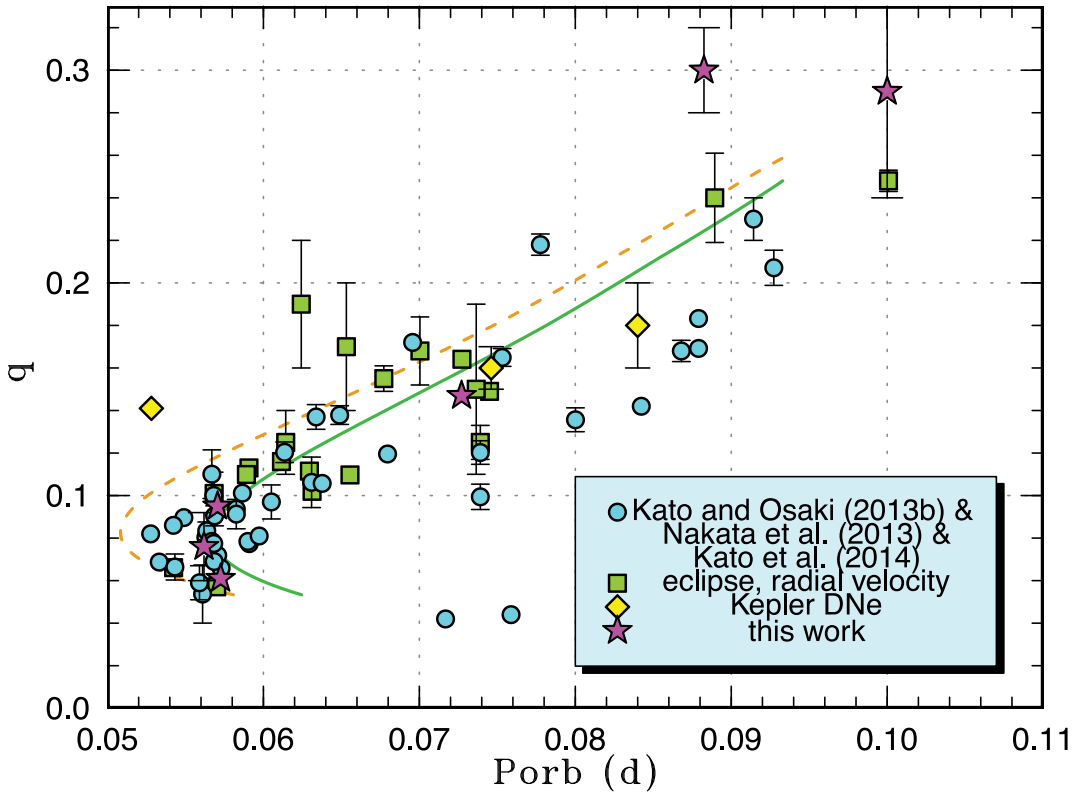

Fig. 82. Mass ratio versus orbital period. The dashed and solid curves represent the standard and optimal evolutionary tracks in Knigge, Baraffe, and Patterson (2011), respectively. The filled circles, filled squares, filled stars, and filled diamonds represent q values from a combination of the estimates from stage A superhumps published in three preceding sources (Kato & Osaki 2013b; Nakata et al. 2013b; Kato et al. 2014a), known q values from quiescent eclipses or radial velocity study (see Kato & Osaki 2013b for the data source), q estimated in this work, and dwarf novae in the Kepler data (see text for the complete reference), respectively.

Table 63. Parameters of WZ Sge-type superoutbursts.

Object	Year	P_{SH}	P_{orb}	P_{dot}*	Error*	ϵ	Type†	N_{reb}‡	Delay§	Max	Min
UZ Boo	2013	0.062066	—	5.1	5.1	—	B	4	3	12.5	19.7
AL Com	2013	0.057323	0.056669	4.9	1.9	0.012	A	1(2)	7	12.7	19.8
ASASSN-13ck	2013	0.056186	0.055348	5.6	0.4	0.015	A	1(3)	≥8	]12.9	20.8
ASASSN-14ac	2014	0.058550	—	−1.7	1.2	—	—	≥1	≥14	]14.5	21.6
MASTER J005740	2013	0.057067	0.056190	4.0	1.0	0.016	—	—	≥6	]15.4	20.9
OT J210016	2013	0.058502	0.05787	2.3	1.5	0.011	—	—	—	]14.2	19.9
PNV J191501	2013	0.058382	0.05706	5.2	0.2	0.023	D	0	≥7	]9.8	18.5
TCP J233822	2013	0.057868	0.057255	2.7	1.1	0.011	B	2	≥12	]13.6	21.5

*Unit: 10^{-5}.
†A: long-lasting rebrightening; B: multiple rebrightenings; C: single rebrightening; D: no rebrightening.
‡Number of rebrightenings.
§Days before ordinary superhumps appeared.

sine curves having different amplitudes (the secondary maximum is assumed to have a half amplitude of the primary maximum). The resultant light curve appears to well reproduce the basic characteristics of the observation (figure 55). The sharp minimum around a phase of 0.0 reflects the eclipse of the central part of the disk; the less clear appearance of this feature in observations may have been the result of the self-obscuration of the central part of the disk.

4.7 Stage A superhumps in long-period systems

In subsections 3.14 and 3.10, likely stage A superhumps were detected in the long-P_{orb} systems MN Dra and GZ Cnc. The identification of stage A superhumps in the former system is almost certain because growing amplitudes of the superhumps were detected.

This finding appears to contradict the earlier interpretation that stage A superhumps reflecting the radius of the

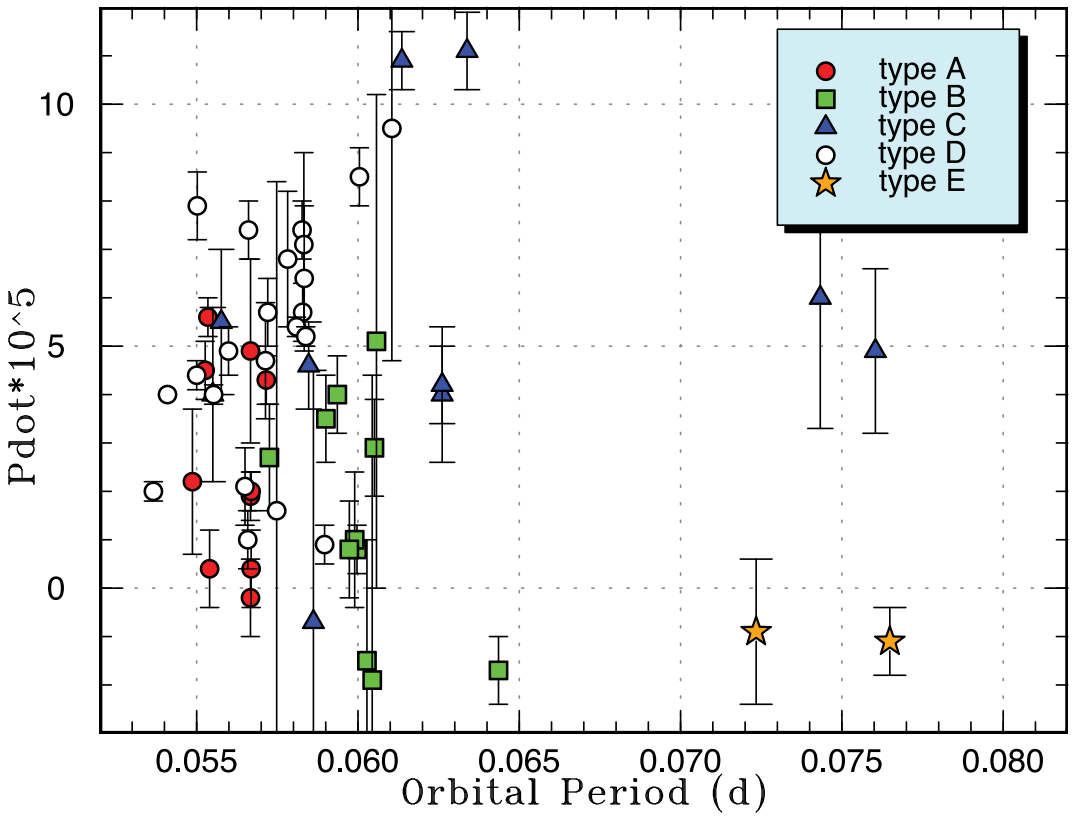

Fig. 83. $P_{\rm dot}$ versus $P_{\rm orb}$ for WZ Sge-type dwarf novae. Symbols represent the type (cf. Kato et al. 2009) of outburst: type A (filled circles), type B (filled squares), type C (filled triangles), type D (open circles), and type E (filled stars) which show double superoutbursts as shown in Kato et al. (2013a).

Table 64. Periods of early superhumps.

Object	$P_{\rm orb}$ (d)	$P_{\rm ESH}$ (d)*	$\varepsilon_{\rm ESH}$†	References
V455 And (2007)	0.05630921(1)	0.0562675(18)	−0.00074(3)	Kato et al. (2009)
AL Com (1995)	0.056668589(9)	0.05666(2)	−0.0002(4)	this work; Kato et al. (1996b)
AL Com (2001)	0.056668589(9)	0.056660(4)	−0.00015(7)	this work
AL Com (2013)	0.056668589(9)	0.056660(8)	−0.00015(14)	this work
EZ Lyn (2010)	0.05900495(3)	0.058973(6)	−0.00054(10)	Kato et al. (2012b)
BW Scl (2011)	0.05432391(1)	0.054308(2)	−0.00029(4)	this work; Kato et al. (2013b)
WZ Sge (2001)	0.0566878460(3)	0.056656(2)	−0.00057(4)	Patterson et al. (2002); Ishioka et al. (2002).
HV Vir (1992)	0.057069(6)	0.05698(8)	−0.0016(14)	Patterson et al. (2003); Kato et al. (2001a)
HV Vir (2008)	0.057069(6)	0.056991(7)	−0.0014(1)	this work
MASTER J005740 (2013)	0.0561904(3)	0.056169(3)	−0.0038(5)	this work

*Period of early superhumps.
†Fractional excess of early superhumps.

3:1 resonance in high-q systems are difficult of detection because the tidal effect is stronger in higher-q systems and their eccentric region spreads more quickly than in low-q systems (Kato & Osaki 2013b). In MN Dra and GZ Cnc, however, the q values are probably critically close to the condition in which the 3:1 resonance occurs, and the resonance may be weak enough to be confined to the radius of the 3:1 resonance for a longer time than in ordinary SU UMa-type dwarf novae. This possibility needs to be studied further. Although some of the objects recorded in our past study with a long $P_{\rm orb}$ and large negative $P_{\rm dot}$ may have been similar ones, we could not find as convincing a case as MN Dra. Since almost all of these systems lack determination of the orbital period, future measurements of the orbital periods may provide a clue to interpreting this phenomenon.

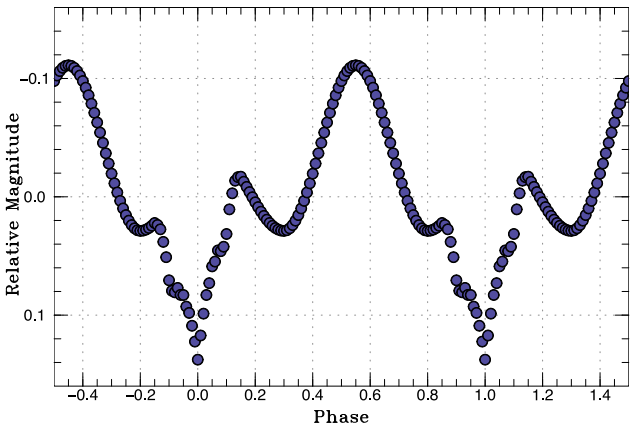

Fig. 84. Model light curve of the early superhump and eclipse of MASTER J005740.

Table 65. Period of negative superhumps in VW Hyi (2012).

JD*−2400000	Period (d)	Error (d)	Amplitude (mag)
56229–56239	0.07252	0.00003	0.05
56240–56254	0.07266	0.00002	0.04
56269–56279	0.07261	0.00003	0.10
56285–56302	0.07279	0.00003	0.07
56305–56327	0.07275	0.00002	0.07
56339–56361	—	—	—
56365–56374	0.07271	0.00005	0.05

*Julian day number.

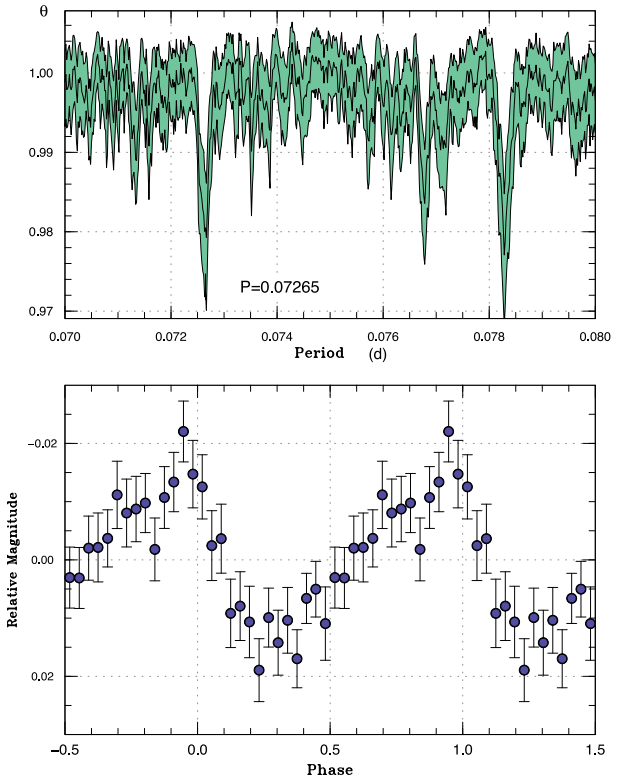

Fig. 85. Negative superhumps in VW Hyi (2012). The observation of BJD 2456229–2456584 (quiescence before the 2012 superoutburst) was analyzed after subtracting the mean orbital variation. Upper: PDM analysis. Lower: Phase-averaged profile.

4.8 Negative superhumps in VW Hydri

In a recent series of papers (Osaki & Kato 2013a, 2013b, 2014), it has been demonstrated by using the Kepler data that the state with negative superhumps tends to suppress normal outbursts in V1504 Cyg and V344 Lyr. The same phenomenon is also reported in ER UMa (Ohshima et al. 2012, 2014; Zemko et al. 2013). This phenomenon has been interpreted as a result of the decreased mass supply to the outermost part of the accretion disk when the disk is tilted, thereby reducing the occurrence of thermal instability in the outer part of the disk (Osaki & Kato 2013a; Ohshima et al. 2014). Osaki & Kato (2013a) called the supercycle type S (short intervals between normal outbursts) or type L (long intervals between normal outbursts), according to the nomenclature originally introduced by Smak (1985) for VW Hyi. Although the result in V1504 Cyg and V344 Lyr suggests that the same mechanism is responsible for type S and L supercycles in VW Hyi, this has not yet been demonstrated observationally.

We conducted an intensive campaign on VW Hyi in 2012–2013 to test this possibility. Since the start of the campaign on 2012 October 29, no outburst was detected (for a duration of 25 d) until the next superoutburst starting on November 23 (the superoutburst reported in subsection 3.18). Although the observations were not as dense as our CCD campaign, visual observations by the AAVSO observers did not reveal an outburst until the last recorded outburst on September 9. If there was no outburst from September 10 through November 22, the interval of normal outbursts may be as long as ∼70 d. Since VW Hyi undergoes normal outbursts as frequently as every 11–23 d in type S supercycles (cf. Smak 1985), in which intervals shorter than 23 d were considered as type S and those longer than ∼30 d were type L), the state before the 2012 superoutburst was most likely in type L.

A PDM analysis of the observation from BJD 2456229 to 2456254 (quiescence before the 2012 superoutburst) after subtracting the mean orbital variation yielded a period of 0.07265(3) d, by 2.2% shorter than the orbital period. Another candidate period is 0.07829(3) d, which is a one-day alias of the 0.07265 d period. Although there remains a possibility that 0.07829 d is the true period and the 0.07265 d period is a one-day alias signal, we consider this possibility less likely because a similar signal was also observed after the superoutburst (figure 86). In this interval, the negative superhump was the strongest signal after subtracting the orbital modulations, and there is no remaining

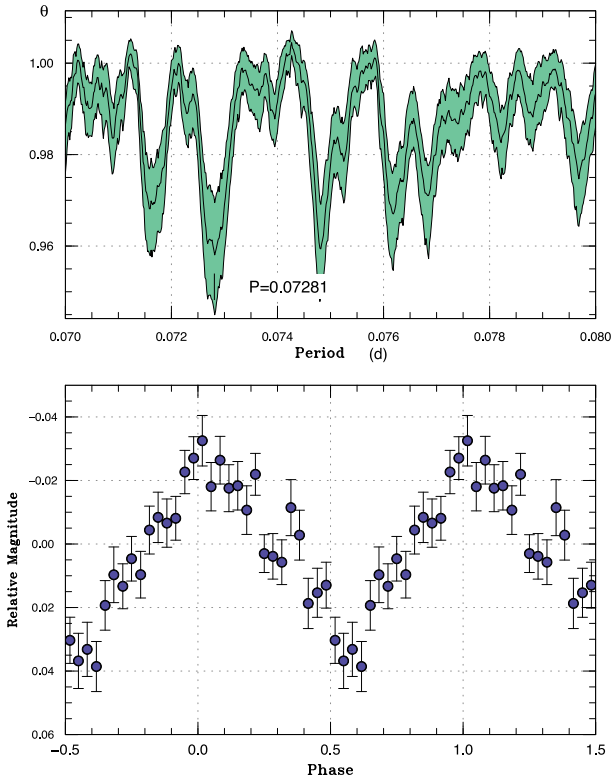

Fig. 86. Negative superhumps in VW Hyi (2012). The observation of BJD 2456282–2456302 (quiescence between the first two normal outbursts after the superoutburst) was analyzed after subtracting the mean orbital variation. Upper: PDM analysis. Lower: Phase-averaged profile.

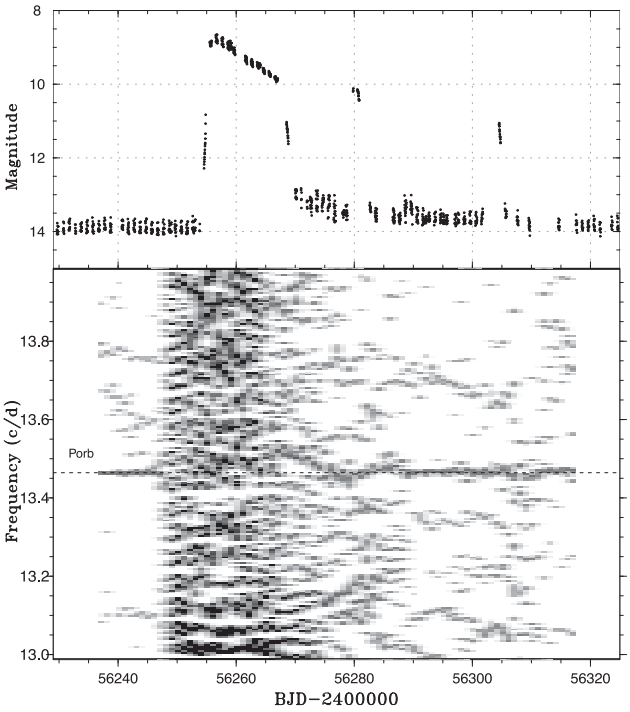

Fig. 87. Two-dimensional Lasso period analysis of VW Hyi (2012). Upper: Light curve. The data were binned to 0.02 d. Lower: Lasso period analysis of the superhump and the orbital signal. The signal of negative superhumps with a frequency around 13.75 cycles d^{-1} before the superoutburst was recorded. A possible signal of negative superhumps with frequencies around 13.65–13.70 cycles d^{-1} was also detected after the superoutburst. The parameter $\log\lambda = -7.8$ was used. The width of the sliding window and the time step used are 15 d and 1 d, respectively.

ambiguity of a one-day alias. The periods of negative superhumps determined for different segments of the data after subtraction of the orbital signal are listed in table 65. During the superoutburst, the period of negative superhumps could not be determined because it was located close to the one-day alias of the (positive) superhump period.

The mean profile (figure 85) is also characteristic of negative superhumps (cf. Osaki & Kato 2013a, 2013b) with a slower rise to the maximum and a faster decline to the minimum. The coexistence of orbital humps and negative superhumps, which is also recorded in both V1504 Cyg and V344 Lyr, suggests that some part of the stream hits the outermost part of the disk to produce the hot spot while some part of the stream reaches the inner disk to produce negative superhumps (cf. Wood & Burke 2007).

A two-dimensional Lasso analysis (figure 87) shows a signal of negative superhumps with a frequency of $\sim$13.75 cycles d^{-1} before the superoutburst. A possible signal of negative superhumps with a frequency of $\sim$13.65–13.70 cycles d^{-1} was also detected after the superoutburst. The decrease in the frequency (also evident as an increase in period is shown in table 65) is compatible with the shrinkage of the accretion disk after the superoutburst. As reported in Osaki and Kato (2013a), the precession frequency of a tilted disk can be expressed as follows (Larwood 1998):

$$\nu_{\rm NSH}/\nu_{\rm orb} = 1 + \frac{3}{7}\frac{q}{\sqrt{1+q}}\cos\theta\left(\frac{R_{\rm d}}{A}\right)^{3/2}, \quad (5)$$

where $\nu_{\rm NSH}$ and $\nu_{\rm orb}$ are the frequency for the negative superhump and the binary's orbital frequency, respectively; $R_{\rm d}$ is the disk radius, A the binary separation, and θ the tilt angle of the disk to the binary's orbital plane. The smallest $|\varepsilon^*|$ (equivalent to $\nu_{\rm NSH}/\nu_{\rm orb}$) before the superoutburst was 0.024 and the largest $|\varepsilon^*|$ after the superoutburst was 0.020. This difference can be explained from a 13% shrinkage of the disk radius after the superoutburst. Assuming $q = 0.21(2)$ (from the radial velocity study by Smith et al. 2006) and a small tilt angle ($\cos\theta \sim 1$), these two values of $|\varepsilon^*|$ correspond to disk radii of $0.42(1)A$ and $0.39(1)A$, respectively.[8]

[8] Smith, Haswell, and Hynes (2006) suggested that this q value is highly insecure. We used this value since there is no other direct determination of q value, and the q determined from stage B superhumps (Patterson et al. 2005) has some unknown uncertainty.

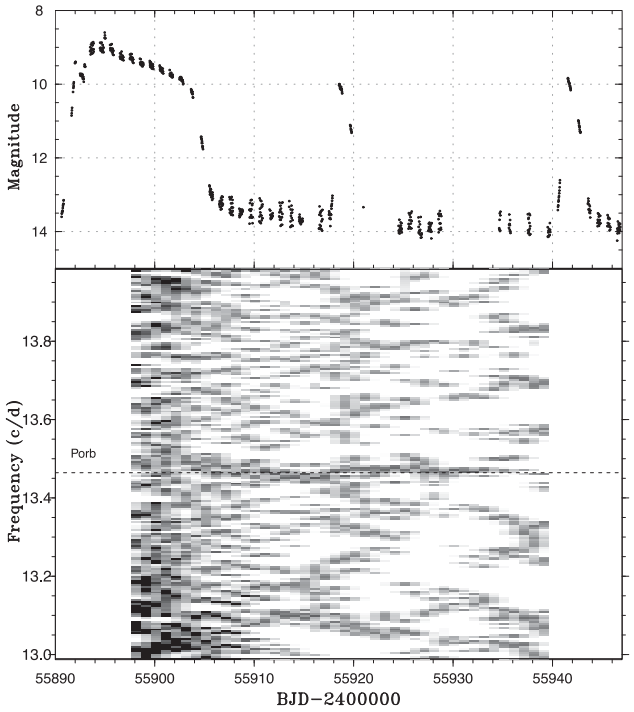

Fig. 88. Two-dimensional Lasso period analysis of VW Hyi (2011). See figure 87 for the explanation. No strong signal of negative superhumps was detected.

For comparison, a two-dimensional Lasso analysis of the 2011 superoutburst is also shown in figure 88. No clear signal of negative superhumps was detected, although the analysis is noisy due to the poorer data coverage than in the 2012 superoutburst and to the persistence of positive superhumps which interferes with the detection of other signals when the data are sparse.

We conclude that the type L supercycle in VW Hyi (reduced number of normal outbursts) is associated with the presence of negative superhumps as in V1504 Cyg and V344 Lyr, and the tilt in the disk can be regarded as a cause of the varying frequency of normal outbursts.

5 Summary

In addition to basic data of superhumps of the objects dealt with in this paper, the major findings we obtained can be summarized as follows.

(i) We report on the detection of negative superhumps in quiescence of VW Hyi in 2012. We conclude that the type L supercycle in VW Hyi (reduced number of normal outbursts) is associated with the presence of negative superhumps as in V1504 Cyg and V344 Lyr.

(ii) MASTER J005740 is the first eclipsing WZ Sge-type dwarf nova showing the probable eclipse of the white dwarf. The sharp structure in the profile of early superhumps is interpreted as an eclipse of the accretion disk, and it has been difficult to distinguish the ecllipse from the profile of the early superhump itself in other WZ Sge-type dwarf novae. The symmetric profile of the eclipse indicates that the disk itself, not the enhanced hot spot, is eclipsed. This finding provides observational support for Osaki and Meyer (2003) who interpreted that the source of early superhumps is not the hot spot such as is explained by an enhanced mass-transfer model (Patterson et al. 1981). We also carried out a model calculation of the eclipse light curve of this object during the phase of early superhumps.

(iii) We detected stage A superhumps with growing amplitude in MN Dra and likely stage A (from the $O-C$ diagram) in GZ Cnc, both of which have a long orbital period. The stage A superhump in these systems lasted longer than expected. We interpreted that the 3:1 resonance was confined to the region of excitement because these objects have a mass ratio critically close to the condition in which tidal instability occurs. This may provide an interpretation of large negative-period derivatives recorded in the past in the system with a long orbital period.

(iv) The 2013 superoutburst of UZ Boo was followed by four post-superoutburst rebrightenings, the same as in the 2003 superoutburst. This observation suggests that the pattern of rebrightening is inclined to be reproducible in the same object.

(v) The WZ Sge-type dwarf novae AL Com and ASASSN-13ck showed a long-lasting (plateau-type) rebrightening. In the early phase of the rebrightening, both objects showed a precursor-like outburst, suggesting that the long-lasting rebrightening is triggered by a precursor outburst. Both objects showed small dip(s) during the rebrightening.

(vi) We have reviewed the observation of early superhumps of WZ Sge-type dwarf novae and found that the fractional superhump excess for early superhumps has a typical value of -0.05%.

(vii) We have succeeded in detecting a positive period derivative of superhumps in the helium CV CP Eri. This object also showed an oscillation-type rebrightening.

(viii) We have established the long-sought superoutburst of the eclipsing dwarf nova V893 Sco. It was 15 years after its rediscovery.

Note added in proof (2014 October 2):

Most recent study indicates that AM CVn-type objects having orbital periods as long as ~ 0.034 d show dwarf

nova-type outbursts (Kato et al. 2014b; Woudt et al. 2013). MASTER J234843 may also fit this category.

Acknowledgments

This work was supported by a Grant-in-Aid "Initiative for High-Dimensional Data-Driven Science through Deepening of Sparse Modeling" from the Ministry of Education, Culture, Sports, Science and Technology (MEXT) of Japan. The authors are grateful to observers of VSNET Collaboration and to VSOLJ observers who supplied vital data. We acknowledge with thanks the variable star observations from the AAVSO International Database, which are contributed by observers world-wide and used in this research. This work is deeply indebted to outburst detections and announcement by a number of variable star observers worldwide, including participants of CVNET and BAA VSS alert. We thank Dr. Brian Skiff for making historical materials about WX Hyi available for our use. The CCD operation of the Bronberg Observatory is partly sponsored by the Center for Backyard Astrophysics. The CCD operation by Peter Nelson is on loan from the AAVSO, funded by the Curry Foundation. We are grateful to the Catalina Real-time Transient Survey team for making their real-time detection of transient objects available for the public use.

References

Abbott, T. M. C., Robinson, E. L., Hill, G. J., & Haswell, C. A. 1992, ApJ, 399, 680
Andronov, I. L. 1986, Astron. Tsirk., 1432, 6
Antipin, S. V., & Pavlenko, E. P. 2002, A&A, 391, 565
Araujo-Betancor, S., et al. 2005, A&A, 430, 629
Armstrong, E., Patterson, J., & Kemp, J. 2012, MNRAS, 421, 2310
Aungwerojwit, A., et al. 2006, A&A, 455, 659
Avery, R., & Sievers, J. 1968, Bamberg Veröff., 7, 76
Bailey, J. 1979a, MNRAS, 188, 681
Bailey, J. 1979b, MNRAS, 189, 41P
Balanutsa, P., et al. 2013a, Astron. Telegram, 5555
Balanutsa, P., et al. 2013b, Astron. Telegram, 5708
Bateson, F. M. 1976, IBVS, 1161
Bateson, F. M. 1982a, Publ. Variable Stars Sect. R. Astron. Soc. New Zealand, 10, 24
Bateson, F. M. 1982b, Publ. Variable Stars Sect. R. Astron. Soc. New Zealand, 10, 12
Bateson, F. M. 1998, Publ. Variable Stars Sect. R. Astron. Soc. New Zealand, 23, 44
Bertola, F. 1964, Ann. Astrophys., 27, 298
Bertola, F. 1965, IBVS, 103
Bond, H. E., Kemper, E., & Mattei, J. A. 1982, ApJ, 260, L79
Boyd, D., Oksanen, A., & Henden, A. 2006, J. Br. Astron. Assoc., 116, 187
Bruch, A. 1989, A&AS, 78, 145
Bruch, A., Fischer, F.-J., & Wilmsen, U. 1987, A&AS, 70, 481
Bruch, A., Steiner, J. E., & Gneiding, C. D. 2000, PASP, 112, 237
Cannizzo, J. K., Still, M. D., Howell, S. B., Wood, M. A., & Smale, A. P. 2010, ApJ, 725, 1393
Cannon, A. J. 1925, Harvard Coll. Obs. Bull., 825, 1
Carter, P. J., et al. 2013, MNRAS, 431, 372
Chen, J.-S., Liu, X.-W., & Wei, M.-Z. 1991, A&A, 242, 397
Cleveland, W. S. 1979, J. Amer. Statist. Assoc., 74, 829
Demartino, R., Kocyla, D., Predom, C., & Wetherbee, E. 1996, IBVS, 4322
Denisenko, D., et al. 2013a, Astron. Telegram, 5572
Denisenko, D., et al. 2013b, Astron. Telegram, 5643
Denisenko, D., et al. 2013c, Astron. Telegram, 5399
Denisenko, D. V., & Sokolovsky, K. V. 2011, Astron. Lett., 37, 91
Downes, R., Webbink, R. F., & Shara, M. M. 1997, PASP, 109, 345
Downes, R. A. 1990, AJ, 99, 339
Downes, R. A., Webbink, R. F., Shara, M. M., Ritter, H., Kolb, U., & Duerbeck, H. W. 2001, PASP, 113, 764
Drake, A. J., et al. 2009, ApJ, 696, 870
Drew, J. E., et al. 2005, MNRAS, 362, 753
Duerbeck, H. W. 1987, Space Sci. Rev., 45, 1
Fernie, J. D. 1989, PASP, 101, 225
Filin, A. Y., & Satyvoldiev, V. 1975, Perem. Zvezdy, 20, 161
Fisher, W. J. H., Walker, W. S. G., Jones, A. F., & Nelson, P. 1971, IAU Circ., 2348
Gill, C. D., & O'Brien, T. J. 1998, MNRAS, 300, 221
Glasby, J. S. 1970, The Dwarf Novae (London: Constable)
Gorbovskoy, E. S., et al. 2013, Astron. Rep., 57, 233
Green, R. F., Ferguson, D. H., Liebert, J., & Schmidt, M. 1982, PASP, 94, 560
Haro, G., & Luyten, W. J. 1962, Bol. Obs. de Tonantzintla y Tacubaya, 3, 37
Harvey, D., Skillman, D. R., Patterson, J., & Ringwald, F. A. 1995, PASP, 107, 551
Hirose, M., & Osaki, Y. 1990, PASJ, 42, 135
Hoffmeister, C. 1936, Astron. Nachr., 259, 37
Hoffmeister, C. 1949, Erg. Astron. Nachr., 12, 12
Hoffmeister, C. 1957, Mitt. Veränderl. Sterne, 1, 245
Hoffmeister, C. 1967, Astron. Nachr., 289, 205
Howell, S. B., De Young, J., Mattei, J. A., Foster, G., Szkody, P., Cannizzo, J. K., Walker, G., & Fierce, E. 1996, AJ, 111, 2367
Howell, S. B., Dobrzycka, D., Szkody, P., & Kreidl, T. J. 1991, PASP, 103, 300
Howell, S. B., & Szkody, P. 1990, ApJ, 356, 623
Iida, M., & York, D. 1994, IAU Circ., 6056, 3
Imada, A., Kubota, K., Kato, T., Nogami, D., Maehara, H., Nakajima, K., Uemura, M., & Ishioka, R. 2006, PASJ, 58, L23
Ishioka, R., et al. 2002, A&A, 381, L41
Ishioka, R., Kato, T., Uemura, M., Iwamatsu, H., Matsumoto, K., Martin, B. E., Billings, G. W., & Novak, R. 2001, PASJ, 53, L51
Itagaki, K., et al. 2013, Cent. Bur. Electron. Telegrams, 3554
Kato, T. 1995a, IBVS, 4152
Kato, T. 1995b, IBVS, 4242
Kato, T. 1996, IBVS, 4369
Kato, T. 2002, PASJ, 54, L11
Kato, T., et al. 2002c, A&A, 396, 929
Kato, T., et al. 2002d, A&A, 395, 541
Kato, T., et al. 2004c, MNRAS, 347, 861
Kato, T., et al. 2009, PASJ, 61, S395
Kato, T., et al. 2010, PASJ, 62, 1525
Kato, T., et al. 2012b, PASJ, 64, 21
Kato, T., et al. 2013b, PASJ, 65, 23
Kato, T., et al. 2014a, PASJ, 66, 30
Kato, T., et al. 2014b, PASJ, 66, L7

Kato, T., Hanson, G., Poyner, G., Muyllaert, E., Reszelski, M., & Dubovsky, P. A. 2000, IBVS, 4932
Kato, T., Haseda, K., Takamizawa, K., Kazarovets, E. V., & Samus, N. N. 1998a, IBVS, 4585
Kato, T., Ishioka, R., & Uemura, M. 2002a, PASJ, 54, 1029
Kato, T., & Kunjaya, C. 1995, PASJ, 47, 163
Kato, T., Lipkin, Y., Retter, A., & Leibowitz, E. 1998b, IBVS, 4602
Kato, T., & Maehara, H. 2013, PASJ, 65, 76
Kato, T., Maehara, H., & Uemura, M. 2012a, PASJ, 64, 62
Kato, T., Matsumoto, K., & Uemura, M. 2002b, IBVS, 5262
Kato, T., Monard, B., Hambsch, F.-J., Kiyota, S., & Maehara, H. 2013a, PASJ, 65, L11
Kato, T., Nogami, D., Baba, H., Masuda, S., Matsumoto, K., & Kunjaya, C. 1999, in Disk Instabilities in Close Binary Systems, ed. S. Mineshige & J. C. Wheeler (Tokyo: Universal Academy Press), p. 45
Kato, T., Nogami, D., Baba, H., Matsumoto, K., Arimoto, J., Tanabe, K., & Ishikawa, K. 1996b, PASJ, 48, L21
Kato, T., Nogami, D., & Masuda, S. 1996a, PASJ, 48, L5
Kato, T., Nogami, D., Matsumoto, K., & Baba, H. 2004a, PASJ, 56, S109
Kato, T., & Osaki, Y. 2013a, PASJ, 65, 97
Kato, T., & Osaki, Y. 2013b, PASJ, 65, 115
Kato, T., & Osaki, Y. 2013c, PASJ, 65, L13
Kato, T., & Osaki, Y. 2014, PASJ, 66, L5
Kato, T., Sekine, Y., & Hirata, R. 2001a, PASJ, 53, 1191
Kato, T., Stubbings, R., Pearce, A., Nelson, P., & Monard, B. 2001b, IBVS, 5119, 1
Kato, T., & Uemura, M. 2012, PASJ, 64, 122
Kato, T., Uemura, M., Buczynski, D., & Schmeer, P. 2001c, IBVS, 5123
Kato, T., Uemura, M., Ishioka, R., Nogami, D., Kunjaya, C., Baba, H., & Yamaoka, H. 2004b, PASJ, 56, S1
Kazarovets, E. V., Samus, N. N., Durlevich, O. V., Kireeva, N. N., & Pastukhova, E. N. 2008, IBVS, 5863
Kholopov, P. N., et al. 1985, General Catalogue of Variable Stars, 4th ed. (Moscow: Nauka Publishing House)
Klose, S. 1995, ApJ, 446, 357
Knigge, C., Baraffe, I., & Patterson, J. 2011, ApJS, 194, 28
Knigge, R., & Bauernfeind, H. 1967, Bamberg Veröff., 6, 45
Kukarkin, B. V. 1971, IAU Circ., 2319
Kukarkin, B. V., et al. 1969, General Catalogue of Variable Stars, 3rd ed. (Moscow: Astronomical Council of the Academy of Sciences in the USSR)
Kunjaya, C., Kinugasa, K., Ishioka, R., Kato, T., Iwamatsu, H., & Uemura, M. 2001, IBVS, 5128
Kuulkers, E., Howell, S. B., & van Paradijs, J. 1996, ApJ, 462, L87
Larwood, J. 1998, MNRAS, 299, L32
Littlefair, S. P., Dhillon, V. S., Marsh, T. R., & Gänsicke, B. T. 2006, MNRAS, 371, 1435
Littlefield, C., et al. 2013, AJ, 145, 145
Liu, Wu., & Hu, J. Y. 2000, ApJS, 128, 387
Liu, Wu., Hu, J. Y., Zhu, X. H., & Li, Z. Y. 1999, ApJS, 122, 243
Lubow, S. H. 1991, ApJ, 381, 259
Lucchetti, S. C., & Usher, P. D. 1972, IBVS, 696
Luyten, W. J. 1932, Astron. Nachr., 245, 211
Luyten, W. J., & Haro, G. 1959, PASP, 71, 469
Martin, D. C., et al. 2005, ApJ, 619, L1
Mason, E., & Howell, S. 2003, A&A, 403, 699
Mason, K. O., Reichert, G. A., Bowyer, S., & Thorstensen, J. R. 1982, PASP, 94, 521
Mason, E., Skidmore, W., Howell, S. B., & Mennickent, R. E. 2001, ApJ, 563, 351
Matsumoto, K., Mennickent, R. E., & Kato, T. 2000, A&A, 363, 1029
McLaughlin, D. B. 1945, AJ, 51, 136
Meinunger, L. 1984a, IBVS, 2483
Meinunger, L. 1984b, Mitt. Veränderl. Sterne, 10, 56
Mennickent, R. E., & Diaz, M. 1996, A&A, 309, 147
Mukai, K., et al. 1990, MNRAS, 245, 385
Mukai, K., Zietsman, E., & Still, M. 2009, ApJ, 707, 652
Munari, U., & Zwitter, T. 1998, A&AS, 128, 277
Nakata, C., et al. 2013b, PASJ, 65, 117
Nakata, C., et al. 2014, PASJ in press
Nakata, C., Kuin, P., Kato, T., & Ohshima, T. 2013a, Astron. Telegram, 5253
Nogami, D., & Kato, T. 1995, IBVS, 4227
Nogami, D., Kato, T., Baba, H., Matsumoto, K., Arimoto, J., Tanabe, K., & Ishikawa, K. 1997, ApJ, 490, 840
Nogami, D., Kato, T., & Hirata, R. 1996, PASJ, 48, 607
Nogami, D., Masuda, S., & Kato, T. 1997, PASP, 109, 1114
Nogami, D., et al. 2003, A&A, 404, 1067
Noguchi, T., Maehara, H., & Kondo, M. 1980, Tokyo Astron. Obs. Ann., Sec. Ser., 18, 55
Noguchi, T., Yutani, M., & Maehara, H. 1982, PASJ, 34, 407
O'Donoghue, D., Chen, A., Marang, F., Mittaz, J. P. D., Winkler, H., & Warner, B. 1991, MNRAS, 250, 363
Ohshima, T., et al. 2012, PASJ, 64, L3
Ohshima, T., et al. 2014, PASJ, 66, 67
Oizumi, S., et al. 2007, PASJ, 59, 643
Olech, A., Mularczyk, K., Kędzierski, P., Złoczewski, K., Wiśniewski, M., & Szaruga, K. 2006, A&A, 452, 933
Olech, A., Wisniewski, M., Zloczewski, K., Cook, L. M., Mularczyk, K., & Kedzierski, P. 2008, Acta Astron., 58, 131
Olech, A., Zloczewski, K., Mularczyk, K., Kedzierski, P., Wisniewski, M., & Stachowski, G. 2004, Acta Astron., 54, 57
Osaki, Y. 1989, PASJ, 41, 1005
Osaki, Y. 1996, PASP, 108, 39
Osaki, Y., & Kato, T. 2013a, PASJ, 65, 50
Osaki, Y., & Kato, T. 2013b, PASJ, 65, 95
Osaki, Y., & Kato, T. 2014, PASJ, 66, 15
Osaki, Y., & Meyer, F. 2002, A&A, 383, 574
Osaki, Y., & Meyer, F. 2003, A&A, 401, 325
Osaki, Y., Shimizu, S., & Tsugawa, M. 1997, PASJ, 49, L19
Otulakowska-Hypka, M., Olech, A., de Miguel, E., Rutkowski, A., Koff, R., & Bąkakowska, K. 2013, MNRAS, 429, 868
Patterson, J. 1979, AJ, 84, 804
Patterson, J., et al. 1998, PASP, 110, 1290
Patterson, J., et al. 2002, PASP, 114, 721
Patterson, J., et al. 2003, PASP, 115, 1308
Patterson, J., et al. 2005, PASP, 117, 1204
Patterson, J., Augusteijn, T., Harvey, D. A., Skillman, D. R., Abbott, T. M. C., & Thorstensen, J. 1996, PASP, 108, 748
Patterson, J., Kemp, J., Saad, J., Skillman, D. R., Harvey, D., Fried, R., Thorstensen, J. R., & Ashley, R. 1997, PASP, 109, 468

Patterson, J., McGraw, J. T., Coleman, L., & Africano, J. L. 1981, ApJ, 248, 1067
Patterson, J., Richman, H., Kemp, J., & Mukai, K. 1998, PASP, 110, 403
Patterson, J., Thomas, G., Skillman, D. R., & Diaz, M. 1993, ApJS, 86, 235
Pavlenko, E. P., et al. 2010, Astron. Rep., 54, 6
Petit, M. 1956, Journal des Observateurs, 39, 37
Philip, A. G. D. 1971, IAU Circ., 2308
Pojmański, G. 2002, Acta Astron., 52, 397
Prager, R., & Shapley, H. 1941, Ann. Astron. Obs. Harvard Coll., 111, 1
Pretorius, M. L., Warner, B., & Woudt, P. A. 2006, MNRAS, 368, 361
Ramsay, G., Barclay, T., Steeghs, D., Wheatley, P. J., Hakala, P., Kotko, I., & Rosen, S. 2012, MNRAS, 419, 2836
Richter, G. A. 1969, Mitt. Veränderl. Sterne, 5, 69
Richter, G. A. 1986, Astron. Nachr., 307, 221
Richter, G. A. 1989, Astron. Nachr., 310, 143
Robertson, J. W., Honeycutt, R. K., & Turner, G. W. 1995, PASP, 107, 443
Rodríguez-Gil, P., Gänsicke, B. T., Hagen, H.-J., Marsh, T. R., Harlaftis, E. T., Kitsionas, S., & Engels, D. 2005, A&A, 431, 269
Rosino, L. 1961, IAU Circ., 1782
Rufanov, A., et al. 2013, Astron. Telegram, 5587
Samsonov, D. A., Pavlenko, E. P., Andreev, M. V., Sklyanov, A., & Zubareva, A. M. 2010, Odessa Astron. Publ., 23, 98
Sanduleak, N. 1976, IBVS, 1218
Satyvoldiev, V. 1972, Astron. Tsirk., 711, 7
Satyvoldiev, V. 1982, Perem. Zvezdy, Prilozh., 4, 127
Schoembs, R., & Vogt, N. 1981, A&A, 97, 185
Semeniuk, I., Nalezyty, M., Gembara, P., & Kwast, T. 1997, Acta Astron., 47, 299
Shafter, A. W., Coelho, E. A., & Reed, J. K. 2007, PASP, 119, 388
Shafter, A. W., & Hessman, F. V. 1988, AJ, 95, 178
Shappee, B. J., et al. 2014a, ApJ, 788, 48
Shappee, B. J., et al. 2014b, Astron. Telegram, 5775
Shears, J. H., Gaensicke, B. T., Brady, S., Dubovsky, P., Miller, I., & Staels, B. 2011b, New Astron., 16, 311
Shears, J., Lloyd, C., Boyd, D., Brady, S., Miller, I., & Pickard, R. 2009, J. Br. Astron. Assoc., 119, 31
Shears, J., Wils, P., Bolt, G., Hambsch, F.-J., Krajci, T., Miller, I., Sabo, R., & Staels, B. 2011a, J. Br. Astron. Assoc., 121, 155
Shumkov, V., et al. 2013, Astron. Telegram, 4814
Shurpakov, S., et al. 2013, Astron. Telegram, 5526
Skvarc, J., & Palcic, R. 2006, Cent. Bur. Electron. Telegrams, 701, 1
Smak, J. 1985, Acta Astron., 35, 357
Smak, J. 2010, Acta Astron., 60, 357
Smith, A. J., Haswell, C. A., & Hynes, R. I. 2006, MNRAS, 369, 1537
Solheim, J.-E. 2010, PASP, 122, 1133
Splittgerber, E. 1971, IBVS, 578
Stellingwerf, R. F. 1978, ApJ, 224, 953
Szkody, P. 1987, ApJS, 63, 685
Szkody, P., & Feinswog, L. 1988, ApJ, 334, 422
Szkody, P., Howell, S. B., Mateo, M., & Kreidl, T. J. 1989, PASP, 101, 899
Szkody, P., & Mattei, J. A. 1984, PASP, 96, 988
Tappert, C., & Bianchini, A. 2003, A&A, 401, 1101
Thorstensen, J. R. 1999, IBVS, 4749
Thorstensen, J. R., Patterson, J. O., Shambrook, A., & Thomas, G. 1996, PASP, 108, 73
Thorstensen, J. R., Wade, R. A., & Oke, J. B. 1986, ApJ, 309, 721
Tibshirani, R. 1996, J. R. Statistical Soc. Ser. B, 58, 267
Tsesevich, V. P. 1969, Astron. Tsirk., 529, 7
Tsesevich, V. P., & Dragomiretskaia, B. A. 1973, Zvezdy tipa RW Voznichego: fotograficheskie nablyudeniya bleska (Naukova dumka: Kiev)
Udalski, A. 1990a, AJ, 100, 226
Udalski, A. 1990b, IBVS, 3425
Uemura, M., et al. 2005, A&A, 432, 261
Uemura, M., et al. 2008, IBVS, 5815
Uemura, M., Kato, T., Ohshima, T., & Maehara, H. 2012, PASJ, 64, 92
Vladimirov, V., et al. 2013, Astron. Telegram, 5481
Vogt, N. 1974, A&A, 36, 369
Vogt, N. 1980, A&A, 88, 66
Vogt, N. 1983, A&A, 118, 95
Vogt, N., & Bateson, F. M. 1982, A&AS, 48, 383
von Gessner, H., & Meinunger, I. 1974, Veröff. Sternw. Sonneberg, 6, 249
Walker, W. S. G., Marino, B. F., & Freeth, G. 1976, IBVS, 1185
Warner, B. 1995, Cataclysmic Variable Stars (Cambridge: Cambridge University Press)
Wegner, G., & McMahan, R. K. 1988, AJ, 96, 1933
Whitehurst, R. 1988, MNRAS, 232, 35
Wolf, M., & Wolf, G. 1906, Astron. Nachr., 170, 361
Wood, M. A., & Burke, C. J. 2007, ApJ, 661, 1042
Wood, M. A., Winget, D. E., Nather, R. E., Hessman, F. V., Liebert, J., Kurtz, D. W., Wesemael, F., & Wegner, G. 1987, ApJ, 313, 757
Woudt, P. A., & Warner, B. 2001, MNRAS, 328, 159
Woudt, P. A., Warner, B., & Motsoaledi, M. 2013, Astron. Telegram, 4726
Woudt, P. A., Warner, B., & Pretorius, M. L. 2004, MNRAS, 351, 1015
Wu, J.-H., Chen, Y., He, X.-T., Zhang, X.-Z., & Voges, W. 2001, Chin. J. Astron. Astrophys., 1, 57
Zemko, P., Kato, T., & Shugarov, S. 2013, PASJ, 65, 54
Zhukov, G. V., Solov'ev, V. Y., & Solovjev, V. Y. 1972, Astron. Tsirk., 729, 8
Zwicky, F. 1965, IAU Circ., 1902
Zwitter, T., & Munari, U. 1995, A&AS, 114, 575